



**Selective dehydroisomerisation of cyclic monoterpenes to
p-cymene over bifunctional metal-acid catalysts**

Thesis submitted in accordance with the requirements of the
University of Liverpool for the degree of Doctor in
Philosophy by

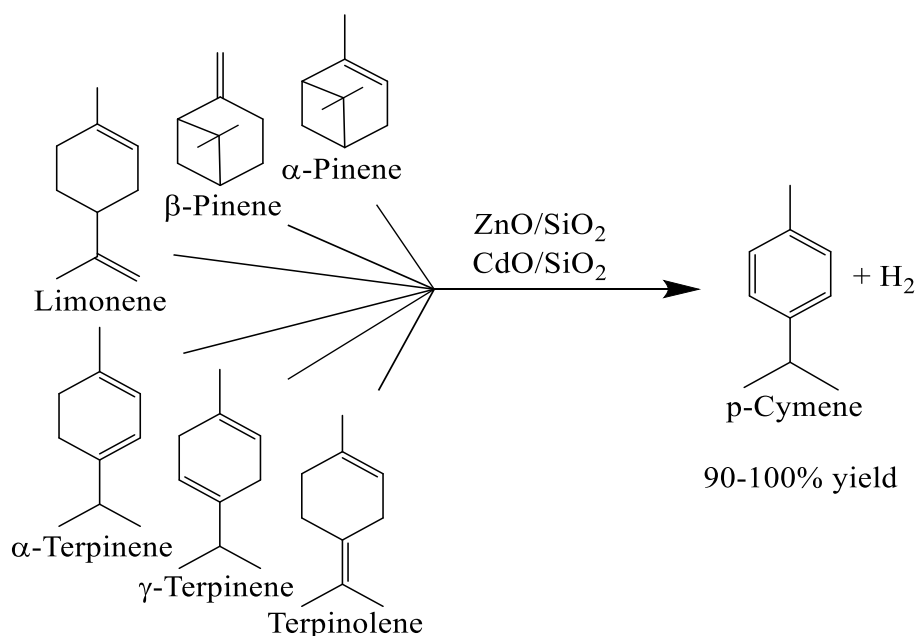
Aliyah Abdullah Alsharif

January 2023

Abstract

The dehydroisomerisation of α -pinene and limonene, naturally occurring abundant monoterpenes, is a clean sustainable route to produce p-cymene, an important intermediate in organic synthesis and ingredient in cosmetics and medicinal products. Currently, p-cymene is produced in a mixture with o- and m-isomers by the Friedel-Crafts alkylation of toluene with propene, followed by isomer separation, with an adverse effect on the environment.

The aim of this work is to study the dehydroisomerisation of cyclic monoterpenes, such as α -pinene, β -pinene, limonene, α -terpinene, γ -terpinene and terpinolene, in the gas phase using silica-supported ZnO and CdO as new bifunctional metal-acid catalysts. It is demonstrated that all these monoterpenes can be converted to p-cymene with excellent yields of 90–100% using ZnO/SiO₂ and CdO/SiO₂ as the catalysts.



The catalysts were prepared by wet impregnation of silica with metal nitrates from an aqueous solution followed by drying and calcination at 400–500 °C and characterised by BET, TGA, XRD, DRIFTS, H₂-TPR and ICP-OES. The dehydroisomerisation reactions were carried out in a continuous flow fixed-bed microreactor with online GC analysis.

It was found that dehydroisomerisation of α -pinene over ZnO/SiO₂ produces p-cymene with 90% yield at 100% conversion at 370 °C and WHSV = 0.020 h⁻¹. The reaction with limonene gives a 100% p-cymene yield at 325 °C and WHSV = 0.080 h⁻¹. ZnO/SiO₂ catalyst shows stable performance for over 70 h without co-feeding hydrogen to the reactor. The reaction over silica-supported ZnO catalysts with β -pinene produces a 100% p-cymene yield

at 400 °C and WHSV = 0.080 h⁻¹. The reaction with monocyclic terpenes such as limonene, α -terpinene, γ -terpinene and terpinolene gives a 100% p-cymene yield at 300–325 °C and WHSV = 0.16–0.08 h⁻¹.

The dehydroisomerisation of bicyclic monoterpenes, such as α -pinene and β -pinene, over CdO/SiO₂ gives 91–95% p-cymene yields at 325–375 °C and WHSV = 0.010–0.020 h⁻¹, whereas the more reactive monocyclic terpenes, such as limonene, α -terpinene, γ -terpinene, and terpinolene, give a 100% yield at 200–250 °C and WHSV = 0.040–0.080 h⁻¹. This catalyst shows stable performance for over 25 h without co-feeding hydrogen. To the best of our knowledge, CdO/SiO₂ has the highest efficiency in monoterpene-to-p-cymene dehydroisomerisation among the catalysts reported to date.

The proposed mechanism of monoterpene dehydroisomerisation to p-cymene on bifunctional ZnO/SiO₂ and CdO/SiO₂ catalysts involves two steps: fast isomerisation of monoterpene reactant on Brønsted acid sites (silanol groups of silica support) to form p-menthadiene intermediates followed by their slow dehydrogenation on oxo-metal sites to p-cymene. The dehydrogenation is suggested to proceed through the abstraction of allylic hydrogen from the substrate by an oxo-metal site followed by the elimination of another hydrogen atom to form p-cymene π -bonded to metal ion (Zn(II) or Cd(II)). Then, the elimination of the p-cymene molecule and H₂ closes the catalytic cycle.

Publications and presentations

1. A. Alsharif, N. Smith, E. F. Kozhevnikova, I. V. Kozhevnikov, Dehydroisomerisation of α -pinene and limonene to p-cymene over silica-supported ZnO in the gas phase, *Catalysts* 11 (2021) 1245.
2. A. Alsharif, E. F. Kozhevnikova, I. V. Kozhevnikov, Selective dehydroisomerisation of cyclic monoterpenes to p-cymene over silica-supported CdO, *Appl. Catal. B Environ.* 325 (2022) 122362.
3. A. Alsharif, E. F. Kozhevnikova, I. V. Kozhevnikov, The 7th UK Catalysis Conference (UKCC2021), Loughborough, UK 2021.
4. A. Alsharif, E. F. Kozhevnikova, I. V. Kozhevnikov, The 8th Edition of Global Conference on Catalysis, Chemical Engineering and Technology (CAT-2021), Paris, France 2021.
5. A. Alsharif, E. F. Kozhevnikova, I. V. Kozhevnikov, Poster Day, University of Liverpool, Liverpool, UK 2022.
6. A. Alsharif, E. F. Kozhevnikova, I. V. Kozhevnikov, 3rd Global Virtual Summit on Catalysis and Chemical Engineering, UK 2022.

Acknowledgments

I would like to thank my primary supervisor, Prof. Ivan V. Kozhevnikov, who guided me throughout my PhD study, for his invaluable patience and advice. Due to his advice and experience, PhD project has been successfully completed.

Words cannot express my gratitude to Dr. Elena F. Kozhevnikova for her kind help in experimental work and for solving technical issues in the laboratory.

I would also like to thank all members of the technical support team in the Department of Chemistry at University of Liverpool, and all members of my group, Reem Ghubayra, Hanan Althikrallah, Rawan Alfaze and Amal Alasmari.

The scholarship and financial support I received from Al-Imam Muhammad Ibn Saud University, Riyadh, Saudi Arabia are gratefully acknowledged. Extended appreciation goes to the Saudi Arabian Cultural Bureau in the UK for taking the responsibility for my scholarship in the United Kingdom.

Let me also extend my great thanks to my family; my mum, my brothers and my sisters. I could not have undertaken this journey without their support and encouragement. Special thanks are due to my husband for his generous support and my children for their patience and love.

Finally, to my father, you have always been in my heart throughout my PhD journey, I never forgot your sweet words, your daughter achieved PhD as you wish, rest in peace, father.

Abbreviations

ZnO	Zinc oxide
CdO	Cadmium oxide
CST	Crude sulfate turpentine
IM	Impregnation method
PM	Physical mixing
TOS	Time on stream
XRD	Powder X-ray diffraction
TGA	Thermogravimetric analysis
DRIFT	Diffuse reflectance infrared Fourier transform
BET	Brunauer-Emmett-Teller method
BJH	Barrett-Joyner-Halenda method
ICP-OES	Inductively coupled plasma optical emission spectroscopy
TPR	Temperature programmed reduction
GC	Gas chromatography
FID	Flame ionisation detector
WHSV	Weight hourly space velocity
XPS	X-ray photoelectron spectroscopy
EXAFS	Extended X-ray adsorption fine structure

Contents

Abstract.....	i
Publications and presentations.....	iii
Acknowledgments.....	iv
Abbreviations.....	v
Contents.....	vi
List of figures.....	ix
List of tables.....	xv
List of schemes.....	xvii
Chapter 1. Introduction.....	1
1. Background and definitions.....	1
1.1. Heterogeneous catalysis.....	3
1.1.1. Key steps of reaction on porous solid catalyst.....	3
1.1.2. Essential properties of catalysts.....	4
1.1.3. Key factors of catalysts development.....	5
1.1.4. Active sites.....	6
1.1.5. Classification of catalysts.....	7
1.1.6. Multifunctional catalysis for tandem reactions.....	8
1.2. Catalysis by ZnO.....	9
1.2.1. Preparation of ZnO catalysts.....	9
1.2.2. Properties of ZnO.....	10
1.3. Catalysis by CdO.....	12
1.3.1. Preparation of CdO catalysts.....	12
1.3.2. The properties of CdO.....	13
1.4. p-Cymene.....	14
1.4.1. The synthesis of p-cymene.....	15
1.4.1.1. Friedel-Crafts alkylation.....	15
1.4.1.2. Synthesis from terpenes.....	16
1.4.1.2.1. Pinene as renewable feedstock for p-cymene synthesis.....	18

1.4.1.2.2. Dehydroisomerisation of α - and β -pinene to p-cymene.....	18
1.4.1.2.3. Limonene as renewable feedstock for p-cymene synthesis.....	21
1.4.1.2.4. Dehydroisomerisation of limonene to p-cymene.....	21
1.5. Objectives and thesis organisation.....	25
References.....	27
Chapter 2. Experimental.....	35
2. Introduction.....	35
2.1. Chemicals and solvents.....	35
2.2. Catalyst preparation.....	35
2.2.1. Preparation of compacted SiO ₂	35
2.2.2. Preparation of bulk ZnO and CdO.....	36
2.2.3. Preparation of silica-supported ZnO and CdO catalysts.....	36
2.3. Catalyst characterisation techniques.....	37
2.3.1. Inductively coupled plasma optical emission spectroscopy (ICP-OES).....	37
2.3.2. Surface area and porosity.....	39
2.3.3. Thermogravimetric analysis (TGA).....	43
2.3.4. Fourier transform infrared spectroscopy (FTIR).....	44
2.3.5. X-ray diffraction (XRD).....	45
2.3.6. Temperature programmed reduction (TPR).....	46
2.3.7. CHN analysis.....	48
2.4. Catalyst testing.....	48
2.4.1. Gas chromatography (GC).....	48
2.4.2. GC calibration.....	51
2.5. Reaction studies.....	53
2.5.1. Gas phase reaction.....	53
2.6. Calculation of conversion, yield and selectivity.....	55
References.....	57
Chapter 3. Dehydroisomerisation of α-pinene and limonene to p-cymene over silica-supported ZnO in the gas phase.....	60
3. Introduction.....	60

3.1. Results and discussion	63
3.1.1. Catalyst characterisation.....	63
3.1.2. Dehydroisomerisation of α -pinene.....	72
3.1.3. Dehydroisomerisation of limonene.....	79
3.2. Conclusions	82
References	84
Chapter 4. Dehydroisomerisation of β-pinene, α-terpinene, γ-terpinene and terpinolene over silica-supported ZnO in the gas phase	88
4. Introduction	88
4.1. Results and discussion	88
4.1.1. Dehydroisomerisation of β -pinene.....	88
4.1.2. Dehydroisomerisation of α -terpinene, γ -terpinene, and terpinolene.....	91
4.2. Conclusions	95
References	96
Chapter 5. Dehydroisomerisation of cyclic monoterpenes to p-cymene over silica-supported CdO in the gas phase	97
5. Introduction	97
5.1. Results and discussion	100
5.1.1. Catalyst characterisation.....	100
5.1.2. Dehydroisomerisation of α -pinene.....	108
5.1.3. Dehydroisomerisation of β -pinene.....	114
5.1.4. Dehydroisomerisation of limonene.....	118
5.1.5. Dehydroisomerisation of α -terpinene, γ -terpinene, and terpinolene.....	122
5.1.6. Reaction mechanism.....	127
5.2. Conclusions	129
References	130
Chapter 6. Conclusions and future outlook	135
References	138

List of figures

Figure 1.1.	Solid catalysts used in the chemical industry.	2
Figure 1.2.	Reaction steps on a porous solid catalyst.	4
Figure 1.3.	The active sites of redox and acid-base catalysts.	6
Figure 1.4.	Traditional step-by-step reaction versus tandem process.	8
Figure 1.5.	Chemical structure of p-cymene.	14
Figure 2.1.	Schematic diagram of ICP-OES instrument.	38
Figure 2.2.	Schematic representation of Micrometrics ASAP 2010 instrument.	41
Figure 2.3.	The four common types of N ₂ adsorption isotherm.	42
Figure 2.4.	Four hysteresis types usually seen in N ₂ adsorption-desorption isotherms.	42
Figure 2.5.	A schematic of TGA apparatus.	44
Figure 2.6.	Diagram of Bragg's reflection.	46
Figure 2.7.	H ₂ -TPR of Ag ₂ O (18.8 mg) in H ₂ -N ₂ (5:95) flow (50 ml min ⁻¹), 10 °C min ⁻¹ temperature ramp rate.	47
Figure 2.8.	Calibration of H ₂ -TPR using Ag ₂ O (0.08–0.20 mmol) in H ₂ -N ₂ (5:95) flow (50 ml min ⁻¹), 10 °C min ⁻¹ temperature ramp rate.	47
Figure 2.9.	Representation of a typical GC set-up: (1) carrier gas, (2) injection port, (3) column, (4) oven, (5) detector and (6) data processor.	49
Figure 2.10.	Split/splitless injector.	49
Figure 2.11.	Flame ionisation detector.	50
Figure 2.12.	The column heating programme used for p-cymene GC analysis.	51
Figure 2.13.	A typical GC trace for α-pinene dehydroisomerisation over 10%ZnO/SiO ₂ .	53
Figure 2.14.	A diagram of the reactor setup for α-pinene and limonene dehydroisomerisation.	55
Figure 3.1.	Nitrogen adsorption (solid circles) and desorption (open circles) isotherms for 10%ZnO/SiO ₂ (300) (a), 20%ZnO/SiO ₂ (300) (b) and 30%ZnO/SiO ₂ (300) (c).	65

Figure 3.2.	Pore size distribution for ZnO/SiO ₂ catalysts.	66
Figure 3.3.	TGA for Zn(NO ₃) ₂ ·6H ₂ O.	67
Figure 3.4.	TGA for fresh 10%ZnO/SiO ₂ (300).	68
Figure 3.5.	XRD patterns (CuKα) for (1) bulk ZnO, (2) 10%ZnO/SiO ₂ (200), (3) 10%ZnO/SiO ₂ (300), (4) 10%ZnO/SiO ₂ (600), (5) 10%ZnO/SiO ₂ (750).	69
Figure 3.6.	XRD patterns for ZnO catalysts (CuKα radiation): (1) bulk ZnO, (2) 30%ZnO/SiO ₂ , (3) 20%ZnO/SiO ₂ and (4) 10%ZnO/SiO ₂ . Aerosil 300 was used as a support.	70
Figure 3.7.	DRIFT spectra of adsorbed pyridine (powdered KBr mixtures vs. KBr): (1) bulk ZnO, (2) 10%ZnO/SiO ₂ (300), (3) 10%ZnO/SiO ₂ (750).	71
Figure 3.8.	DRIFT spectra of SiO ₂ supports (A) and 10%ZnO/SiO ₂ catalysts (B) calcined at 400 °C in air for 2 h (powdered KBr mixtures vs. KBr). Support surface area (m ² g ⁻¹): (1) 200, (2) 300, (3) 600 and (4) 750.	72
Figure 3.9.	Time course for α-pinene dehydroisomerisation over 10%ZnO/SiO ₂ (300): 0.40 g catalyst, 370 °C, 0.48 kPa α-pinene partial pressure, 5 ml min ⁻¹ flow rate, WHSV = 0.020 h ⁻¹ .	74
Figure 3.10.	α-Pinene conversion and p-cymene selectivity over 10%ZnO/SiO ₂ (300) versus contact time at 370 °C and 0.48 kPa α-pinene partial pressure; the contact time varied by changing flow rate (5–50 ml min ⁻¹) and catalyst amount (0.4–0.8 g).	75
Figure 3.11.	Effect of temperature on α-pinene dehydroisomerisation over 10%ZnO/SiO ₂ (300): 0.80 g catalyst, 0.48 kPa α-pinene partial pressure, 5 ml min ⁻¹ flow rate, WHSV = 0.010 h ⁻¹ .	76
Figure 3.12.	Long-term time course for α-pinene dehydroisomerisation over 10%ZnO/SiO ₂ (300) with catalyst regeneration: 0.80 g catalyst, 370 °C, 0.48 kPa α-pinene partial pressure, 10 ml min ⁻¹ flow rate, WHSV = 0.020 h ⁻¹ ; the catalyst regenerated in situ by air flow (10 ml min ⁻¹) at 370 °C for 3 h. Average p-cymene selectivity 85% at 100% p-cymene conversion over 70 h TOS.	78
Figure 3.13.	Time course for limonene dehydroisomerisation over 20%ZnO/SiO ₂ (300): 0.20 g catalyst, 300 °C, 0.47 kPa limonene partial pressure, 10 ml min ⁻¹ flow rate, WHSV = 0.080 h ⁻¹ .	80
Figure 3.14.	Limonene conversion and product selectivity over 30%ZnO/SiO ₂ (300) (0.20 g) versus contact time at 275 °C and 0.47 kPa limonene partial pressure; the contact time varied by changing the flow rate (10–50 ml min ⁻¹).	81

Figure 3.15.	Effect of temperature on limonene dehydroisomerisation over 20%ZnO/SiO ₂ (300) and 30%ZnO/SiO ₂ (300): 0.20 g catalyst, 0.47 kPa limonene partial pressure, 10 ml min ⁻¹ flow rate, 4 h TOS, WHSV = 0.080 h ⁻¹ ; 100% limonene conversion in all cases.	82
Figure 4.1.	Time course for β-pinene dehydroisomerisation over 10%ZnO/SiO ₂ : 0.20 g catalyst, 400 °C, 0.47 kPa β-pinene partial pressure, 10 ml min ⁻¹ flow rate, WHSV = 0.08 h ⁻¹ .	90
Figure 4.2.	Effect of temperature on β-pinene dehydroisomerisation over 10%ZnO/SiO ₂ : 0.20 g catalyst, 0.47 kPa α-pinene partial pressure, 10 ml min ⁻¹ flow rate, WHSV = 0.08 h ⁻¹ .	90
Figure 4.3.	Plot of β-pinene conversion and p-cymene selectivity over 10%ZnO/SiO ₂ versus contact time at 400 °C and 0.47 kPa β-pinene partial pressure; the contact time varied by changing flow rate (5–20 ml min ⁻¹) and catalyst amount (0.2–0.8 g).	91
Figure 4.4.	Time course for α-terpinene dehydroisomerisation over 30%ZnO/SiO ₂ : 0.20 g catalyst, 325 °C, 0.47 kPa α-terpinene partial pressure, 10 ml min ⁻¹ flow rate, WHSV = 0.08 h ⁻¹ .	92
Figure 4.5.	Time course for γ-terpinene dehydroisomerisation over 30%ZnO/SiO ₂ : 0.20 g catalyst, 325 °C, 0.47 kPa γ-terpinene partial pressure, 10 ml min ⁻¹ flow rate, WHSV = 0.08 h ⁻¹ .	93
Figure 4.6.	Time course for terpinolene dehydroisomerisation over 30%ZnO/SiO ₂ : 0.20 g catalyst, 325 °C, 0.47 kPa terpinolene partial pressure, 10 ml min ⁻¹ flow rate, WHSV = 0.08 h ⁻¹ .	93
Figure 4.7.	Effect of temperature on p-cymene yield in monoterpene dehydroisomerisation over 30%ZnO/SiO ₂ : 0.20 g catalyst, 0.47 kPa monoterpene partial pressure, 10 ml min ⁻¹ flow rate, 4 h TOS, WHSV = 0.08 h ⁻¹ .	94
Figure 4.8.	Plot of terpinolene conversion and p-cymene selectivity over 30%ZnO/SiO ₂ versus contact time at 325 °C and 0.47 kPa terpinolene partial pressure; the contact time varied by changing the flow rate (5–20 ml min ⁻¹) and catalyst weight (0.2–0.8 g).	95
Figure 5.1.	TGA of Cd(NO ₃) ₂ ·4H ₂ O in air flow, 10 °C min ⁻¹ (1); and TGA of CdO calcined at 500 °C, in H ₂ -N ₂ (5:95) flow, 20 °C min ⁻¹ (2).	100
Figure 5.2.	Powder XRD (CuKα) for bulk CdO (1), 5%CdO/SiO ₂ (2), 10%CdO/SiO ₂ (3), 20%CdO/SiO ₂ (4) and 30%CdO/SiO ₂ (5); all calcined at 400 °C for 2 h, 5 °C min ⁻¹ temperature ramp rate.	101
Figure 5.3.	Nitrogen adsorption and desorption isotherms for 10%CdO/SiO ₂ (a), 20%CdO/SiO ₂ (b) and 30%CdO/SiO ₂ (c) calcined at 400 °C.	102

Figure 5.4.	Pore size distribution for CdO/SiO ₂ catalysts.	103
Figure 5.5.	H ₂ -TPR of 10%CdO/SiO ₂ (40 mg) calcined at 500 °C in H ₂ -N ₂ (5:95) flow (40 ml min ⁻¹), 20 °C min ⁻¹ .	105
Figure 5.6.	DRIFT spectra of adsorbed pyridine (powdered KBr mixtures versus KBr): anhydrous Cd(NO ₃) ₂ calcined at 300 °C (1), Aerosil 300 silica (2), 5% CdO/SiO ₂ (3), and 10% CdO/SiO ₂ (4).	106
Figure 5.7.	TGA of 10% CdO/SiO ₂ (1) and 20% CdO/SiO ₂ (2) under nitrogen, 20 °C min ⁻¹ temperature ramp rate.	107
Figure 5.8.	DRIFT spectra of SiO ₂ (1), 5% CdO/SiO ₂ (2), 10% CdO/SiO ₂ (3), 20% CdO/SiO ₂ (4), and 30% CdO/SiO ₂ (5) calcined at 400 °C in air for 2 h (powdered KBr mixtures versus KBr).	107
Figure 5.9.	Time course for α-pinene dehydroisomerisation over 10% CdO/SiO ₂ calcined at 400 °C: 0.20 g catalyst, 250 °C, 0.48 kPa α-pinene partial pressure, 10 ml min ⁻¹ flow rate, WHSV = 0.08 h ⁻¹ .	109
Figure 5.10.	GC-TCD trace showing H ₂ product evolved in α-pinene dehydroisomerisation at 250 °C and WHSV = 0.08 h ⁻¹ over 10% CdO/SiO ₂ (0.20.g) calcined at 400 °C (Agilent 8860 GC instrument fitted with TCD and 1.5 m packed Molsieve 5A column).	109
Figure 5.11.	α-Pinene conversion (solid circles) and p-cymene selectivity for 10% CdO/SiO ₂ calcined at 400 °C (open squares) and calcined at 500 °C (solid squares) at different contact times (250 °C, 0.48 kPa α-pinene partial pressure, 4 h TOS).	110
Figure 5.12.	Long-term time course (25 h TOS) for α-pinene dehydroisomerisation over 10% CdO/SiO ₂ calcined at 500 °C: 0.60 g catalyst, 250 °C, 0.48 kPa α-pinene partial pressure, 5 ml min ⁻¹ flow rate, WHSV = 0.013 h ⁻¹ .	111
Figure 5.13.	Long-term time course for α-pinene dehydroisomerisation over 20% CdO/SiO ₂ calcined at 400 °C with catalyst regeneration: 0.20 g catalyst, 275 °C, 0.48 kPa α-pinene partial pressure, 10 ml min ⁻¹ flow rate, WHSV = 0.08 h ⁻¹ ; the catalyst regenerated in situ by air flow (10 ml min ⁻¹) at 400 °C for 3 h.	112
Figure 5.14.	Powder XRD (CuKα) for spent 10% CdO/SiO ₂ (1), 20% CdO/SiO ₂ (2), and 30% CdO/SiO ₂ (3) calcined at 400 °C after α-pinene dehydroisomerisation (250 °C, WHSV = 0.08 h ⁻¹ , 4 h TOS). Reflections at 33.0° and 38.3° in 20% and 30% CdO/SiO ₂ are attributed to CdO. No Cd metal phase (JCPDS 03-065-3363) is present.	112

Figure 5.15.	Effect of temperature on α -pinene dehydroisomerisation over 10%CdO/SiO ₂ calcined at 500 °C: 0.20 g catalyst, 0.48 kPa α -pinene partial pressure, 10 ml min ⁻¹ flow rate, WHSV = 0.08 h ⁻¹ .	113
Figure 5.16.	α -Pinene conversion and p-cymene selectivity for 10%CdO/SiO ₂ calcined at 500 °C at different contact times (325 °C, 0.48 kPa α -pinene partial pressure, 4 h TOS); the contact time varied by changing flow rate (5–20 ml min ⁻¹) and catalyst amount (0.2–0.8 g).	114
Figure 5.17.	Time course for β -pinene dehydroisomerisation over 10%CdO/SiO ₂ calcined at 500 °C: 0.20 g catalyst, 375 °C, 0.47 kPa β -pinene partial pressure, 10 ml min ⁻¹ flow rate, WHSV = 0.08 h ⁻¹ .	116
Figure 5.18.	Effect of temperature on β -pinene dehydroisomerisation over 10%CdO/SiO ₂ calcined at 500 °C: 0.20 g catalyst, 0.47 kPa α -pinene partial pressure, 10 ml min ⁻¹ flow rate, WHSV = 0.08 h ⁻¹ .	117
Figure 5.19.	Plot of β -pinene conversion and p-cymene selectivity over 10%CdO/SiO ₂ calcined at 500 °C versus contact time at 375 °C; the contact time varied by changing flow rate (5–20 ml min ⁻¹), catalyst amount (0.2–0.8 g) and β -pinene partial pressure (0.36–0.66 kPa).	118
Figure 5.20.	Effect of temperature on limonene dehydroisomerisation over 20%CdO/SiO ₂ and 30%CdO/SiO ₂ : 0.20 g catalyst, 0.47 kPa limonene partial pressure, 10 ml min ⁻¹ flow rate, 4 h TOS, WHSV = 0.08 h ⁻¹ ; 100% limonene conversion in all cases.	120
Figure 5.21.	Plot of limonene conversion and p-cymene selectivity over 20%CdO/SiO ₂ calcined at 400 °C (0.2–0.8 g) versus contact time at 225 °C and 0.47 kPa limonene partial pressure; the contact time varied by changing the flow rate (5–20 ml min ⁻¹).	121
Figure 5.22.	Plot of limonene conversion and p-cymene selectivity over 20%CdO/SiO ₂ calcined at 400 °C (0.2–0.8 g) versus contact time at 250 °C and 0.47 kPa limonene partial pressure; the contact time varied by changing the flow rate (5–20 ml min ⁻¹).	121
Figure 5.23.	Long-term test for limonene dehydroisomerisation over 20%CdO/SiO ₂ : 0.20 g catalyst, 250 °C, 0.47 kPa limonene partial pressure, 10 ml min ⁻¹ flow rate, WHSV = 0.08 h ⁻¹ .	122
Figure 5.24.	Time course for α -terpinene dehydroisomerisation over 20%CdO/SiO ₂ calcined at 400 °C: 0.20 g catalyst, 250 °C, 0.47 kPa α -terpinene partial pressure, 10 ml min ⁻¹ flow rate, WHSV = 0.08 h ⁻¹ .	123

- Figure 5.25.** Time course for γ -terpinene dehydroisomerisation over 20%CdO/SiO₂ 124
calcined at 400 °C: 0.20 g catalyst, 250 °C, 0.47 kPa γ -terpinene partial
pressure, 10 ml min⁻¹ flow rate, WHSV = 0.08 h⁻¹.
- Figure 5.26.** Time course for terpinolene dehydroisomerisation over 20%CdO/SiO₂ 124
calcined at 400 °C: 0.20 g catalyst, 250 °C, 0.47 kPa terpinolene partial
pressure, 10 ml min⁻¹ flow rate, WHSV = 0.08 h⁻¹.
- Figure 5.27.** Effect of temperature on p-cymene yield in monoterpene 125
dehydroisomerisation over 20%CdO/SiO₂ calcined at 400 °C: 0.20 g
catalyst, 0.47 kPa monoterpene partial pressure, 10 ml min⁻¹ flow rate,
4 h TOS, WHSV = 0.08 h⁻¹.
- Figure 5.28.** Plot of terpinolene conversion and p-cymene selectivity over 126
20%CdO/SiO₂ calcined at 400 °C versus contact time at 250 °C and 0.47
kPa terpinolene partial pressure; the contact time varied by changing the
flow rate (5–20 ml min⁻¹) and catalyst weight (0.2–0.8 g).

List of tables

Table 1.1.	Examples of metal oxide catalysts and their applications.	3
Table 1.2.	Properties of p-cymene.	14
Table 1.3.	Chemical structure of some monoterpene compounds.	17
Table 2.1.	The mass of reagents used for the preparation of ZnO/SiO ₂ catalysts.	37
Table 2.2.	The mass of reagents used for the preparation of CdO/SiO ₂ catalysts.	37
Table 2.3.	ICP-OES analysis of ZnO/SiO ₂ catalysts.	39
Table 2.4.	ICP-OES analysis of CdO based catalysts.	39
Table 2.5.	The calibration data for dehydroisomerisation of α -pinene and limonene.	52
Table 2.6.	Partial vapour pressure of monoterpenes at saturation temperatures used in experiments.	54
Table 3.1.	Information about catalysts.	64
Table 3.2.	Dehydroisomerisation of α -pinene to p-cymene over ZnO/SiO ₂ (300).	74
Table 3.3.	Dehydroisomerisation of α -pinene to p-cymene over ZnO/SiO ₂ : effect of support.	77
Table 3.4.	C and H combustion analysis for 10%ZnO/SiO ₂ used in α -pinene dehydroisomerisation for a specified time on stream (TOS).	77
Table 3.5.	Dehydroisomerisation of limonene to p-cymene over ZnO/SiO ₂ (300).	79
Table 4.1.	Effect of temperature on β -pinene dehydroisomerisation over 10%ZnO/SiO ₂ .	89
Table 4.2.	Dehydroisomerisation of monoterpenes to p-cymene over 30%ZnO/SiO ₂ .	92
Table 5.1.	Information about catalysts.	104
Table 5.2.	Dehydroisomerisation of α -pinene to p-cymene over CdO/SiO ₂ .	108
Table 5.3.	Effect of temperature on β -pinene dehydroisomerisation over 10%CdO/SiO ₂ .	116
Table 5.4.	Dehydroisomerisation of limonene to p-cymene over CdO/SiO ₂ .	119

Table 5.5. Dehydroisomerisation of monoterpenes to p-cymene over 123 20% CdO/SiO₂.

List of schemes

Scheme 1.1.	Friedel-Crafts alkylation of toluene.	16
Scheme 1.2.	The proposed mechanism of dehydroisomerisation of α -pinene to p-cymene.	19
Scheme 1.3.	Dehydroisomerisation of limonene to p-cymene.	22
Scheme 3.1.	Dehydroisomerisation of α -pinene to p-cymene.	62
Scheme 3.2.	Dehydroisomerisation of limonene to p-cymene.	63
Scheme 5.1.	Dehydroisomerisation of β -pinene to p-cymene.	115
Scheme 5.2.	Proposed mechanism of monoterpene dehydrogenation on oxo-metal sites of CdO/SiO ₂ catalyst.	128

Chapter 1. Introduction

1. Background and definitions

Catalysis is a phenomenon known since ancient centuries when Cordus reported a catalytic reaction in 1552 [1]. He used sulfuric acid as an inorganic catalyst to convert alcohol to ether. In 1811, Kirchhoff explored that starch can be converted into gum and raisin sugar over mineral acids [1]. Humphry Davy discovered the first operations of catalysis in the gas phase using platinum and palladium in 1817 [2]. The first utilisation of heterogeneous catalysis was in the middle of the 18th century when Faraday conducted an oxidation reaction using platinum [3].

Berzelius was the first who coined the term catalysis in 1836 [4]. The word catalysis is derived from the Greek word kata, which means down, and lysein, which means loosen. A catalyst is a chemical substance that is required in a small amount to expedite the rate of a chemical reaction without undergoing any chemical change itself [5]. The catalyst provides an alternative path to lower the activation energy of a chemical reaction. Catalysts can be solids, liquids or gases. The process of accelerating a chemical reaction by using a catalyst is called catalysis.

Today, catalysis plays an important role in industrial applications, especially in chemical, pharmaceutical and petrochemical industries, which have an extremely strong economic and environmental influence on the world. Around 90% of industrial chemical processes include one catalytic step or more [6]. Green chemistry [7–9], nanotechnology [10,11], fuels [12,13] and fuel cells [14–18] are the most significant areas of catalytic applications.

Catalysis can be homogeneous or heterogeneous, based on the catalytic system [19]. In homogeneous catalysis, reactants and catalyst are in the same phase, while in heterogeneous catalysis, reactants and catalyst are in different phases [20]. Heterogeneous catalysis has become more attractive, because it has great advantages over homogeneous catalysis. Heterogeneous catalysis allows easy separation of catalyst from reaction medium to make the catalyst recyclable, hence facilitating economic and environmental benefits. In contrast, the most serious disadvantage of homogeneous catalysis is the separation problem which means it is difficult to separate the catalyst from product [21].

Metal oxides are commonly used in heterogeneous catalysis. 30% of chemical process are catalysed by oxides (Figure 1.1). Oxides constitute a large group of active catalytic materials which can be categorised by their behaviour as acidic, basic or amphoteric.

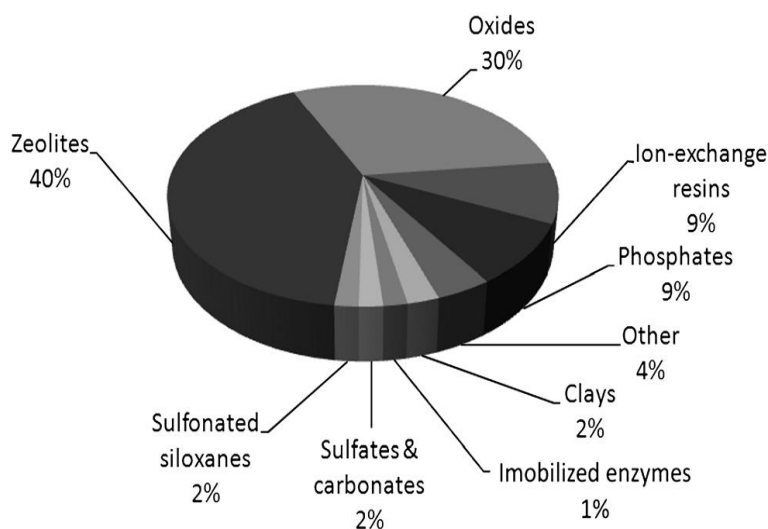


Figure 1.1. Solid catalysts used in the chemical industry [22].

Metal oxides are usually solid materials, and their catalytic properties rely on the interaction between the metal and inherent oxygen. Some examples of metal oxide catalysts and their applications are listed in Table 1.1.

Table 1.1. Examples of metal oxide catalysts and their applications [19].

Catalyst	Catalytic Process
ZnCr ₂ O ₄ , ZnO	Methanol synthesis (high pressure)
ZnFe ₂ O ₄	Oxidative dehydrogenation
Cu _x Zn _{1-x} Cr ₂ O ₄ , CuO	Methanol synthesis (low pressure)
CuCr ₂ O ₄ , CuO	Oxidation, hydrogenation
Cr _x Al _{2-x} O ₃	Light alkane dehydrogenation

1.1. Heterogeneous catalysis

1.1.1. Key steps of reactions on porous solid catalysts

Figure 1.2 illustrates schematically the reaction steps occurring on the surface of a porous solid catalyst. Seven key steps can be recognised [23–26]:

- 1) External transport of substrate molecules by gas phase diffusion to the outer surface of the catalyst (film diffusion).
- 2) Internal transport of substrate molecules through the pores to active sites on the interior surface of the catalyst (pore diffusion).
- 3) Adsorption of substrate molecules onto the surface (chemisorption).
- 4) Reaction between adsorbed molecules at the surface to form a product (chemical reaction).
- 5) Desorption of product.
- 6) Internal transport of product through the pores to the outer surface of the catalyst.
- 7) External transport of product through the boundary layer to bulk fluid phase.

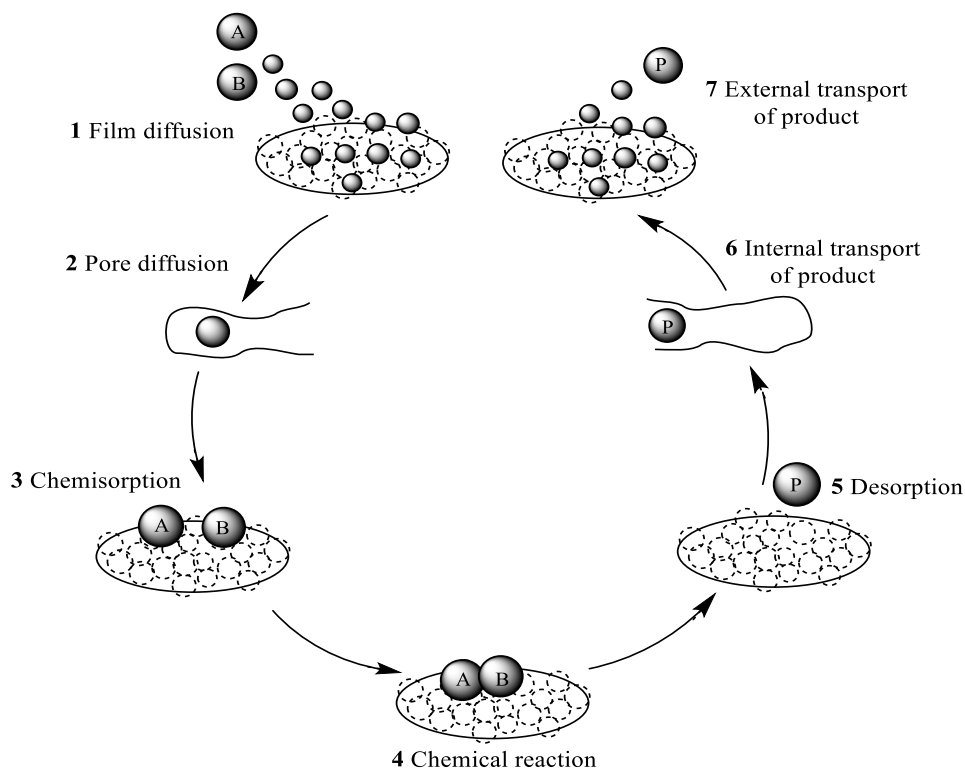


Figure 1.2. Reaction steps on a porous solid catalyst.

1.1.2. Essential properties of catalysts

Chemical reactions occur under specific conditions and the rate at which reactants are converted to products is known as the catalyst activity [5]. Catalyst activity is determined by measuring the rate of reactant consumption or product accumulation. In heterogeneous catalysis, catalyst activity is calculated based on the catalyst weight or catalyst surface area. Turnover frequency (TOF) defined as the number of molecules consumed or produced per unit time per active site is a more rigorous measure of catalyst activity [20].

Catalyst selectivity can be defined as the preference of the catalyst to accelerate the formation of a particular product among all other products that can form in the system. Catalyst selectivity is the choice of the catalytic activity based on the desired output of the reaction in relation to the other activities of the system.

Catalyst lifetime can be defined as the period of time during which the catalyst keeps its activity at an acceptable level. The lifetime of catalysts varies greatly for different reactions. It can last as long as 10 years in the case of synthesis of ammonia over iron and just a few seconds for the catalytic cracking of paraffins over HY zeolite.

1.1.3. Key factors of catalyst development

Several factors should be considered for developing or designing a catalyst to be suitable for use in a particular chemical reaction. These factors involve [25,27]:

- i. *Active phase*. It is important to accomplish maximum catalytic activity. This is usually characterised as the yield of product per unit time.
- ii. *Surface area/porosity*. Moderate surface area of catalyst is required to achieve high yield of the main product and avoid undesired products (e.g. to avoid over-oxidation).
- iii. *Longevity*. Catalyst stability is crucial as the catalyst activity can decline during the chemical reaction. It can be a result of poisoning, deposition of metals, formation of coke, etc..
- iv. *Catalyst shape*. Structural stability is essential for the efficiency of the catalyst.
- v. *Cost*. Using an expensive catalyst is not favoured in commercial reactions as it results in the increased prices of products.
- vi. *Eco-friendliness*. Climate-friendly and non-polluting catalysts are ideal for reducing the toxic by-product levels.

1.1.4. Active sites

The concept of active sites is fundamental to heterogeneous catalysis. It was first introduced in 1925 by Taylor (defects, 1930s) and developed by Balandin and Kohozev (ensembles, 1940s) [28].

Taylor proposed that only small proportion of active sites, which can be formed of an atom or a group of atoms located at the surface defects such as edges and corners of catalyst particles, is catalytically active. Taylor claimed that the structure of solid surfaces is exceptionally complex, irregular on the atomic scale, with heterogeneity of flaws and imperfections. These defects and imperfections exhibit atoms with low coordination that are capable of bonding reactant molecules and thereby able to act as active sites [29]. This notion suggests that numerous catalytic surfaces are not consistently active but show activity only at the sites that are distinguished by a particular positioning or a certain chemical formation of the surface atoms [28–31]. Nevertheless, the exact nature of active sites and the mechanism of how they act remains a matter of debate.

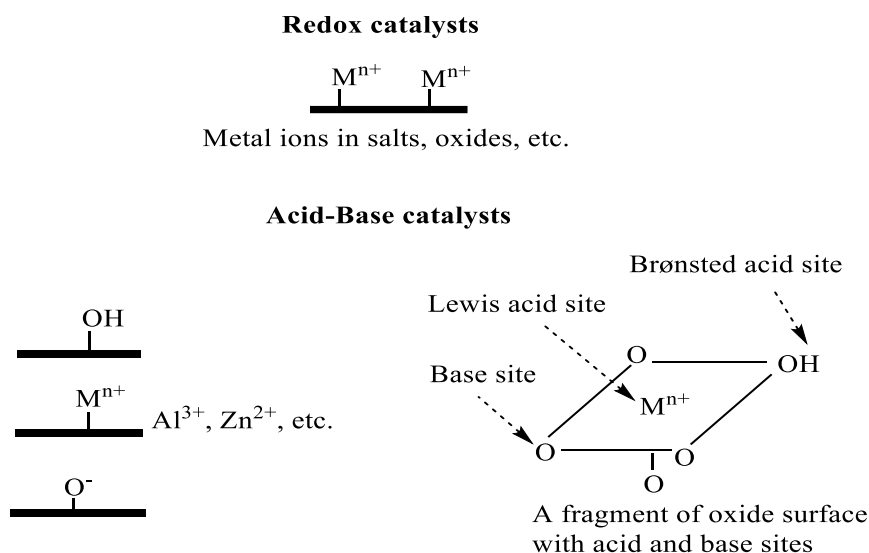


Figure 1.3. The active sites of redox and acid-base catalysts [32].

1.1.5. Classification of catalysts

Catalytic processes occur through chemical interaction between reactants and the catalyst, without chemical change of the nature of the catalyst [33]. Consequently, the catalysts, both homogeneous and heterogeneous, are classified according to reactions they catalyse: (i) redox catalysts, (ii) acid-base catalysts and (iii) multifunctional catalysts.

Transition metals such as Fe, Ni, Pd, Pt and Ag are used as redox catalysts because they have metal active sites on their surface. For example, they catalyse transformation of hydrogen or hydrocarbons, and can be used for hydrogenation, dehydrogenation and hydrogenolysis. Meanwhile, noble metals such as Pd, Pt and Ag can be used for oxidation reactions, because they are resistant to oxidation by oxygen.

Solid acids and bases such as zeolites, ZnO, H₃PO₄/SiO₂, MgO, CaO, etc. are used as acid-base catalysts because they have acidic or basic active sites, which can be Brønsted and Lewis acids and bases. These catalysts can be used for cracking, alkylation, hydration and other reactions. The interaction between these catalysts and reactants occurs according to an acid-base mechanism [32].

Catalysts which possess more than one catalytic function such as redox and acid-base functions are called multifunctional catalysts. For example, Cu/SiO₂ has been used for the dehydrogenation of methanol [34]; this reaction involves decomposition of methanol into CO and H₂ on the metal active sites, and dehydration of methanol on the acid sites of the catalyst. Pt supported on HZSM-5 zeolite is another example of bifunctional metal-acid catalyst which is used for the isomerisation of alkanes in industry [32,33].

1.1.6. Multifunctional catalysis for tandem reactions

Particular attention has been paid to the development of tandem processes using multifunctional catalysis. This can offer environmentally friendly technologies with high selectivity for desirable products and high reactant conversion. Multifunctional catalysts possess two or more different active sites (metal, acid, base, etc.) that can act simultaneously in one step (one-pot, tandem) chemical reaction to produce desired products without intermediate isolation steps [35,36].

Figure 1.4 illustrates a step-by-step reaction in which product D is obtained from reactant A through the formation of two intermediate compounds B and C via three consecutive steps. These intermediates should be isolated and purified, after each step, with a large quantity of waste formed (solid arrows), which makes the operation costly and time consuming. These disadvantages can be overcome by using a tandem process with a multifunctional catalyst (dotted arrow) [37].

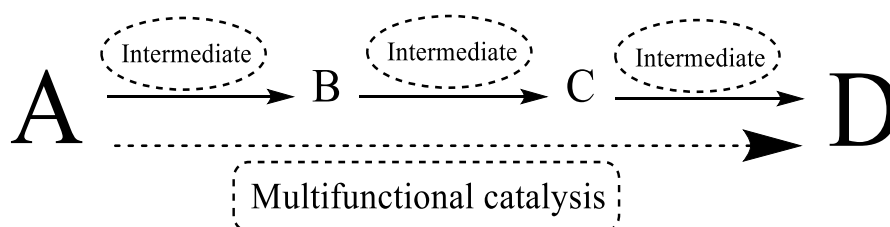


Figure 1.4. Traditional step-by-step reaction versus tandem process.

Utilisation of one-pot reactions to produce the final products without intermediate isolation is an attractive alternative to traditional multistep organic synthesis. Multifunctional catalysts have been widely utilised in the production of organic compounds by tandem processes. In most common cases, these catalysts contain one or two transition metals on an acidic and/or basic support, for example, Pt/HZSM-5 [32]. The major issue in their utilisation

is that these active sites must be precisely tuned to suit the reaction system and work simultaneously [38].

1.2. Catalysis by ZnO

Zinc oxide (ZnO), with its unique physical and chemical properties, is an attractive bifunctional catalyst. ZnO has been used as the catalyst in many reactions including CO hydrogenation to methanol [39,40], hydrogen production [41–44], isomerisation of butene [45], dehydrogenation of ethanol to acetaldehyde [46], dehydrocyclisation of ethylenediamine with propylene glycol to 2-methylpyrazine [47], transformation of glycerol to glycerol carbonate [48], biomass valorisation, biodiesel production [49] and many other reactions.

1.2.1. Preparation of ZnO catalysts

Zinc oxide can be prepared utilising various methods, for example, by precipitation of zinc hydroxide using zinc nitrate as a starting material [50–54]. Thus, Bayahia and co-workers [55] prepared ZnO by adding drop-wise 10% aqueous ammonia into a stirred solution of zinc nitrate at 70 °C until pH 7.0 was reached. After filtration, the precipitate was washed with distilled water to be freed from ammonia and air dried overnight at 110 °C. Then, the product was calcined under N₂ atmosphere for 5 h at 300 °C and finally ground to 45 µm particle size. The preparation of the silica-supported Zn oxide catalyst was performed via impregnation of zinc nitrate onto Aerosil 300 from an aqueous solution. Then water was rotatory evaporated followed by oven drying overnight at 110 °C. Finally, the solid was calcined in air at 400 °C for 2 h to achieve the decomposition of zinc nitrate to zinc oxide.

10% ZnO/SiO₂ catalyst has been prepared through the dissolution of Zn(NO₃)₂·6H₂O in distilled water and adjusting the pH to 11.0 by adding 10% aqueous NH₃. Then, SiO₂ with variant surface areas (60–700 m² g⁻¹) was added. After stirring for 2 h, the mixture was dried under reduced pressure at 80 °C overnight. Finally, the powder was calcined at 250 °C for 2 h to produce 10% ZnO/SiO₂ [46]. Cu-ZnO/SiO₂ bimetal catalyst was also prepared by co-impregnation method using nitrates as a source of oxides and using aqueous ammonia to control pH [46].

Krisnandi *et al.* [48] applied direct precipitation technique to prepare ZnO/SiO₂ catalyst using zinc sulfate and Aerosil 300 silica support. Typically, ZnSO₄ was dissolved in distilled water with continuous stirring. Simultaneously, K₂C₂O₄ was dissolved separately in distilled water. The solutions of potassium oxalate and zinc sulphate were mixed under constant stirring for 30 min. Then, the mixture was left to stand until the white precipitate of ZnC₂O₄ was formed. The product was filtered, washed with distilled water, dried at 100 °C and calcined at 400 °C to afford ZnO as a white powder. The preparation of ZnO/SiO₂ catalyst was carried out using a similar technique. Before adding the solution of potassium oxalate, Aerosil 300 silica was added to the vigorously stirred ZnSO₄ solution at 60 °C for 30 min. Then K₂C₂O₄ was added and the preparation procedure was continued as above.

1.2.2. Properties of ZnO

The texture of ZnO catalysts has been the subject of several studies [45–48]. Krisnandi *et al.* [48] have reported the surface area and porosity of ZnO/SiO₂ catalysts with different ZnO loadings. The dispersion of ZnO on the silica surface has been analysed by STEM.

The composition of ZnO catalysts has been investigated by many researchers [56–59]. In these catalysts, ZnO can be either amorphous or crystalline as shown by X-ray diffraction.

Sumiyoshi *et al.* [45] observed that if the content of ZnO was less than 30% in mixed oxide catalysts with air calcination at 500 °C, the catalysts were amorphous. The crystalline pattern of ZnO occurred in the samples with ZnO content over 50%. Also, Miyake *et al.* [46] reported that XRD diffraction peaks of ZnO were seen only when ZnO loading was higher than 30%. They suggested that ZnO finely dispersed when the loading was < 20%.

The composition of Zn-Cr mixed oxide was examined by Bayahia *et al.* [55]. They found that Zn-rich catalysts had crystalline structure, whereas Cr-rich catalysts were amorphous. They also found that the surface area of crystalline material was lower than that of amorphous material.

Furthermore, the particles of ZnO have a wurtzite crystal structure similar to the pattern observed in nanosized ZnO powder [59]. The diffraction peaks reported were ascribed to the hexagonal-phase ZnO [60]. The ZnO peaks intensity first reduced with an increase in the silica support amount starting from 30% to 50% followed by a slight increase at 60% SiO₂ [48].

The thermal behaviour of the amorphous and crystalline ZnO and Zn-Cr oxides has been characterised by the thermal gravimetric analysis. The TGA of Zn(NO₃)₂ hydrate gives three main stages of weight loss in the temperature range of 25–1000 °C. The weight loss in the first stage from room temperature to ~110 °C refers to the removal of physisorbed water from the external surface of catalyst [61], while the second stage between 110 and 270 °C is due to the removal of water resulting from hydroxyl groups. The weight loss at third stage >270 °C can be attributed to the decomposition of zinc nitrate to ZnO [62]. Kozhevnikova *et al.* [52] reported that ZnO and Zn-Cr oxides have different water content. Amorphous oxide calcined at 300 °C, contains 8.3 wt% water, whereas crystalline oxide calcined at 350 °C only 2.0 wt%.

The nature of acidity in solid catalysts can be identified by the infrared spectra of adsorbed pyridine in the IR range of 1410–1590 cm⁻¹. Sumiyoshi *et al.* [45] determined the

nature of active sites in ZnO/SiO₂. They found that the catalyst showed a band at 1450 cm⁻¹ characteristic of Lewis acid sites and no bands were detected at 1540 cm⁻¹ characteristic of Brønsted acid sites. Therefore, the ZnO/SiO₂ catalyst has predominantly Lewis acidity. The type of acid sites of ZnO and Cr₂O₃ catalysts has also been characterised [55]. It was observed that these catalysts showed Lewis acid sites, as indicated by a strong adsorption band at 1450 cm⁻¹. Only the Zn-Cr oxide with the highest chromium content Cr/Zn = 10:1, showed the presence of Brønsted acid sites, which was indicated by an adsorption band at 1540 cm⁻¹.

1.3. Catalysis by CdO

Cadmium oxide (CdO) is known as a multifunctional catalyst. It has been reported as a Lewis acid-base and dehydrogenation catalyst, for example, for condensation of aldehydes [63], dehydration of ethanol [64,65] and dehydrogenation of ethylbenzene and cycloalkanes [66].

1.3.1. Preparation of CdO catalysts

The common preparation method of cadmium oxide is through precipitation using ammonia or sodium hydroxide. For example, CdO has been prepared by adding 15% aqueous ammonia into a stirred solution of cadmium nitrate at room temperature. The precipitate of hydroxide was washed with distilled water to be freed from nitrate and ammonia and dried at 110 °C overnight. Then, the Cd(OH)₂ was calcined at 300 °C under a stream of CO₂-free air. Finally, the product was crushed into 0.5–1 mm particle size [67].

CdO has also been prepared by adding potassium hydroxide (KOH) to a cadmium nitrate solution. The obtained precipitate was washed by distilled water, and then dried in

vacuum desiccator over P_2O_5 . The product was calcined at different temperatures from 150 to 500 °C for 5 h [64,68].

Dahi-Azar *et al.* [63] have applied the precipitation method to prepare CdO using cadmium nitrate and sodium hydroxide. 2 M NaOH was added to a stirred $Cd(NO_3)_2$ aqueous solution for 20 min. The produced white precipitate of $Cd(OH)_2$ was centrifuged and then dried at 70 °C in a vacuum oven for 5 h. The solid was calcined for 2 h at 400 °C to finally afford a brown powder of CdO.

1.3.2. The properties of CdO

The phase composition of CdO has been investigated using XRD analysis [64,65,67–70]. X-ray diffraction patterns for CdO prepared at various calcination temperatures (150–500 °C) have been reported [64]. The crystal phase of CdO was observed for the samples prepared at calcination temperatures above 300 °C. X-ray diffraction showed that CdO had a cubic crystal structure with XRD pattern similar to the pattern of CdO nanoparticles [63,70].

The texture of CdO catalysts has been characterised using nitrogen adsorption at 77 K. Nitrogen adsorption/desorption isotherms of CdO exhibit a type IV isotherm with a H1 hysteresis loop, which is typical of mesoporous materials [71]. Macroporosity was also observed at higher relative pressure, and this result was confirmed by SEM and TEM studies [69].

Thermal gravimetric analysis has been reported for the precursor $Cd(NO_3)_2 \cdot 4H_2O$ under helium atmosphere in the temperature range of 25–500 °C [72]. The TGA trace presented three main weight losses. The first step between 50 and 110 °C was attributed to the loss of two water molecules from $Cd(NO_3)_2 \cdot 4H_2O$. In the second step, anhydrous cadmium nitrate was formed

by the loss of another two H₂O molecules at 250 °C. The third step from 250 to 500 °C gave the large weight loss due to Cd(NO₃)₂ decomposition to form CdO as the final product [73].

1.4. p-Cymene

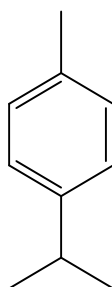


Figure 1.5. Chemical structure of p-cymene.

p-Cymene (Figure 1.5) is one of the most important monocyclic monoterpene compounds, which is also known as 4-isopropyltoluene, 1-isopropyl-4-methylbenzene or 1-methyl-4-isopropylbenzene. It has two isomers: m-cymene (meta-substituted alkyl groups) and o-cymene (ortho-substituted alkyl groups) [74]. p-Cymene naturally occurs in the essential oils of over 100 plants and can be found in more than 200 foods. It is also present in several species of herbs [75]. Some physicochemical properties of p-cymene are given in Table 1.2.

Table 1.2. Properties of p-cymene [76].

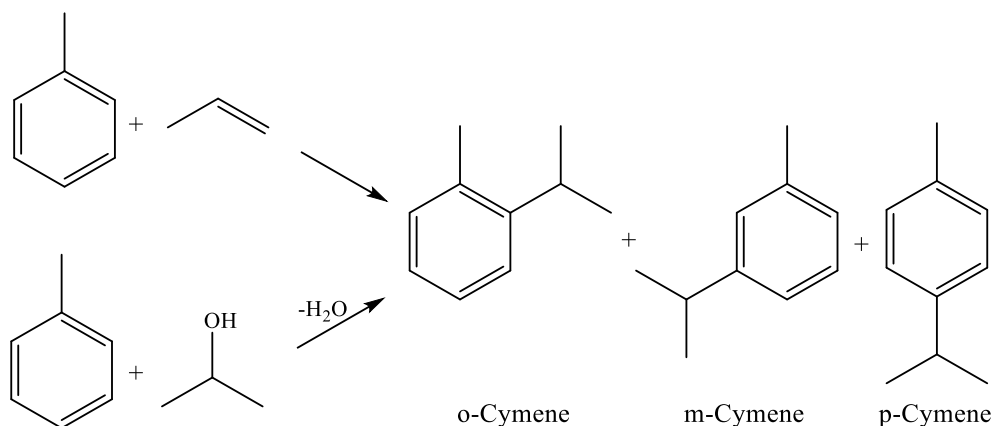
Property	Value
Chemical formula	C ₁₀ H ₁₄
Molecular mass	134.22 g/mol
Vapour pressure	1.46 mm Hg at 25 °C
Boiling point	177.1 °C
Water solubility	23.4 mg/L at 25 °C
Density	0.855 g/mL at 25 °C

p-Cymene is a valuable product in the organic chemical industry. Important industrial applications of p-cymene include its use as a solvent for dyes and varnishes, and in inks and adhesives, and also as an additive in flavours and fragrances [77]. Furthermore, it is used as a starting material for the synthesis of p-cresol. p-Cresol is an important intermediate for the synthesis of antioxidants. p-Cresol is converted into 2,6-di-tert-butyl-p-cresol which is a widely used antioxidant [78]. Moreover, p-cymene can be used in the synthesis of terephthalic acid. Terephthalic acid is used as a monomer for polycondensation. The production of terephthalic acid occurs via the oxidation of p-cymene using a Mn-Fe mixed oxide heterogeneous catalyst [79]. Finally, p-cymene is widely used in the synthesis of non-nitrated musks. The synthesis of non-nitrated musks from p-cymene is a more preferable method than the methods of synthesis of nitrated musks which contain high amounts of toxic nitroaromatic compounds [80–82]. Overall, due to the diversity of applications of p-cymene, it is desirable to produce it in a high yield using a sustainable catalytic process from a renewable feedstock such as α -pinene and limonene.

1.4.1. The synthesis of p-cymene

1.4.1.1. Friedel-Crafts alkylation

Friedel-Crafts alkylation of toluene with propene or 2-propanol catalysed by Lewis acids, such as AlCl₃, BF₃, etc., is the conventional industrial method to produce p-cymene (Scheme 1.1) [79,83,84]. This method produces mixtures of cymene isomers which requires further separation of p-cymene.



Scheme 1.1. Friedel-Crafts alkylation of toluene.

Although this is the leading method of p-cymene synthesis today, it causes a serious environmental and sustainability concerns. This is because of the use of corrosive and toxic Lewis acid catalysts in stoichiometric quantities. Furthermore, these reactions are carried out in liquid phase and produce large amounts of waste, which increases costs for waste disposal and also causes pollution [76].

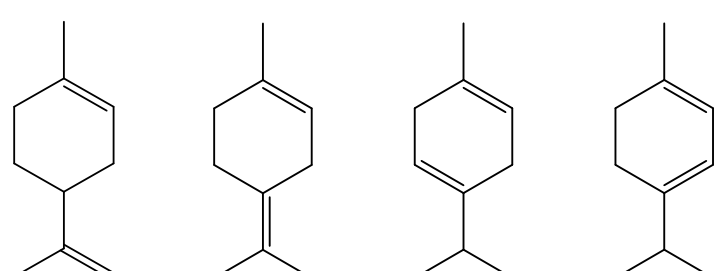
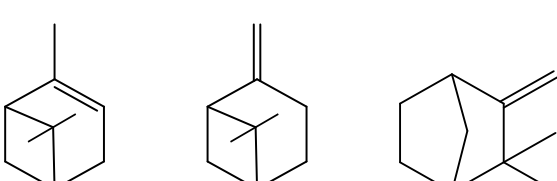
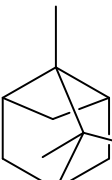
Due to the diminishing amounts of petroleum-based resources and the environmental concerns surrounding the Friedel-Crafts alkylation, this method of synthesising p-cymene is not sustainable in a long-term perspective. Additionally, this method produces mixtures of cymene isomers which must then undergo further separation. For this reason, research has been directed towards the selective synthesis of p-cymene from renewable feedstocks such as biomass using solid acid catalysts in the gas phase.

1.4.1.2. Synthesis from terpenes

Turpentine is a term used to describe a mixture of C₁₀H₁₆ monoterpene isomers [84], including monocyclic compounds such as limonene and terpinolene, bicyclics such as α- and

β -pinenes, 3-carene and camphene, and tricyclics such as tricyclene (Table 1.3) [85]. Terpenes represent a type of renewable materials which are naturally occurring and widely found in essential oils [86]. Terpenes are more desirable as starting materials in organic synthesis than crude oil derivatives, like benzene or toluene, for reasons that were discussed above. They are considered as a cheap feedstock and they exhibit high reactivity in various chemical reactions such as isomerisation, dehydroisomerisation, oxidation, hydration, hydrogenation, etc.. In this section, dehydroisomerisation of limonene and α -pinene to p-cymene will be discussed in more detail because of its relevance to our work.

Table 1.3. Chemical structure of some monoterpene compounds [87].

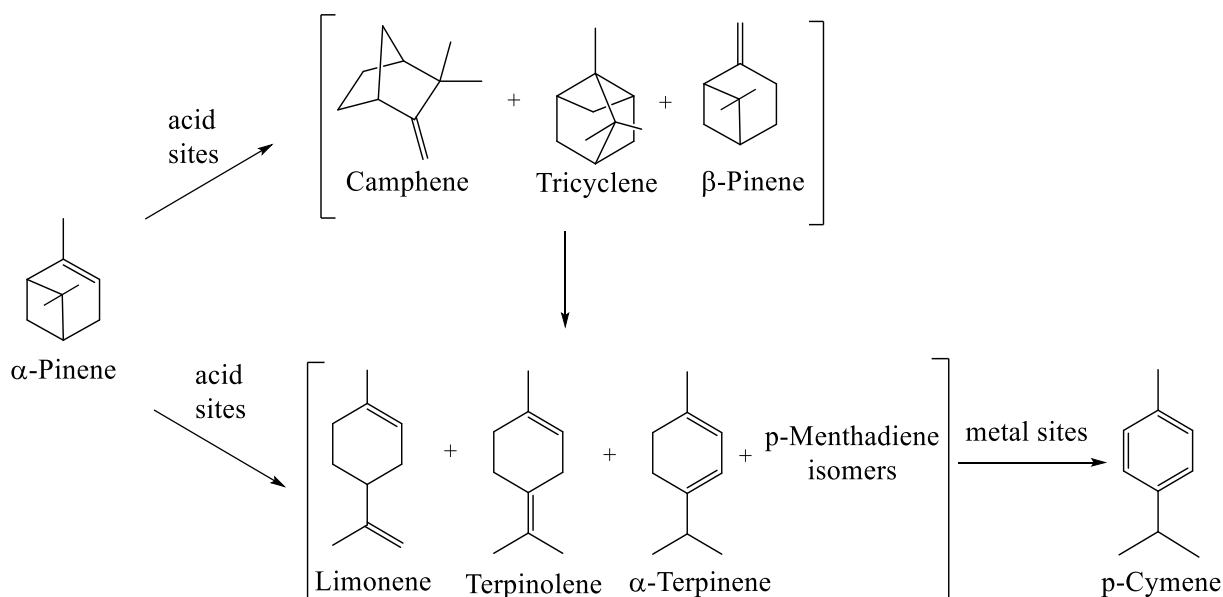
Compound	Structure
Monocyclic	 <p>Four monocyclic monoterpene structures are shown in a row. From left to right: Limonene (a cyclohexane ring with a double bond and an isopropenyl group), Terpinolene (a cyclohexane ring with a double bond and an isopropenyl group in a different orientation), γ-Terpinene (a cyclohexane ring with a double bond and an isopropenyl group), and α-Terpinene (a cyclohexane ring with a double bond and an isopropenyl group).</p> <p>Limonene Terpinolene γ-Terpinene α-Terpinene</p>
Bicyclic	 <p>Three bicyclic monoterpene structures are shown in a row. From left to right: α-Pinene (a bicyclic structure with a double bond), β-Pinene (a bicyclic structure with a double bond), and Camphene (a bicyclic structure with a double bond).</p> <p>α-Pinene β-Pinene Camphene</p>
Tricyclic	 <p>A tricyclic monoterpene structure is shown, consisting of three fused cyclohexane rings.</p> <p>Tricyclene</p>

1.4.1.2.1. Pinene as renewable feedstock for p-cymene synthesis

α -Pinene and β -pinene are bicyclic terpenes that are the main components of wood turpentine. α -Pinene (2,6,6-trimethyl bicyclo[3.1.1]hept-2-ene) is a colourless liquid, which exists in at least 400 essential oils. The largest resource of α -pinene is biomass. It is naturally present in Italian rosemary, wild thyme, French lavender, coriander, cumin, labdanum, neroli, lemon and Litsea cubeba, and it is also found in high concentration in coniferous trees [88]. α -Pinene represents about 60–65% and β -pinene 25–35% of by-products of pulp and paper industry which are commonly known as crude sulfate turpentine (CST) [89,90]. α -Pinene and β -pinene can be directly extracted from these sources or obtained by distillation of turpentine [90]. The purity of turpentine is highly dependent on the type of pulping process applied. The alkaline sulfate pulping process produces around 2–16 kg/ton of turpentine by condensing crude terpentine, while the acidic sulfate process produces approximately 0.3 kg/ton of turpentine by skimming crude terpentine. About 0.3 kg/ton of very pure turpentine is produced by steam distillation [87]. Overall, the low cost and abundance of α - and β -pinene in nature makes the synthesis of value-added chemicals from α - and β -pinene a more desired route in organic synthesis.

1.4.1.2.2. Dehydroisomerisation of α - and β -pinene to p-cymene

The transformation of α - and β -pinene to p-cymene in the presence of acid catalyst is a promising route to p-cymene synthesis. Dehydroisomerisation of α -pinene to p-cymene occurs via a bifunctional catalysis mechanism as proposed by Roberge *et al.* [91]. It involves α -pinene isomerisation on acid sites of the catalyst by two parallel pathways: one pathway leading to bicyclic and tricyclic products such as camphene, tricyclene and β -pinene, and the other to monocyclic products such as limonene and p-menthadienic products. This is followed by p-menthadiene dehydrogenation on metal or oxo-metal sites to produce p-cymene (Scheme 1.2).



Scheme 1.2. The proposed mechanism of dehydroisomerisation of α -pinene to *p*-cymene.

Several studies have been reported on *p*-cymene synthesis from α -pinene using bifunctional catalysts in a gas-phase process [53,79,92,93]. The principal purpose of these studies has been to discover active catalysts with optimal acid strength that are selective towards *p*-cymene and stable for a long time.

Crude sulfate turpentine (CST) containing α -pinene (65 wt.%) and β -pinene (25 wt.%) was used for *p*-cymene production in high yield in the presence of supported Pd catalysts [91]. Roberge and co-workers [91] prepared Pd supported on various high surface area materials and tested in the conversion of CST to *p*-cymene. The catalyst supports used included: H-ZSM-5 zeolite (strong acid), silica D-11-10, γ -alumina D-10-10 (moderate acids), and activated carbon (weak acid). The reaction was carried out in the gas phase at 300 °C using H_2 as a carrier gas. It was observed that the reaction was affected by catalyst acidity. The highest *p*-cymene yield (67%) was obtained over Pd/D-10-10 and Pd/D-11-10. In the case of zeolite, light cracking hydrocarbons and heavy oligomer products were formed in high yield. On the other hand, the

rate of hydrogenation and saturation of bicyclic pinenes increased when using the weakly acidic Pd/C catalyst. Also, the deactivation of catalyst by sulfur present in CST was observed.

Ajaikumar *et al.* [92] studied the effect of different preparation methods of bimetallic AuNi-TiO₂/SBA-15 catalysts in the dehydroisomerisation of α -pinene under H₂ pressure. The preparation methods applied were: (i) deposition-precipitation (DP), (ii) impregnation (IM), and (iii) physical mixing (PM). The optimal reaction conditions were: 0.25 g catalyst amount, 1.8 mL h⁻¹ α -pinene feeding, 10 mL min⁻¹ H₂ flow rate at 300 °C for 6 h time on stream (TOS). The maximum selectivity of 54% for p-cymene was obtained over AuNi-TiO₂/SBA-15 (DP), while the catalysts prepared by IM and PM methods gave 20% and 31% p-cymene, respectively. This was explained in terms of interaction between metal and support.

Golets *et al.* [78] studied Pd-Zn bimetallic catalysts with various Pd/Zn ratios with different loadings on Al-SBA-15 supports in α -pinene dehydroisomerisation. Pd-Zn/Al-SBA-15 (1:1) (5 wt%) was the most promising catalyst which yielded 77% of p-cymene with 100% α -pinene conversion at 300 °C under H₂ atmosphere after 30 min TOS. This catalyst, however, suffered from deactivation, and p-cymene yield was 67% after 5 h TOS. The catalyst was regenerated under air at 500 °C and reused with the loss of selectivity but the conversion remained unchanged.

Al-Wadaani *et al.* [53] reported a new noble-metal-free catalyst based on Zn-Cr mixed oxides for the dehydroisomerisation of α -pinene to p-cymene. A series of Zn-Cr oxide were prepared with various Zn/Cr atomic ratios by co-precipitation and characterised by BET, XRD, TGA and DRIFT spectroscopy of adsorbed pyridine. FTIR of adsorbed pyridine showed that most of Zn-Cr mixed oxides had Lewis acid sites, while Zn-Cr with a high Cr content (Cr/Zn = 10:1) had also Brønsted acid sites. The reaction was carried out in a fixed bed reactor at 350 °C using N₂ as a carrier gas and 0.3 g of catalyst for 2 h TOS. The results showed that Zn-Cr

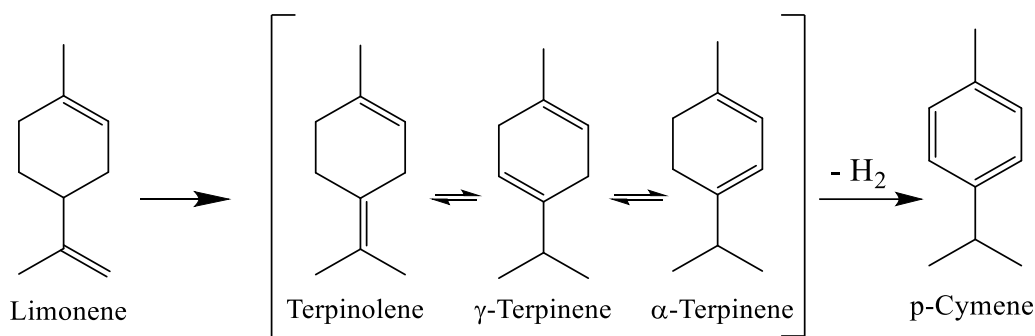
(1:1) catalyst had strong Lewis acid sites and weak Brønsted acidity, which was favourable for its activity and selectivity. Zn-Cr (1:1) provided 100% α -pinene conversion and 78% p-cymene selectivity and showed stable performance without H₂ supply.

1.4.1.2.3. Limonene as renewable feedstock for p-cymene synthesis

Limonene and related terpenes, such as terpinolene, α - and γ -terpinene, are widely available feedstocks. Limonene (4-isopropenyl-1-methylcyclohexene) is one of the most common monoterpene molecules that can be converted to p-cymene. The main source of limonene is orange peels, which are industrial waste from citrus juice process. Globally, the waste of juice production reaches 7 million tons per year [93,94]. As limonene is easily available from inexpensive sources like the waste of the juice industry, it makes limonene an attractive substrate for the synthesis of valuable products such as 1,2-epoxylimonene [95], α - and γ -terpinene, terpinolene, and p-cymene [86,96].

1.4.1.2.4. Dehydroisomerisation of limonene to p-cymene

Dehydroisomerisation of limonene to p-cymene occurs via isomerisation of limonene to terpinenes and terpinolenes followed by their dehydrogenation to p-cymene (Scheme 1.3) as suggested by Wroblewska *et al.* [96]. This transformation requires a dual functional catalyst, namely acid sites for the isomerisation step, while metallic sites are required for the dehydrogenation step. The mechanism is proposed that involves limonene double bond protonation to form carbocation intermediate. Secondly, this carbocation rearranges to form p-menthadiene isomers. Finally, the p-menthadienes are dehydrogenated on metal sites of the catalyst to form p-cymene.



Scheme 1.3. Dehydroisomerisation of limonene to p-cymene.

Solid acids such as zeolites and modified clays have been the most investigated catalysts for the dehydroisomerisation of limonene. For example, Hölderich and Weyrich [97] investigated the limonene dehydroisomerisation in the gas phase over unmodified H-ZSM-5 and Pd/Ce modified ZSM-5 zeolite at 250 °C. They observed that the conversion of limonene dropped from 99% to 64% for a period of 16 h over unmodified H-ZSM-5, and selectivity to p-cymene decreased from 18% to 2.5%. However, an increase of the acidity of the zeolite increased the dehydrogenation properties of H-ZSM-5. Therefore, the maximum yield of limonene to p-cymene over a Pd/Ce modified ZSM-5 catalyst was 80% with 98% conversion after 8 h TOS. The catalyst showed deactivation with increasing TOS.

Pd/Ce supported on ZSM-5 zeolite was also tested for p-cymene production from dipentene [98]. The yield of p-cymene increased up to 70% for a period of 8 h at 250 °C using 3.2 g of the catalyst. Whereas, the conversion of dipentene over 2 g of Pd/SiO₂ produced 90% p-cymene yield at 300 °C under H₂ atmosphere, and no catalyst deactivation was observed for 100 h.

Zhao *et al.* [99] investigated the catalytic activity of Pd/HZSM-5 in limonene dehydroisomerisation to p-cymene in the presence of H₂ or N₂ gas in the liquid phase. It was

found that p-cymene selectivity reached 83% under 8 bar N₂ pressure at 260 °C, while p-cymene selectivity decreased to 69% after adding H₂ to the system.

Silica supported Pd and pure silica catalysts were examined on dehydroisomerisation of limonene to p-cymene using hydrogen as a carrier gas [100]. The reaction was carried out in a fixed-bed reactor at the temperature between 200 and 400 °C. In the case of pure silica, the main products were p-menthadiene isomers like α -, γ -terpinene and terpinolene, and the selectivity to p-cymene was 25%. With Pd/SiO₂ catalyst, the selectivity of p-cymene increased to 96% at 300 °C and to 100% at 400 °C. The catalyst showed stable performance for 500 h.

Furthermore, Akgün *et al.* [77] studied the dehydroisomerisation of limonene into p-cymene using Ni/Al₂O₃, Pt/Al₂O₃ and Pd/Al₂O₃ metal catalysts under supercritical alcohol conditions. They found that Ni/Al₂O₃ catalyst did not show any activity on limonene conversion under such conditions. In contrast, Pt/Al₂O₃ showed catalytic activity on limonene transformation at high temperature. Pd/Al₂O₃ was the most active catalyst and achieved 100% limonene conversion and 80% p-cymene selectivity at 8.0 MPa and 300 °C.

Mesoporous materials have been used for the catalytic dehydrogenation of both limonene and dipentene. Kamitsou and co-workers [101] studied dehydroisomerisation of limonene to p-cymene over mesoporous catalysts γ -Al₂O₃, TiO₂, SiO₂, MCM-41. Among these oxides, TiO₂ achieved the best catalytic activity and produced 90% yield of p-cymene at 100% limonene conversion at 300 °C for 6 h TOS under H₂ pressure.

The conversion of dipentene to p-cymene has also been investigated by Du *et al.* [102] over Al and Zn supported on SBA-15 which were prepared by an impregnation method and characterised by X-Ray diffraction, BET, FTIR and other techniques. p-Cymene was obtained as the main product with 87% yield over Zn/SBA-15 at 450 °C. While, cracking products in large amount were found in the dipentene conversion over Al/SBA-15. The conversion of

dipentene over Zn/SBA-15 and Al/SBA-15 was 97% and 92% respectively. The authors suggested that the strong Brønsted acidity of Al/SBA-15 was responsible for high yields of undesired cracking products, whereas a moderate Lewis acidity of Zn/SBA-15 was more favourable for p-cymene formation.

Mesoporous titanium-silicate catalysts, such as Ti-MCM-41, Ti-SBA-15 and Ti-SBA-16, were prepared and tested for p-cymene synthesis from limonene [96,103,104]. The highest p-cymene yield of 56% with 99% of limonene conversion was obtained over Ti-SBA-15 at 160 °C and 23 h TOS in the liquid phase. Under the same reaction conditions, Ti-MCM-41 gave terpinolene as the main product together with a mixture of α -terpinene, γ -terpinene and p-cymene, with 92% limonene conversion.

Other clays modified by mineral acids have been reported for transformation of limonene into p-cymene such as HCl/bentonite, H₂SO₄/mordenite and HCl/mordenite. Fernandes *et al.* [105] evaluated the activity of HCl activated bentonite in the limonene conversion in the liquid phase at 80 °C under atmospheric pressure. It has been found that the selectivity towards p-cymene was very low (15%). To achieve higher selectivity, it is necessary to control the catalyst acid strength.

Makarouni *et al.* [94] and Lycourghiotis *et al.* [106] also studied the catalytic activity of H₂SO₄ and HCl modified mordenite in the liquid phase at 140 °C for 7 h. p-Cymene was the main product found at a yield of 63% and 65% with 58% and 68% limonene conversion, over H₂SO₄/mordenite and HCl/mordenite, respectively.

Recently, supported heteropolyacid (HPA) catalysts have been used to transform limonene into p-cymene under N₂ atmosphere at 250 °C [107]. A series of HPAs such as H₃PW₁₂O₄₀, H₃PMo₁₂O₄₀, and H₄SiW₁₂O₄₀ were supported on amorphous mesoporous silicas (Q-10, SBA-15, KIT-6, and MCM-41). The H₃PMo₁₂O₄₀/Q-10 catalyst gave a 44% limonene

conversion with a 28% p-cymene yield. The low p-cymene yield may be explained by the very strong Brønsted acidity of HPA.

1.5. Objectives and thesis organisation

p-Cymene is a valuable chemical which has numerous applications, including organic synthesis and medicinal and cosmetic products [53,78–80]. The Friedel–Crafts alkylation of toluene with propene using corrosive liquid acids catalysts is an industrial method to produce p-cymene which poses a threat to the safety and environment. To eliminate the problems associated with the conventional Friedel–Crafts alkylation, the search is directed to sustainable, economic and eco-friendly alternative routes by which value-added chemicals such p-cymene can be produced from renewable sources.

In this context, the dehydroisomerisation of biomass-derived renewable feedstocks such as α -pinene and limonene to p-cymene has received much attention. In this study, we aim to investigate the gas phase dehydroisomerisation of α -pinene and limonene over heterogeneous multifunctional catalysts based on zinc and cadmium oxides supported on silica. Our goal is to understand how these catalysts operate and to optimise the reaction conditions for maximising the yield of p-cymene. In addition to α -pinene and limonene, we also aim to test other monoterpenes as starting materials, such as β -pinene, terpinolene, α - and γ -terpinene.

The catalyst comprising ZnO and CdO supported on silica will be prepared by wet impregnation of silica using aqueous solutions of metal nitrates followed by calcination to decompose the metal nitrites to the corresponding oxides.

The oxide catalysts will be characterised using various techniques such as BET (Brunauer-Emmett-Teller), TGA (thermogravimetric analysis), DRIFT (diffuse reflectance infrared Fourier transform) spectroscopy, XRD (powder X-ray diffraction), H₂-TPR

(temperature programmed reduction) and ICP–OES (inductively coupled plasma optical emission spectroscopy).

The catalysts will be tested for their activity and selectivity in terpene-to-p-cymene dehydroisomerisation using a continuous flow fixed-bed reactor with online gas chromatographic analysis of products.

Chapter 1 gives a general introduction to heterogeneous catalysis and reviews recent literature on the dehydroisomerisation of terpenes to p-cymene.

Chapter 2 describes the materials and methods used for the preparation of metal oxides catalysts, along with the techniques that are used for the characterisation of catalysts and gas phase catalyst reaction testing procedure.

Chapter 3 describes the performance of ZnO/SiO₂ catalysts in the dehydroisomerisation of α -pinene and limonene in the gas phase under varied reaction conditions.

Chapter 4 describes the performance of ZnO/SiO₂ catalysts in the dehydroisomerisation of other cyclic monoterpenes (β -pinene, α -terpinene, γ -terpinene and terpinolene) in the gas phase.

Chapter 5 describes the performance of CdO/SiO₂ catalysts on α -pinene, limonene, β -pinene, α -terpinene, γ -terpinene and terpinolene dehydroisomerisation in the gas phase. It also describes the results of the catalyst characterisation in detail.

Chapter 6 provides conclusions and future outlook.

References

- [1] J. Wisniak, The history of catalysis. From the beginning to Nobel prizes, *Educ. Quim.* 21 (2010) 60–69.
- [2] H. Davy, Some new experiments and observations on the combustion of gaseous mixtures, *R. Soc.* 107 (1817) 77–85.
- [3] M. Faraday, Experimental researches in electricity, *R. Soc.* 124 (1834) 77–122.
- [4] J. J. Berzelius, Berzelius and the platinum metals, *Platin. Met. Rev.* 23 (1979) 155–156.
- [5] J. C. Védrine, Fundamentals of heterogeneous catalysis, *Met. Oxides Heterog. Catal.* (2018) 1–41.
- [6] J. C. Védrine, Metal oxides in heterogeneous oxidation catalysis: State of the art and challenges for a more sustainable world, *ChemSusChem* 12 (2019) 577–588.
- [7] P. T. Anastas, M. M. Kirchhoff, T. C. Williamson, Catalysis as a foundational pillar of green chemistry, *Appl. Catal. A Gen.* 221 (2001) 3–13.
- [8] M. Castro-Puyana, M. L. Marina, M. Plaza, Water as green extraction solvent: Principles and reasons for its use, *Curr. Opin. Green Sustain. Chem.* 5 (2017) 31–36.
- [9] R. A. Sheldon, I. Arends and U. Hanefeld, in *Green Chemistry and Catalysis*, Wiley-VCH Verlag GmbH & Co. KGaA, Editon edn., 2007, 1–47.
- [10] H. Liu, C. Song, L. Zhang, J. Zhang, H. Wang, D. P. Wilkinson, A review of anode catalysis in the direct methanol fuel cell, *J. Power Sources* 155 (2006) 95–110.
- [11] A. Santasalo-Aarnio, M. Borghei, I. V. Anoshkin, A. G. Nasibulin, E. I. Kauppinen, V. Ruiz, T. Kallio, Durability of different carbon nanomaterial supports with PtRu catalyst in a direct methanol fuel cell, *Int. J. Hydrogen Energy* 37 (2012) 3415–3424.
- [12] G. Centi, S. Perathoner, Redesign chemical processes to substitute the use of fossil fuels: A viewpoint of the implications on catalysis, *Catal. Today* 387 (2022) 216–223.
- [13] S. Lopatin, A. Elyshev, A. Zagoruiko, Catalytic device for environmentally friendly combustion of liquid fuels on the base of structured glass-fiber catalyst, *Catal. Today* 383 (2022) 259–265.
- [14] H. Zhang, J. Xuan, H. Xu, M. K. H. Leung, D. Y. C. Leung, L. Zhang, H. Wang, L. Wang, Enabling high-concentrated fuel operation of fuel cells with microfluidic principles: A feasibility study, *Appl. Energy* 112 (2013) 1131–1137.
- [15] H. Xu, H. Zhang, H. Wang, D.Y.C. Leung, L. Zhang, J. Cao, K. Jiao, J. Xuan, Counter-flow formic acid microfluidic fuel cell with high fuel utilization exceeding 90%, *Appl. Energy* 160 (2015) 930–936.
- [16] D. D. Ye, B. Zhang, X. Zhu, P. C. Sui, N. Djilali, Q. Liao, Computational modeling of alkaline air-breathing microfluidic fuel cells with an array of cylinder anodes, *J. Power Sources* 288 (2015) 150–159.

- [17] J. W. Lee, E. Kjeang, Chip-embedded thin film current collector for microfluidic fuel cells, *Int. J. Hydrogen Energy* 37 (2012) 9359–9367.
- [18] M. R. Thorson, F. R. Brushett, C. J. Timberg, P. J. A. Kenis, Design rules for electrode arrangement in an air-breathing alkaline direct methanol laminar flow fuel cell, *J. Power Sources* 218 (2012) 28–33.
- [19] H. Knözinger and K. Kochloefl, in *Ullmann's Encyclopedia of Industrial Chemistry*, Wiley-VCH Verlag GmbH & Co. KGaA, Editon edn., 2000.
- [20] V. V. Ranade, S. S. Joshi, *Catalysis and Catalytic Processes, Industrial Catalytic Processes for Fine and Specialty Chemicals*, 2016.
- [21] W. Keim, Multiphase catalysis and its potential in catalytic processes: the story of biphasic homogeneous catalysis, *Green Chem.* 5 (2003) 105–111.
- [22] R. Rinaldi, F. Schüth, Design of solid catalysts for the conversion of biomass, *Energy Environ. Sci.* 2 (2009) 610–626.
- [23] M. Bowker, *The Basis and Applications of Heterogeneous Catalysis*, Oxford University Press Inc., New York, 1998.
- [24] G. Ertl, Elementary steps in heterogeneous catalysis, *Angew. Chem. Int.* 29 (1990) 1219–1227.
- [25] P. Unnikrishnan, D. Srinivas, Heterogeneous catalysis, *Ind. Catal. Process. Fine Spec. Chem.* (2016) 41–111.
- [26] R. Klaewkla, M. Arend, F. Hoelderich, A review of mass transfer controlling the reaction rate in heterogeneous catalytic systems, *Chem. Technol. Heterog. Catal.* 3 (2011) 667–684.
- [27] G. Ertl, H. Knozinger, J. Weitkamp, *Preparation of Solid Catalysts*, Wiley-VCH, Germany, 1999.
- [28] H. S. Taylor, A theory of the catalytic surface, *R. Soc.* 108 (1925) 105–108.
- [29] Y. Pan, X. Shen, L. Yao, A. Bentalib, Z. Peng, Active sites in heterogeneous catalytic reaction on metal and metal oxide: Theory and practice, *Catalysts* 8 (2018) 1–20.
- [30] J. K. Nørskov, F. Abild-Pedersen, F. Studt, T. Bligaard, Density functional theory in surface chemistry and catalysis, *Proc. Natl. Acad. Sci. U. S. A.* 108 (2011) 937–943.
- [31] T. Zambelli, J. Winterlin, J. Trost, G. Ertl, Identification of the "Active Sites" of a Surface-Catalyzed Reaction, *Science* 273 (1996) 1688–1690.
- [32] J. M. Thomas, W. J. Thomas, *Principle and Pracice of Heterogeneous Catalysis*, VCH, Weinheim, 1997.
- [33] G. C. Bond, *Heterogeneous Catalysis: Principles and Applications*, Second ed., Oxford, 1987.

- [34] A. Vedyagin, Y. Kotolevich, P. Tsyru'nikov, E. Khramov, A. Nizovskii, Methanol dehydrogenation over Cu/SiO₂ catalysts, *Int. J. Nanotechnol.* 13 (2016) 185–198.
- [35] J. C. Wasilke, S. J. Obrey, R. T. Baker, G. C. Bazan, Concurrent tandem catalysis, *Chem. Rev.* 105 (2005) 1001–1020.
- [36] F. X. Felpin, E. Fouquet, Heterogeneous multifunctional catalysts for tandem processes: An approach toward sustainability, *ChemSusChem* 1 (2008) 718–724.
- [37] A. Bruggink, R. Schoevaart, T. Kieboom, Concepts of nature in organic synthesis: Cascade catalysis and multistep conversions in concert, *Org. Process Res. Dev.* 7 (2003) 622–640.
- [38] A. Dhakshinamoorthy, H. Garcia, Cascade reactions catalyzed by metal organic frameworks, *ChemSusChem* 7 (2014) 2392–2410.
- [39] Y. Sun, L. Chen, Y. Bao, Y. Zhang, J. Wang, M. Fu, J. Wu, D. Ye, The applications of morphology controlled ZnO in catalysis, *Catalysts* 6 (2016) 1–44.
- [40] S. Schimpf, A. Rittermeier, X. Zhang, Z. A. Li, M. Spasova, M. W. E. van den Berg, M. Farle, Y. Wang, R. A. Fischer, M. Muhler, Stearate-based Cu colloids in methanol synthesis: Structural changes driven by strong metal–support interactions, *ChemCatChem* 2 (2010) 214–222.
- [41] H. Zhang, J. Sun, V. L. Dagle, B. Halevi, A. K. Datye, Y. Wang, Influence of ZnO facets on Pd/ZnO catalysts for methanol steam reforming, *ACS Catal.* 4 (2014) 2379–2386.
- [42] Y. Matsumura, H. Ishibe, High temperature steam reforming of methanol over Cu/ZnO/ZrO₂ catalysts, *Appl. Catal. B Environ.* 91 (2009) 524–532.
- [43] Y. Matsumura, H. Ishibe, Suppression of CO by-production in steam reforming of methanol by addition of zinc oxide to silica-supported copper catalyst, *J. Catal.* 268 (2009) 282–289.
- [44] S. Liu, K. Takahashi, K. Fuchigami, K. Uematsu, Hydrogen production by oxidative methanol reforming on Pd/ZnO: Catalyst deactivation, *Appl. Catal. A Gen.* 299 (2006) 58–65.
- [45] T. Sumiyoshi, K. Tanabe, H. Hattori, Isomerization of butene over ZnO-SiO₂ by ZnO-SiO₂, *Nuevos Sist. Comun. e Inf.* 17 (1975) 65–70.
- [46] M. Ohira, H. Liu, D. He, Y. Hirata, M. Sano, T. Suzuki, T. Miyake, Catalytic performance and reaction pathways of Cu/SiO₂ and ZnO/SiO₂ for dehydrogenation of ethanol to acetaldehyde, *J. Japan Pet. Inst.* 61 (2018) 205–212.
- [47] I. Park, Y. Rhee, J. Lee, Y. Han, J. Jeon, H. Kim, Metal oxide-modified ZnO/SiO₂ catalysts for cyclo-dehydrogenation of ethylenediamine with propyleneglycol to 2-methylpyrazine, *Res. Chem. Intermed.* 29 (2003) 575–587.
- [48] Y. K. Krisnandi, R. Eckelt, H. Atia, ZnO/SiO₂ composite as catalyst for the transformation of glycerol to glycerol carbonate, *Makara J. Sci.* 24 (2020) 40–49.

- [49] F. Liu, Y. Zhang, Controllable growth of “multi-level tower” ZnO for biodiesel production, *Ceram. Int.* 37 (2011) 3193–3202.
- [50] J. J. Bravo-Suárez, R. V. Chaudhari, B. Subramaniam, Design of heterogeneous catalysts for fuels and chemicals processing: An overview, *ACS Symp. Ser.* 1132 (2013) 3–68.
- [51] F. Simard, U. A. Sedran, J. Sepúlveda, N. S. Fígoli, H. I. de Lasa, ZnO-Cr₂O₃ + ZSM-5 catalyst with very low Zn/Cr ratio for the transformation of synthesis gas to hydrocarbons, *Appl. Catal. A Gen.* 125 (1995) 81–98.
- [52] E. F. Kozhevnikova, I. V. Kozhevnikov, One-step synthesis of methyl isobutyl ketone from acetone catalysed by Pd supported on Zn^{II}-Cr^{III} mixed oxide, *J. Catal.* 238 (2006) 286–292.
- [53] F. Al-Wadaani, E. F. Kozhevnikova, I. V. Kozhevnikov, Zn(II)-Cr(III) mixed oxide as efficient bifunctional catalyst for dehydroisomerisation of α -pinene to p-cymene, *Appl. Catal. A Gen.* 363 (2009) 153–156.
- [54] H. Bayahia, E. F. Kozhevnikova, I. V. Kozhevnikov, Ketonisation of carboxylic acids over Zn-Cr oxide in the gas phase, *Appl. Catal. B Environ.* 165 (2015) 253–259.
- [55] V. V. Costa, H. Bayahia, E.F. Kozhevnikova, E. V. Gusevskaya, I. V. Kozhevnikov, Highly active and recyclable metal oxide catalysts for the Prins condensation of biorenewable feedstocks, *ChemCatChem* 6 (2014) 2134–2139.
- [56] N. Liu, Z. Yuan, C. Wang, S. Wang, C. Zhang, S. Wang, The role of CeO₂-ZrO₂ as support in the ZnO-ZnCr₂O₄ catalysts for autothermal reforming of methanol, *Fuel Process. Technol.* 89 (2008) 574–581.
- [57] A. Patil, C. Dighavkar, R. Borse, S. Patil, R. Khadayate, Effect of Cr₂O₃ by doping and dipping on gas sensing characteristic of ZnO thick films, *J. Electron Devices* 15 (2012) 1274–1281.
- [58] S. R. Naidu, A. K. Banerjee, N. C. Ganguli, S. P. Sen, Stoichiometric modifications of ZnO-Cr₂O₃ catalyst system in oxidizing and reducing atmospheres, *J. Res. Inst. Catal. Hokkaido Univ.* 21 (1974) 172–186.
- [59] C. C. Chen, P. Liu, C. H. Lu, Synthesis and characterization of nano-sized ZnO powders by direct precipitation method, *Chem. Eng. J.* 144 (2008) 509–513.
- [60] H. Wang, C. Li, H. Zhao, R. Li, J. Liu, Synthesis, characterization, and electrical conductivity of ZnO with different morphologies, *Powder Technol.* 239 (2013) 266–271.
- [61] M. Del Arco, V. Rives, R. Trujillano, P. Malet, Thermal behaviour of Zn-Cr layered double hydroxides with hydrotalcite-like structures containing carbonate or decavanadate, *J. Mater. Chem.* 6 (1996) 1419–1428.

- [62] R. M. Gabr, M. M. Girgis, A. M. El-Awad, B. M. Abou-Zeid, Effect of spinel (ZnCr_2O_4) formation on the texture, electrical conduction and catalytic behaviour of the $\text{ZnO-Cr}_2\text{O}_3$ system, *Mater. Chem. Phys.* 39 (1994) 53–62.
- [63] S. Dahi-Azar, S. Abdolmohammadi, J. Mokhtari, CdO Nanoparticles: A highly effective catalyst in cyclocondensation reaction of 3,4-methylenedioxyphenol, aromatic aldehydes, and active methylene compounds under ultrasonic irradiation, *J. Nanostructures* 11 (2021) 57–65.
- [64] K. M. Abd El-Salaam, E. A. Hassan, Active surface centres in a heterogeneous CdO catalyst for ethanol decomposition, *Surf. Technol.* 16 (1982) 121–128.
- [65] B. M. Abu-Zied, A. M. El-Awad, The synergism of cadmium on the catalytic activity of Cd–Cr–O system II. Ethanol decomposition, catalysts reducibility, and in situ electrical conductivity measurements, *J. Mol. Catal. A Chem.* 176 (2001) 227–246.
- [66] V. A. Ferapontov, A. A. Balandin, A. A. Tolstopyatova, Catalytic dehydrogenation of ethylbenzene to styrene on cadmium oxide in the presence of water vapor, *Bull. Acad. Sci. USSR, Div. Chem. Sci* 3 (1962) 414–423.
- [67] A. A. Balandin, V. A. Ferapontov, A. A. Tolstopyatova, The activity of cadmium oxide as a catalyst for hydrogen dehydrogenation, *Russ Chem Bull* 10 (1960) 1751–1758.
- [68] R. B. Fahim, K. M. Abd El-salaam, Surface Properties and Hydration of Cadmium Oxide, *J. Catal.* 9 (1967) 63–69.
- [69] B. S. Anandakumar, M. B. Madhusudana Reddy, K. V. Thipperudraiah, M. A. Pasha, G. T. Chandrappa, Combustion-derived CdO nanopowder as a heterogeneous basic catalyst for efficient synthesis of sulfonamides from aromatic amines using p-toluenesulfonyl chloride, *Chem. Pap.* 67 (2013) 135–144.
- [70] M. Tariq, A. K. Qureshi, S. Karim, M. Sirajuddin, N. Abbas, M. Imran, J. H. Shirazi, Synthesis, characterization and fuel parameters analysis of linseed oil biodiesel using cadmium oxide nanoparticles, *Energy* 222 (2021) 1–8.
- [71] H. Yang, Q. Lu, F. Gao, Q. Shi, Y. Yan, F. Zhang, S. Xie, B. Tu, D. Zhao, One-step synthesis of highly ordered mesoporous silica monoliths with metal oxide nanocrystals in their channels, *Adv. Funct. Mater.* 15 (2005) 1377–1384.
- [72] K. T. Wojciechowski, A. Małcki, Mechanism of thermal decomposition of cadmium nitrate $\text{Cd}(\text{NO}_3)_2 \cdot 4\text{H}_2\text{O}$, *Thermochim. Acta* 331 (1999) 73–77.
- [73] K. Kalpanadevi, C. R. Sinduja, R. Manimekalai, Characterisation of zinc oxide and cadmium oxide nanostructures obtained from the low temperature thermal decomposition of inorganic precursors, *ISRN Inorg. Chem.* 2013 (2013) 1–5.
- [74] A. Balahbib, N. El Omari, N. EL Hachlafi, F. Lakhdar, N. El Menyiy, N. Salhi, H. N. Mrabti, S. Bakrim, G. Zengin, A. Bouyahya, Health beneficial and pharmacological properties of p-cymene, *Food Chem. Toxicol.* 153 (2021) 1–16.

- [75] J. D. S. S. Quintans, P. P. Menezes, M. R. V. Santos, L. R. Bonjardim, J. R. G. S. Almeida, D. P. Gelain, A. A. D. S. Araújo, L. J. Quintans, Improvement of p-cymene antinociceptive and anti-inflammatory effects by inclusion in β -cyclodextrin, *Phytomedicine* 20 (2013) 436–440.
- [76] A. Marchese, C. R. Arciola, R. Barbieri, A. S. Silva, S. F. Nabavi, A. J. T. Sokeng, M. Izadi, N. J. Jafari, I. Suntar, M. Daglia, S. M. Nabavi, Update on monoterpenes as antimicrobial agents: A particular focus on p-cymene, *Materials* 10 (2017) 1–15.
- [77] E. Yılmazoğlu, M. Akgün, p-Cymene production from orange peel oil using some metal catalyst in supercritical alcohols, *J. Supercrit. Fluids* 131 (2018) 37–46.
- [78] M. Golets, S. Ajaikumar, M. Mohln, J. Wärnå, S. Rakesh, J. -P. Mikkola, Continuous production of the renewable p-cymene from α -pinene, *J. Catal.* 307 (2013) 305–315.
- [79] Y. Takebayashi, K. Sue, S. Yoda, Y. Hakuta, T. Furuya, Solubility of terephthalic acid in subcritical water, *J. Chem. Eng. Data* 57 (2012) 1810–1816.
- [80] L. Vallecillos, F. Borrull, E. Pocurull, Recent approaches for the determination of synthetic musk fragrances in environmental samples, *Trends Anal. Chem.* 72 (2015) 80–92.
- [81] K. -S. Ju, R. E. Parales, Nitroaromatic compounds, from synthesis to biodegradation, *Microbiol. Mol. Biol. Rev.* 74 (2010) 250–272.
- [82] P. Mäki-Arvela, B. Holmbom, T. Salmi, D. Y. Murzin, Recent progress in synthesis of fine and specialty chemicals from wood and other biomass by heterogeneous catalytic processes, *Catal. Rev. Sci. Eng.* 49 (2007) 197–340.
- [83] S. Barman, S. K. Maity, N. C. Pradhan, Alkylation of toluene with isopropyl alcohol catalyzed by Ce-exchanged NaX zeolite, *Chem. Eng. J.* 114 (2005) 39–45.
- [84] O. Akpolat, G. Gündüz, F. Ozkan, N. Beşün, Isomerization of α -pinene over calcined natural zeolites, *Appl. Catal. A Gen.* 265 (2004) 11–22.
- [85] M. Golets, S. Ajaikumar, J. P. Mikkola, Catalytic upgrading of extractives to chemicals: Monoterpenes to “EXICALS”, *Chem. Rev.* 115 (2015) 3141–3169.
- [86] A. Corma, S. Iborra, A. Vely, Chemical routes for the transformation of biomass into chemicals, *Chem. Rev.* 107 (2007) 2411–2502.
- [87] M. L. Henriksson, *Biotransformations of Turpentine Constituents: Oxygenation and Esterification*, 2003.
- [88] K. A. C. Vespermann, B. N. Paulino, M. C. S. Barcelos, M. G. Pessôa, G. M. Pastore, G. Molina, Biotransformation of α - and β -pinene into flavor compounds, *Appl. Microbiol. Biotechnol.* 101 (2017) 1805–1817.
- [89] R. Rachwalik, M. Hunger, B. Sulikowski, Transformations of monoterpene hydrocarbons on ferrierite type zeolites, *Appl. Catal. A Gen.* 427–428 (2012) 98–105.
- [90] R. G. Berger, *Flavours and Fragrances*, Springer Berlin Heidelberg New York, 2007.

- [91] D. M. Roberge, D. Buhl, J. P. M. Niederer, W. F. Hölderich, Catalytic aspects in the transformation of pinenes to p-cymene, *Appl. Catal. A Gen.* 215 (2001) 111–124.
- [92] S. Ajaikumar, M. Golets, W. Larsson, A. Shchukarev, K. Kordas, A. R. Leino, J. P. Mikkola, Effective dispersion of Au and Au–M (M= Co, Ni, Cu and Zn) bimetallic nanoparticles over TiO₂ grafted SBA-15: Their catalytic activity on dehydroisomerization of α -pinene, *Microporous Mesoporous Mater.* 173 (2013) 99–111.
- [93] G. Rubulotta, E. A. Quadrelli, *Terpenes: A Valuable Family of Compounds for the Production of Fine Chemicals*, 1st ed., Elsevier B.V., 2019.
- [94] D. Makarouni, S. Lycourghiotis, E. Kordouli, K. Bourikas, C. Kordulis, V. Dourtoglou, Transformation of limonene into p-cymene over acid activated natural mordenite utilizing atmospheric oxygen as a green oxidant: A novel mechanism, *Appl. Catal. B Environ.* 224 (2018) 740–750.
- [95] A. Wróblewska, The epoxidation of limonene over the TS-1 and Ti-SBA-15 catalysts, *Molecules* 19 (2014) 19907–19922.
- [96] M. Retajczyk, A. Wróblewska, The isomerization of limonene over the Ti-SBA-15 catalyst: The influence of reaction time, temperature, and catalyst content, *Catalysts* 7 (2017) 1–14.
- [97] P. A. Weyrich, W. F. Hölderich, Dehydrogenation of α -limonene over Ce promoted, zeolite supported Pd catalysts, *Appl. Catal. A Gen.* 158 (1997) 145–162.
- [98] D. Buhl, P. A. Weyrich, W. M. H. Sachtler, W. F. Hölderich, Support effects in the Pd catalyzed dehydrogenation of terpene mixtures to p-cymene, *Appl. Catal. A Gen.* 171 (1998) 1–11.
- [99] H. Cui, J. Zhang, Z. Luo, C. Zhao, Mechanisms into dehydroaromatization of bio-derived limonene to p-cymene over Pd/HZSM-5 in the presence and absence of H₂, *RSC Adv.* 6 (2016) 66695–66704.
- [100] D. Buhl, D. M. Roberge, W. F. Hölderich, Production of p-cymene from α -limonene over silica supported Pd catalysts, *Appl. Catal. A Gen.* 188 (1999) 287–299.
- [101] M. Kamitsou, G. D. Panagiotou, K. S. Triantafyllidis, K. Bourikas, A. Lycourghiotis, C. Kordulis, Transformation of α -limonene into p-cymene over oxide catalysts: A green chemistry approach, *Appl. Catal. A Gen.* 474 (2014) 224–229.
- [102] J. Du, H. Xu, J. Shen, J. Huang, W. Shen, D. Zhao, Catalytic dehydrogenation and cracking of industrial dipentene over M/SBA-15 (M= Al, Zn) catalysts, *Appl. Catal. A Gen.* 296 (2005) 186–193.
- [103] M. Retajczyk, A. Wróblewska, Isomerization and dehydroaromatization of R(+)-limonene over the Ti-MCM-41 Catalyst: Effect of temperature, reaction time and catalyst content on product yield, *Catalysts* 9 (2019) 1–11.

- [104] M. Retajczyk, A. Wróblewska, A. Szymańska, P. Miadlicki, Z. C. Koren, B. Michalkiewicz, Synthesis, characterization, and catalytic applications of the Ti-SBA-16 porous material in the selective and green isomerizations of limonene and S-carvone, *Catalysts* 16 (2020) 1–17.
- [105] C. Fernandes, C. Catrinescu, P. Castilho, P. A. Russo, M. R. Carrott, C. Breen, Catalytic conversion of limonene over acid activated Serra de Dentro (SD) bentonite, *Appl. Catal. A Gen.* 318 (2007) 108–120.
- [106] S. Lycourghiotis, D. Makarouni, E. Kordouli, K. Bourikas, C. Kordulis, V. Dourtoglou, Activation of natural mordenite by various acids: Characterization and evaluation in the transformation of limonene into p-cymene, *Mol. Catal.* 450 (2018) 95–103.
- [107] C. P. Tavera Ruiz, P. Gauthier-Maradei, M. Capron, C. Pirez, O. Gardoll, B. Katryniok, F. Dumeignil, Transformation of dl limonene into aromatic compounds using supported heteropolyacid catalysts, *Catal. Letters* 149 (2019) 328–337.

Chapter 2. Experimental

2. Introduction

This chapter focuses on the experimental methods applied in our investigation of the dehydroisomerisation of monoterpenes to p-cymene. This includes the procedures for the preparation of ZnO/SiO₂ and CdO/SiO₂ catalysts. The characterisation techniques that were used to determine the catalyst properties such as thermal stability, water content, surface area, porosity, crystallinity and acidity will also be described in detail. This chapter will also provide a description of the reactor setup and the catalyst testing procedure.

2.1. Chemicals and solvents

All chemicals and solvents used in the experiments were purchased from Sigma-Aldrich and used as supplied without further purification. These include Zn(NO₃)₂·6H₂O, Cd(NO₃)₂·4H₂O, α-pinene (>98%), β-pinene (99%), limonene (>97%), terpinolene (>85%), α-terpinene (85%) and γ-terpinene (>97%). Aerosil 300 silica support (S_{BET} , 300 m² g⁻¹) was from Degussa. Other silicas with S_{BET} = 200, 600 and 750 m² g⁻¹ were from Grace Catalysts & Carriers. Hydrogen and nitrogen gases were supplied by the British Oxygen Company (BOC) Ltd.

2.2. Catalyst preparation

2.2.1. Preparation of compacted SiO₂

Aerosil 300 silica (5 g, 83.2 mmol) was added to a beaker and wetted in a minimum amount of distilled water (100 mL). The mixture was left to stir overnight at room temperature. After stirring, water was removed using a rotary evaporator at 60 °C. Then, the resulting solid

was dried in an oven overnight at 100 °C. The solid was ground into a coarse powder and calcined under air at 400 °C for 2 h, then stored in a desiccator over P₂O₅ at room temperature. The compacted silica was used for diluting catalysts in the fixed-bed reactor when required.

2.2.2. Preparation of bulk ZnO and CdO

Bulk ZnO and CdO were prepared by calcining respectively Zn(NO₃)₂·6H₂O and Cd(NO₃)₂·4H₂O under air at 400 °C (for ZnO) and 400 or 500 °C (for CdO) for 2 h at 5 °C min⁻¹ temperature ramp rate. The oxides thus obtained were ground into a coarse powder then stored in a desiccator over P₂O₅ at room temperature. *Cadmium is a very toxic metal. It has a variety of toxic effects including nephrotoxicity, carcinogenicity, teratogenicity and endocrine and reproductive toxicities [1]. The preparation and handling of CdO catalysts must be carried out with great care, especially at high temperatures, using appropriate personal protective equipment.*

2.2.3. Preparation of silica-supported ZnO and CdO catalysts

A series of ZnO/SiO₂ and CdO/SiO₂ catalysts was prepared by the wet impregnation of metal nitrates onto silica support in water at room temperature. The mass of the reagents used for the preparation of these catalysts is given in Table 2.1 and Table 2.2.

Zn(NO₃)₂·6H₂O and Cd(NO₃)₂·4H₂O were dissolved in a minimum amount of distilled water (60–70 mL) at room temperature. This solution was added to silica support and the resulting slurry was left to stir overnight at room temperature. Water was removed using a rotary evaporator at 60 °C and the resulting solid was dried in an oven at 100 °C overnight. The catalysts were then ground to a coarse powder and calcined in air at 400 or 500 °C for 2 h at 5 °C min⁻¹ temperature ramp rate. The catalysts were stored in a desiccator over P₂O₅ at room temperature.

Table 2.1. The mass of reagents used for the preparation of ZnO/SiO₂ catalysts.

Catalyst	Zn(NO ₃) ₂ ·6H ₂ O		SiO ₂
	(mmol)	(g)	(g)
5% ZnO/SiO ₂	3.102	0.914	4.75
10% ZnO/SiO ₂	6.151	1.830	4.50
15% ZnO/SiO ₂	9.217	2.742	4.25
20% ZnO/SiO ₂	12.286	3.655	4.00
30% ZnO/SiO ₂	18.431	5.483	3.50

Table 2.2. The mass of reagents used for the preparation of CdO/SiO₂ catalysts.

Catalysts	Cd(NO ₃) ₂ ·4H ₂ O		SiO ₂
	(mmol)	(g)	(g)
5% CdO/SiO ₂	1.945	0.600	4.75
10% CdO/SiO ₂	3.890	1.200	4.50
20% CdO/SiO ₂	7.780	2.400	4.00
30% CdO/SiO ₂	11.670	3.600	3.50

2.3. Catalyst characterisation techniques

2.3.1. Inductively coupled plasma optical emission spectroscopy (ICP-OES)

This analytical technique is used to quantitatively detect elements that are present at low concentrations in the sample. Plasma is generated by heating argon gas at high temperatures from 5000 to 7000 K, to be able to excite atoms of the sample, which has a high proportion of ions and free electrons [2]. The ICP instrument (Figure 2.1) consists of a unit of light source, a spectrophotometer, a detector and a unit of data processing.

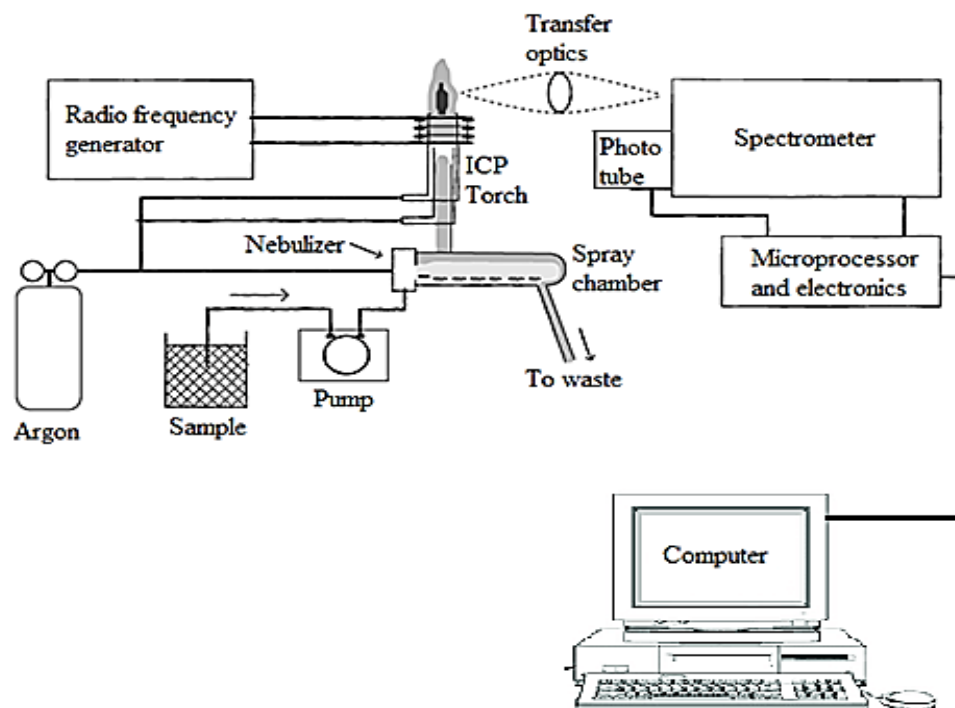


Figure 2.1. Schematic diagram of ICP-OES instrument [2].

The sample to be analysed should be dissolved in an appropriate solvent. The formed solution is introduced into plasma in an atomised state using nebulizer, and excited by plasma. The emitted radiation with characteristic wavelength of the analysed elements is collected by a lens [2]. The intensity of the emissions from various wavelengths of light are proportional to the concentrations of the elements within the sample.

Samples for analysis (~20 mg) were dissolved in concentrated HCl at room temperature, then analysed using ICP. The ICP analysis, for all prepared catalysts, was performed by Mr. S. Moss using a Spectro Ciros CCD Inductively Coupled Plasma source, linked to an Optical Emission Spectroscopy (OES) in the Department of Chemistry, University of Liverpool.

As shown in Table 2.3 and Table 2.4, the content of ZnO and CdO in the catalysts was close to the values expected from the preparation stoichiometry.

Table 2.3. ICP-OES analysis of ZnO/SiO₂ catalysts.

Catalyst	Metal oxide content (%)	
	Calculated	Found
5% ZnO/SiO ₂	5.0	5.3
10% ZnO/SiO ₂	10	10
15% ZnO/SiO ₂	15	15
20% ZnO/SiO ₂	20	19
30% ZnO/SiO ₂	30	29

Table 2.4. ICP-OES analysis of CdO based catalysts.

Catalyst	Metal oxide content (%)	
	Calculated	Found
5% CdO/SiO ₂	5.0	7.0
10% CdO/SiO ₂	10	10
20% CdO/SiO ₂	20	22
30% CdO/SiO ₂	30	32

2.3.2. Surface area and porosity

Determining the surface area and porosity for catalysts is very important in order to characterise catalyst activity. According to the IUPAC classification, the pore size of solid substances is divided into three groups [3]:

Microporous < 2 nm

Mesoporous = 2–50 nm

Macroporous > 50 nm

The surface area of catalysts was determined using Brunauer-Emmett-Teller (BET) method [4]. The BET equation can be presented as:

$$\frac{P}{V(P_o-P)} = \frac{1}{V_m C} + \frac{C-1}{V_m C} \frac{P}{P_o} \quad (2.1)$$

In this equation:

P = equilibrium pressure of adsorbate gas

P_o = saturated pressure of adsorbate gas

V = volume of adsorbed gas

V_m = volume of monolayer adsorbed gas corresponding to monolayer coverage

C = BET constant.

A plot of $P/[V(P_o-P)]$ against P/P_o should give a straight line, where:

$$\text{Slope } (S) = \frac{C-1}{V_m C}$$

$$\text{Intercept } (I) = \frac{1}{V_m C}$$

V_m can be calculated according to: $V_m = \frac{1}{S+I}$.

The total surface area (S_t) can be calculated using the following formula:

$$S_t = V_m \frac{N_A}{V_A} A \quad (2.2)$$

A = the cross section of the nitrogen molecule = (0.162 nm²)

N_A = Avogadro's number = (6.022 x 10²³ mol⁻¹)

V_A = the molar volume of N₂ = (22.4 L mol⁻¹)

The specific surface area (S_s) can be calculated according to the following formula:

$$S_s = \frac{S_t}{m}$$

Where m is the catalyst weight in grams.

The porosity of porous solids was described using the single point total pore volume and the average pore diameter [4-6]. The single point total pore volume is estimated from the amount of adsorbed N₂ at $P/P_o = 0.99$ and converted to the liquid volume. The gas/liquid

volume ratio is 647 for N₂ at 77 K. Then the pore diameter can be calculated from equation (2.3) assuming a cylindrical pore geometry.

$$\text{Pore diameter} = \frac{4 \times \text{pore volume}}{S_s} \quad (2.3)$$

Typically, ~250 mg of a catalyst was placed on the Micromeritics ASAP 2010 adsorption instrument (Figure 2.2) and degassed at 250 °C.

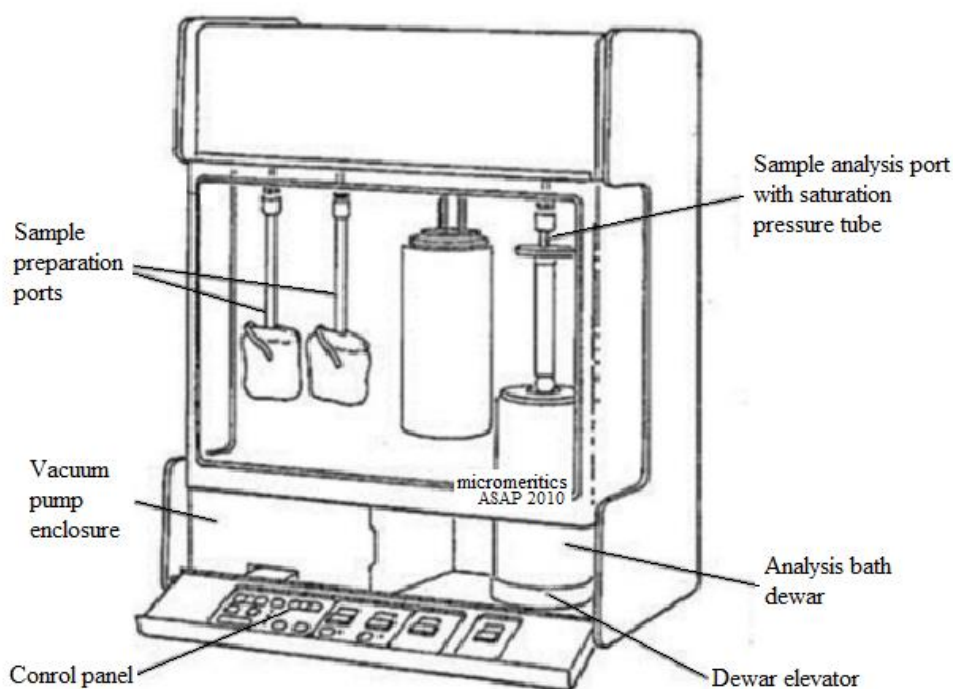


Figure 2.2. Schematic representation of Micromeritics ASAP 2010 instrument [8].

The information about catalyst's porosity and surface area can be obtained by measuring physisorption of nitrogen at 77 K. Plotting the volume of N₂ adsorbed against its relative pressure generates the nitrogen adsorption isotherm. According to the IUPAC classification, there are six types of adsorption isotherms depending on the porous texture of individual solid materials [6,8–12]. Figure 2.3 shows four most common types of isotherm which are observed in solid catalysts. Type I, II, IV and VI isotherms are representative of

microporous, macroporous, mesoporous and uniform ultramicroporous solids, respectively. Types IV will be discussed in detail due to its relevance to the catalysts used in this study.

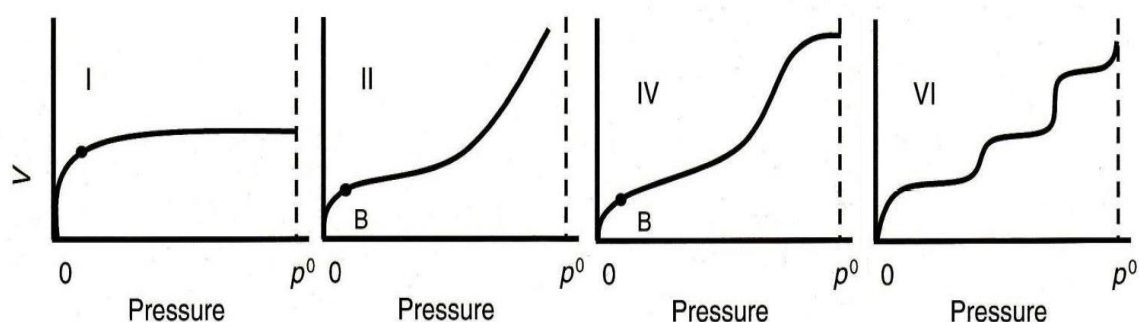


Figure 2.3. The four common types of N_2 adsorption isotherm [13].

Type IV isotherms are characteristic of mesoporous solids. The monolayer adsorption forms at low relative pressure, while multilayer adsorption occurs at high relative pressure, until condensation takes place causing a sharp rise in the adsorbed gas volume. The adsorption on external surface continues as mesopores are completely filled. The vast majority of catalysts exhibit this type of porosity [10]. After adsorption reached saturation, desorption process takes place at low pressure to evaporate the adsorbate from the surface and pores. In mesoporous materials, adsorption causes capillary condensation which leads to a hysteresis loop. Figure 2.4 shows four typical hysteresis types that are classified by the IUPAC [13].

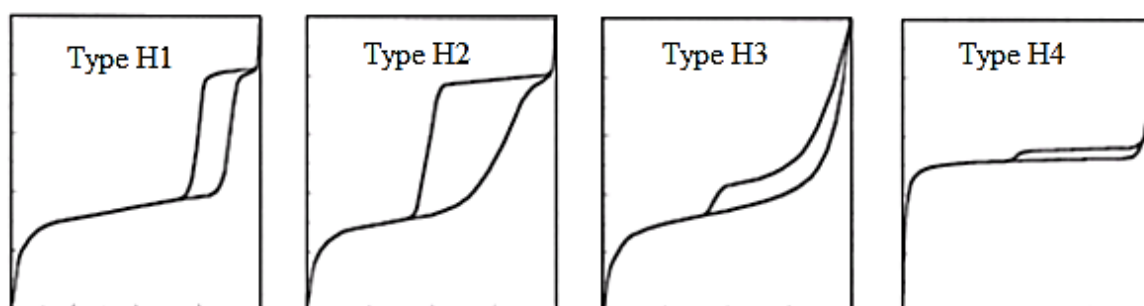


Figure 2.4. Four hysteresis types usually seen in N_2 adsorption-desorption isotherms on porous catalysts [13].

Types H1 and H2 hysteresis loops are observed in the case of uniform and non-uniform pores, respectively, created when the particles of solid materials form cylindrical channels or spheroidal aggregates or agglomerates. These hysteresis types refer to the difference of pore size between body and mouth of the pore (e.g. ink-bottle shaped pores) or to the difference in the behaviour of adsorption and desorption in near cylindrical pores. Most common mesoporous catalysts exhibit these two hysteresis types [4,5].

Types H3 and H4 hysteresis loops are observed with the pores that have a uniform (type H4) or non-uniform (type H3) size and presented in slit-shaped pores (plates or edged particles analogous to cubes) caused by aggregates or agglomerate particles of solids. These hystereses are due to the differences in adsorption and desorption behaviour. Active carbon and zeolites are examples of the catalysts exhibiting H3 and H4 hysteresis, respectively.

Furthermore, no hysteresis is observed in the case of solid materials that possess wedge-shaped, cone-shaped, and blind cylindrical pores. However, the solids with irregular pores exhibit much reduced hysteresis loops.

2.3.3. Thermogravimetric analysis (TGA)

The TGA technique can be used to determine the thermal stability of a catalyst by measuring the change of sample weight during an increase in the temperature. The change of weight may be caused by chemical or physical processes, such as water loss, or thermal decomposition [14]. A TGA apparatus (Figure 2.5) consist of a sensitive balance, usually made of platinum, and a sample container inside a programmed furnace under N₂ or air flow. The results of TGA are displayed as a thermogravimetric curve representing weight loss as a function of temperature [15].

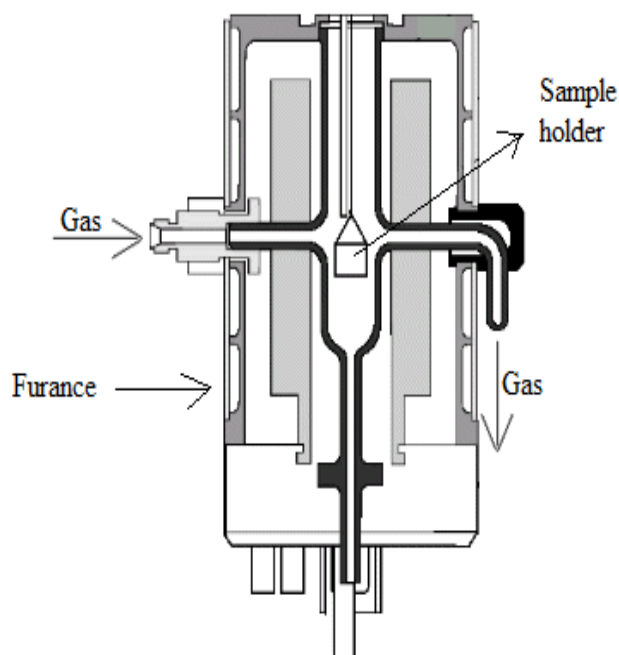


Figure 2.5. A schematic of TGA apparatus.

Our TGA experiments were carried out on 5–20 mg catalyst samples using a TA TGA55 instrument under N₂ flow with a heating rate of 20 °C/min to raise the temperature from room temperature to 600 °C.

2.3.4. Fourier transform infrared spectroscopy (FTIR)

Fourier transform infrared spectroscopy is used to obtain information about the structural framework of molecules [16]. In this study, diffuse reflectance infrared Fourier transform (DRIFT) spectroscopy was used to examine the state of silica supports in the region of 3000–4000 cm⁻¹. It was also utilised to determine the nature of acidity of catalysts, *i.e.* Brønsted and Lewis acid sites, by pyridine adsorption in the range between 1400 and 1600 cm⁻¹.

DRIFT spectra were measured using a Nicolet NEXUS FTIR at room temperature under dry N₂ atmosphere. For the DRIFT measurements, the catalyst samples were mixed 1:10

with dried KBr and thoroughly ground to create a diffusely scattering matrix that lowers light absorption and hence increases the throughput of the beam to enhance the resolution of the analysis. DRIFT spectroscopy was used to characterise the silanol group in silica-supported catalysts, with KBr used as a background.

DRIFT spectra of adsorbed pyridine were obtained for supported ZnO and CdO. For analysis, 10 mg of catalyst was mixed with 90 mg KBr and pre-treated under vacuum at 150 °C to remove physisorbed water. Then the sample was cooled to room temperature under N₂ atmosphere and two drops of pyridine were added to the powder mixture. After that, the sample was degassed again under vacuum at 150 °C for 1 hour to remove physisorbed pyridine. Finally, the DRIFT spectrum was recorded at room temperature, using the mixture of KBr and the catalyst as a background.

2.3.5. X-ray diffraction (XRD)

The XRD is an analytical technique which provides valuable information about the phase composition of catalysts. A pure crystalline solid substance has intensive X-ray fingerprint and the powder diffraction analysis is a convenient method to characterise the crystalline phase [17].

X-rays interact with electrons in atoms. As X-ray photons collide with electrons, certain photons from the incident radiation will be reflected, with the reflection angle equivalent to the incidence angle as shown in (Figure 2.6).

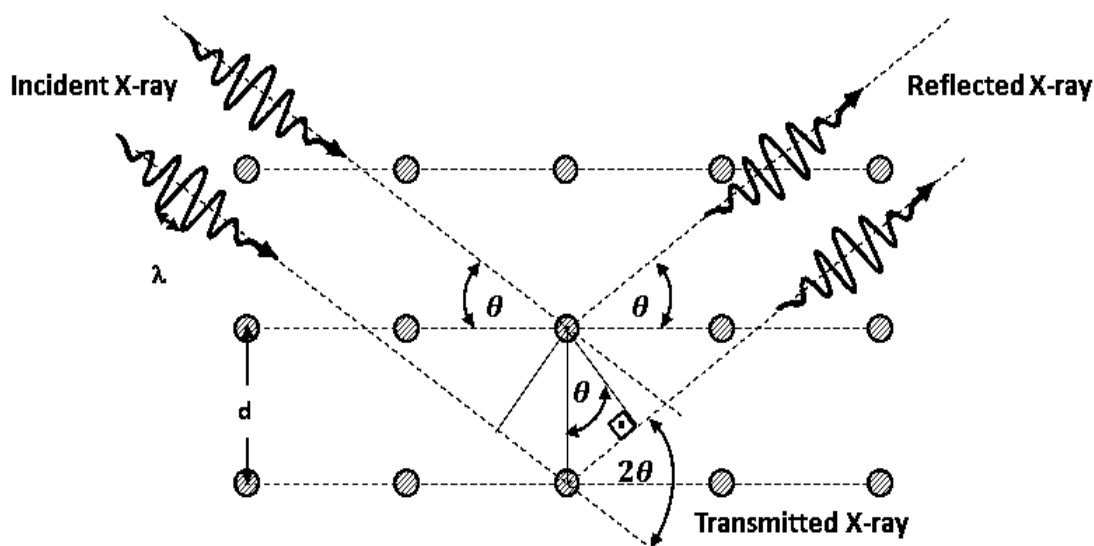


Figure 2.6. Diagram of Bragg's reflection [18].

The directions of X-rays distribution depend on several factors as set out in Bragg's law (equation 2.4) [14]:

$$n \lambda = 2d \sin\theta \quad (2.4)$$

Where n is an integer, the order of reflection, λ is the X-ray wavelength, d is the lattice plane spacing and θ is the diffraction angle.

The XRD patterns were recorded on a Bruker D8 Discover diffractometer with a monochromatic $\text{CuK}\alpha$ radiation ($\lambda = 1.541 \text{ \AA}$). Typically, a small amount of the powdered sample was placed on a sample holder and exposed to X-ray beam at room temperature. This operation was kindly performed by Mr. R. Feetham. The patterns were recorded in the range of 2θ between 20° and 80° and attributed using JCPDS database for comparison with literature.

2.3.6. Temperature programmed reduction (TPR)

TPR is a technique commonly used to identify the redox properties of catalysts by providing information about catalyst reduction with a hydrogen containing flow [19]. In this work, H_2 -TPR of CdO/SiO_2 catalysts was carried out on a Micromeritics TPD/TPR 2900

apparatus equipped with a thermal conductivity detector (TCD). A U-shaped sample tube was packed with 20–40 mg of catalyst and heated up to 600 °C at a rate of 20 °C/min under 40–50 ml min⁻¹ H₂-N₂ (5:95) flow. For quantitative analysis, H₂-TPR was calibrated using Ag₂O as a redox standard. Figure 2.7 shows the H₂-TPR of Ag₂O and Figure 2.8 the calibration plot.

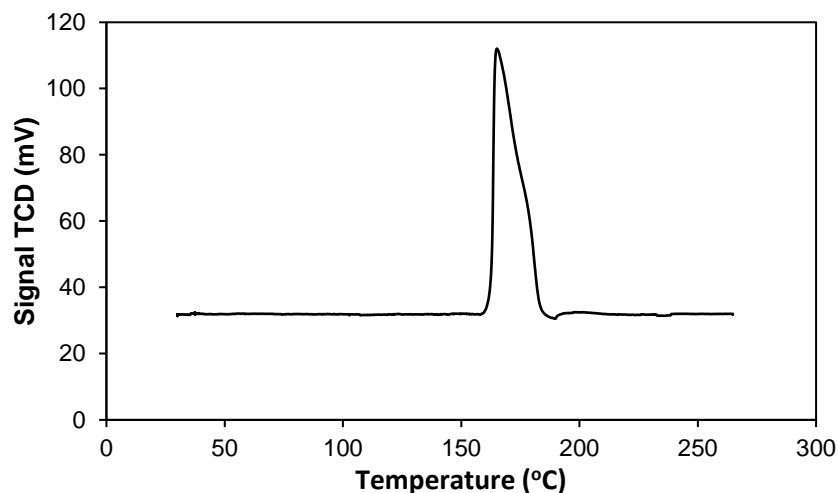


Figure 2.7. H₂-TPR of Ag₂O (18.8 mg) in H₂-N₂ (5:95) flow (50 ml min⁻¹), 10 °C min⁻¹ temperature ramp rate.

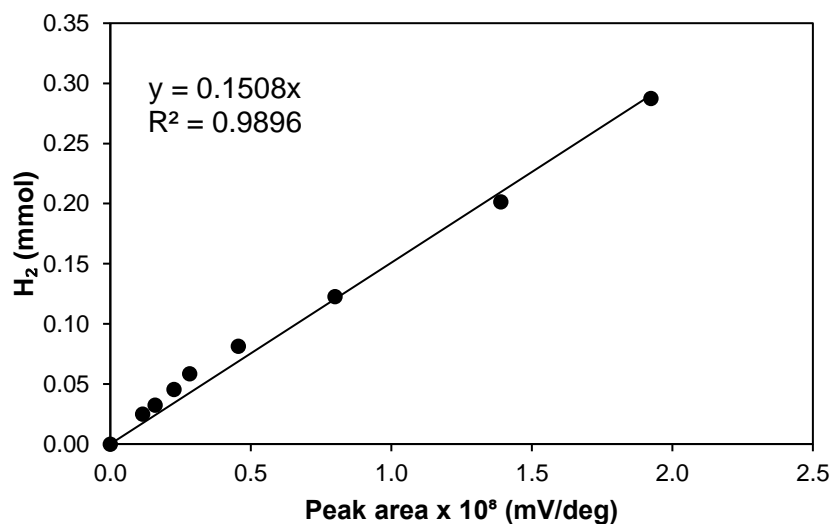


Figure 2.8. Calibration of H₂-TPR using Ag₂O (0.08–0.20 mmol) in H₂-N₂ (5:95) flow (50 ml min⁻¹), 10 °C min⁻¹ temperature ramp rate.

2.3.7. CHN analysis

Evaluation of chemical elements such as carbon, hydrogen, nitrogen and sulfur in organic compounds is one of the most important chemical quantitative analyses [20]. In this analysis, a milligram size sample is weighed, and injected into the reactor at 2000 °C under streaming helium gas, which is then enriched with pure oxygen, leading to flash combustion. The combustion product mixture of gases is then quantified by gas chromatography.

In our work, the purpose of CHN analysis was to detect coke formation caused by carbonaceous deposits which can affect catalyst performance. The coke formation on the surface of a catalyst can cause catalyst deactivation, which reduces the catalytic activity.

In this study, carbon and hydrogen analysis was carried out by Mr. S. Moss using a Thermo Flash EA 1112 instrument which is available in the Department of Chemistry, University of Liverpool.

2.4. Catalyst testing

2.4.1. Gas chromatography (GC)

Gas chromatography is employed for quantitative analysis of reaction products. In this technique, a volatile compound mixture is vaporised and transported by the carrier gas through the GC column to the GC detector [21]. Usually, N₂, He or Ar are used as a carrier gas (mobile phase). The mixture is separated upon passing through the GC column depending on the boiling point and polarity of components of the mixture [22]. A typical GC set-up is shown in Figure 2.9.

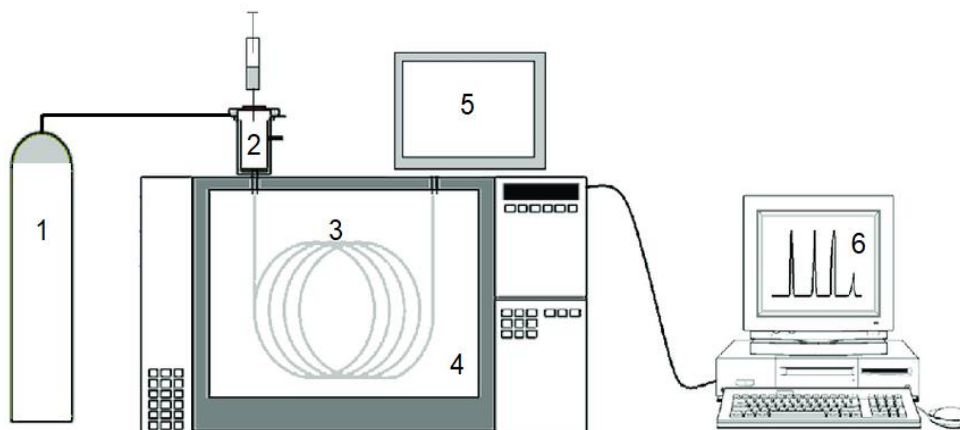


Figure 2.9. Representation of a typical GC set-up: (1) carrier gas, (2) injection port, (3) column, (4) oven, (5) detector and (6) data processor [23].

The column is a long capillary tube, often made of glass or metal, fitted with an injection port at one end and a detector at the other. A split/splitless injector (Figure 2.10) is normally used to insert the samples into the column. The injector is heated to a temperature higher than the temperature of the column to avoid condensation [24].

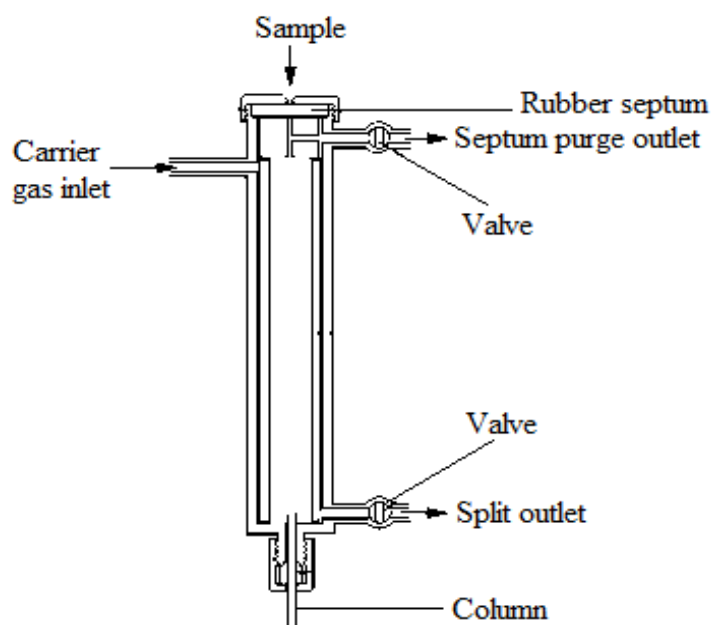


Figure 2.10. Split/splitless injector [25].

Flame ionisation detector (FID) (Figure 2.11) is widely used to detect most organic compounds. These compounds are burned by a hydrogen-air flame using a small metal jet. This produces ionised species, with the amount of charge produced proportional to the quantity of organic compound present. The ionic current is then transformed into a chromatogram.

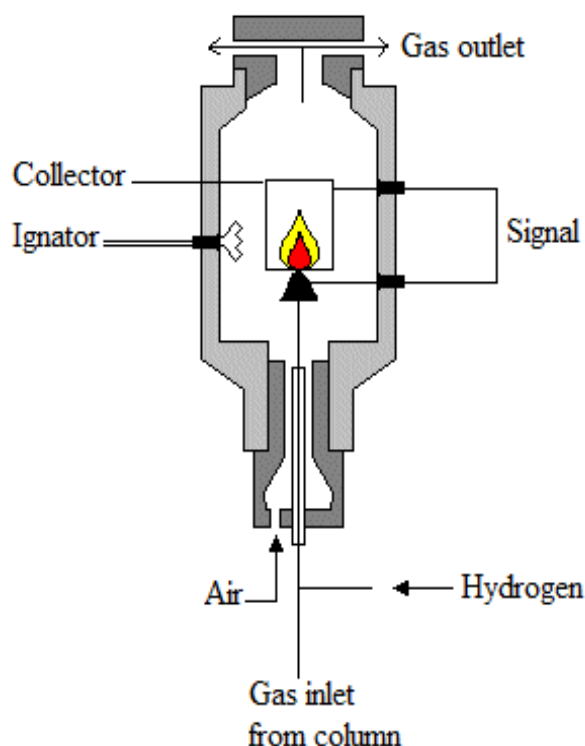


Figure 2.11. Flame ionisation detector [26].

For p-cymene synthesis, the gas phase reactor was equipped with an online Varian Star 3800 Gas Chromatograph and a flame ionisation detector (FID). A medium polarity Zebron ZB-1701 capillary column (30 m length, 0.25 mm internal diameter, 0.25 μ m film thickness) containing a 14% cyanopropyl-phenyl-methyl polysiloxane as a stationary phase was used for the GC analysis. Nitrogen gas was used as a carrier gas with a flow rate of 10 mL min⁻¹. Temperature of injector and detector was set to 250 °C. The column heating programme is shown in Figure 2.12.

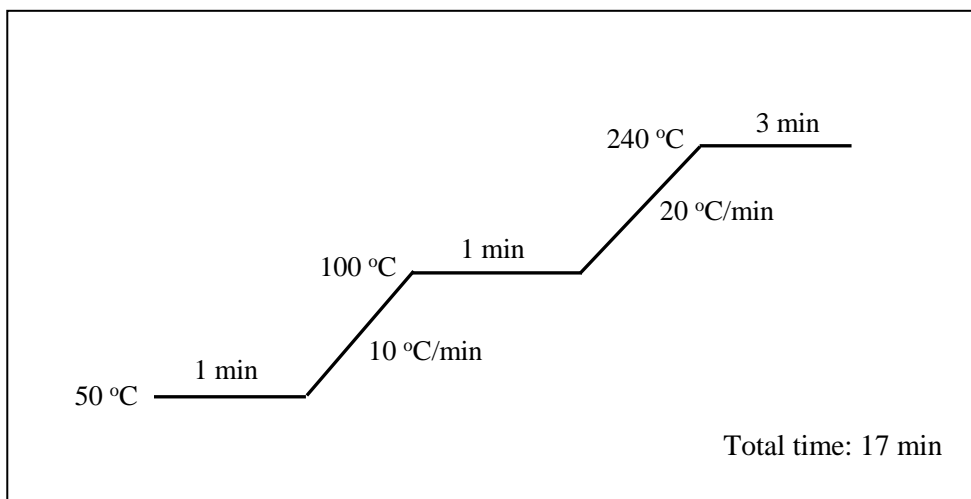


Figure 2.12. The column heating programme used for p-cymene GC analysis.

2.4.2. GC calibration

GC response factors were assumed to be the same for all monoterpenes and p-cymene since they have practically the same hydrocarbon composition. The calibration data (molecular weights, boiling points, retention times and response factors) for dehydroisomerisation of monoterpenes are given in Table 2.5. Figure 2.13 shows a typical GC trace for the gas phase dehydroisomerisation of α -pinene.

Table 2.5. The calibration data for dehydroisomerisation of α -pinene and limonene.

Compound	Molecular weight (g/mol)	Boiling point (°C)	Retention time (min)	Response factor
Lights ^a	-	-	-	1.00
α -Pinene	136.24	156	3.8-3.9	1.00
Camphene	136.24	195	4.3-4.4	1.00
β -Pinene	136.23	166	4.5-4.6	1.00
α -Terpinene	136.23	175	5.2-5.3	1.00
Limonene	136.24	176	5.3-5.4	1.00
p-Cymene	134.22	177	5.5-5.6	1.00
γ -Terpinene	136.23	183	5.8-5.9	1.00
β -Terpinene	136.23	173	6.1-6.2	1.00
Terpinolene	136.24	184	6.4-6.5	1.00
Others ^b	-	-	-	1.00

^a Cracking products. ^b Unidentified p-menthadienes.

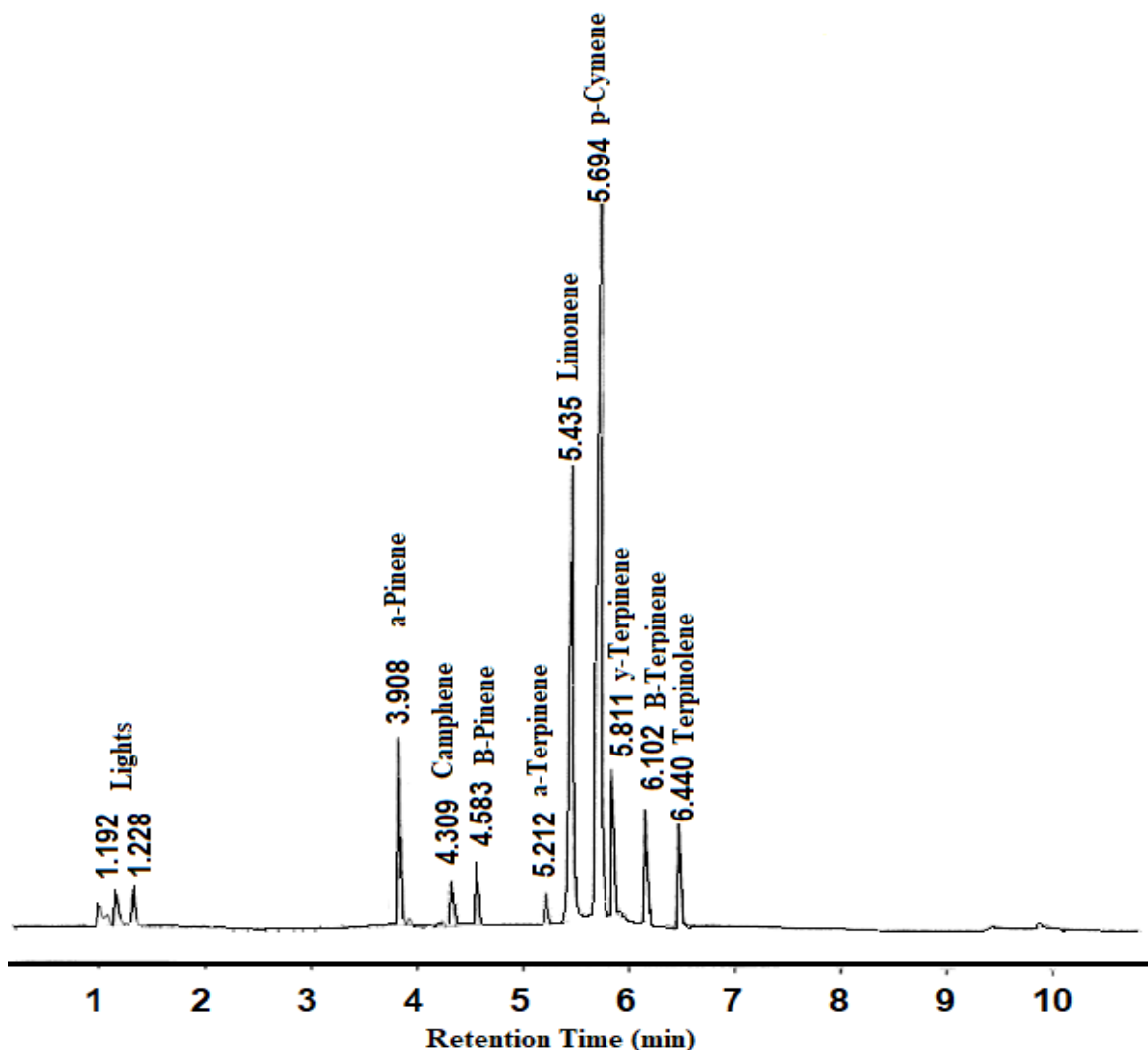


Figure 2.13. A typical GC trace for α -pinene dehydroisomerisation over 10%ZnO/SiO₂.

2.5. Reaction studies

2.5.1. Gas phase reaction

The dehydroisomerisation of α -pinene and limonene was carried out at 200–400 °C and ambient pressure using nitrogen as a carrier gas in a continuous flow fixed-bed quartz tubular downflow reactor (9 mm internal diameter) with online GC analysis (Varian Star 3800 gas chromatograph equipped with a flame ionisation detector and Zebron ZB-1701 capillary column of 30 m length, 0.25 mm internal diameter and 0.25 μ m film thickness). The catalyst

powder (0.2–0.8 g) was loaded in the reactor supported by a glass wool plug. The temperature in the reactor was controlled by a Eurotherm controller using a thermocouple placed at the top of the catalyst bed. All reactor gas lines were made of stainless steel. The downstream lines and sampling valves were heated to 150 °C to prevent product condensation. Prior to reaction, the catalyst was pre-treated at the reaction temperature for 1 h in nitrogen flow. Gas feed containing α -pinene or limonene at 0.2–1.0 kPa partial pressure was supplied to the reactor by passing nitrogen flow controlled by a Brooks mass flow controller through a stainless steel saturator holding liquid substrate at a certain temperature to maintain the required substrate partial pressure (Table 2.6). The downstream gas flow was analysed using the online GC to obtain terpene conversion and product selectivity. A diagram of the reactor setup used for α -pinene and limonene dehydroisomerisation in the gas phase is shown in Figure 2.14. Product selectivity was defined as a molar percentage of monoterpenes converted to a particular reaction product. Each catalyst test was repeated at least twice. The mean absolute percentage error in conversion and product selectivity was usually $\leq 5\%$ and the carbon balance was maintained within 95%. The reactions were carried out for 4 h time on stream (TOS) unless stated otherwise.

Table 2.6. Partial vapour pressure of monoterpenes at saturation temperatures used in experiments (calculated from the reference book [27]).

Reactant	Temperature (°C)	Partial vapour pressure (kPa)
α -Pinene	25	0.48
β -Pinene	31	0.47
Limonene	35	0.47
Terpinolene	51.5	0.47
α -Terpinene	38	0.47
γ -Terpinene	45	0.47

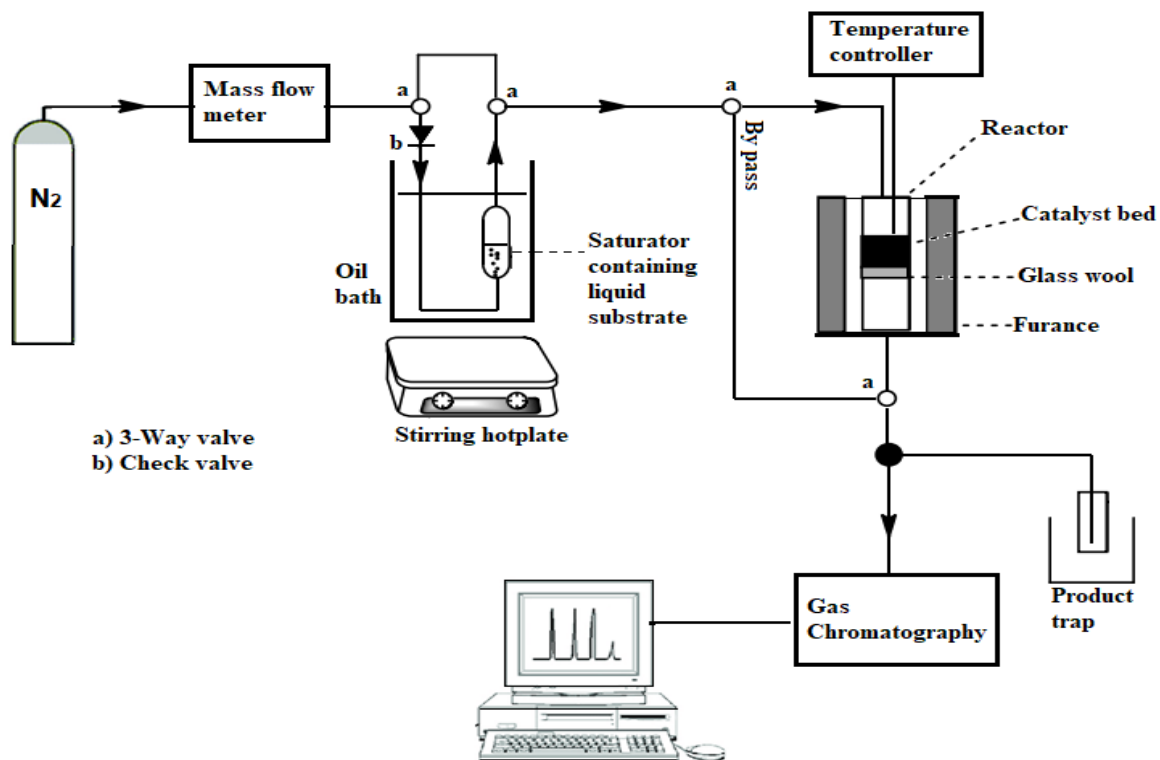


Figure 2.14. A diagram of the reactor setup for dehydroisomerisation of terpenes.

2.6. Calculation of conversion, yield and selectivity

The terpene conversion (C), the yield of each individual product (Y_p) and the selectivity of a particular product ($S_{p,s}$) were calculated using equations (2.5), (2.6) and (2.7), respectively:

$$C (\%) = \sum Y_p \quad (2.5)$$

$$Y_p (\%) = \frac{S_p \times K \times A}{S_r + (\sum S_p \times K \times A)} \times 100 \quad (2.6)$$

$$S_{p,s} (\%) = \frac{Y_p}{C} \times 100 \quad (2.7)$$

In these equations:

S_p = peak area of product

K = response factor

A = stoichiometry factor of the product relative to the substrate, $A = 1$

S_r = peak area of reactant

$\sum S_p \times K \times A$ = summation for all reaction products.

The weight hourly space velocity (WHSV) and catalyst contact time (τ) were calculated using equations (2.8) and (2.9), respectively.

$$WHSV = \frac{F \times 60}{W} \times M \quad (2.8)$$

$$\tau = \frac{1}{WHSV} \quad (2.9)$$

In these equations, F is the molar flow rate of substrate (mol h^{-1}), W is the weight of catalyst (g) and M is the molecular mass of the substrate ($M = 136.24 \text{ g mol}^{-1}$ for all cyclic monoterpenes used as the substrates).

References

- [1] A. Rani, A. Kumar, A. Lal, M. Pant, Cellular mechanisms of cadmium-induced toxicity: a review, *Int. J. Environ. Health Res.* 24 (2014) 378–399.
- [2] S. Ghosh, V. L. Prasanna, B. Sowjanya, P. Srivani¹, M. Alagaraja¹, D. Banji, Inductively coupled plasma-Optical emission spectroscopy: A review, *Asian J. Pharm. Ana.* 3 (2013) 24–33.
- [3] G. C. Bond, *An Introduction to Polysaccharide Biotechnology*, Taylor & Francis, London, 1998.
- [4] G. Leofanti, M. Padovan, G. Tozzola, B. Venturelli, Surface area and pore texture of catalysts, *Catal. Today* 41 (1998) 207–219.
- [5] S. Lowell, J. E. Shields, M. A. Thomas, M. Thommes, *Characterization of Porous Solids and Powders: Surface Area, Pore Size, and Density*, 2004.
- [6] K. Y. Foo, B. H. Hameed, Insights into the modeling of adsorption isotherm systems, *Chem. Eng. J.* 156 (2010) 2–10.
- [7] K. S. W. Sing, R. T. Williams, Physisorption hysteresis loops and the characterization of nanoporous materials, *Adsorpt. Sci. Technol.* 22 (2004) 773–782.
- [8] A. Alsalmeh, *Solid Acid Catalysts Based on Heteropoly Acids for Conversion of Renewable Feedstocks*, 2010.
- [9] R. M. Gabr, M. M. Girgis, A. M. El-Awad, B. M. Abou-Zeid, Effect of spine1 ($ZnCr_2O_4$) formation on the texture, electrical conduction and catalytic behaviour of the $ZnO-Cr_2O_3$, system, *Mater. Chem. Phys.* 39 (1994) 53–62.
- [10] H. M. Tasdemir, S. Yasyerli, N. Yasyerli, Selective catalytic oxidation of H_2S to elemental sulfur over titanium based Ti-Fe, Ti-Cr and Ti-Zr catalysts, *Int. J. Hydrogen Energy* 40 (2015) 9989–10001.

- [11] I. Jasińska, W. Arabczyk, Kinetic studies of the recrystallization process of iron catalyst for ammonia synthesis, *Chem. Pap.* 59 (2005) 496–499.
- [12] H. P. Barrett, L. G. Joyner, P. P. Halenda, The determination of pore volume and area distributions in porous substances I. Computations from nitrogen isotherms, *J. Am. Chem. Soc.* 73 (1951) 373–380.
- [13] K. Kaneko, Determination of pore size and pore size distribution 1. Adsorbents and catalysts, *J. Memb. Sci.* 96 (1994) 59–89.
- [14] A. K. Singh, *Experimental Methodologies for the Characterization of Nanoparticles*, 2016, 125–168.
- [15] D. Kealey, P. J. Haines, *Analytical Chemistry*, the Taylor & Francis e-Library, 2002. Available from: [BIOS Instant Notes in Analytical Chemistry | David Kealey, P J Haines \(taylorfrancis.com\)](https://www.taylorfrancis.com/books/9780429244444).
- [16] I. W. Levin, R. Bhargava, Fourier transform infrared vibrational spectroscopic imaging: integrating microscopy and molecular recognition, *Annu. Rev. Phys. Chem.* 56 (2005) 429–474.
- [17] M. J. Buerger, Partial Fourier syntheses and their application to the solution of certain crystal structures, *Proc. Natl. Acad. Sci.* 42 (1956) 776–781.
- [18] P. Atkins, J. Paula, *Atkins' Physical Chemistry*, 7th ed., Oxford, 2002.
- [19] F. Pinna, Supported metal catalysts preparation, *Catal. Today* 41 (1998) 129–137.
- [20] E. Pella, B. Colombo, Study of carbon, hydrogen and nitrogen determination by combustion-gas chromatography, *Mikrochim. Acta* 61 (1973) 697–719.
- [21] G. Schomburg, Two-dimensional gas chromatography: principles, instrumentation, methods, *J. Chromatogr. A* 703 (1995) 309–325.
- [22] G. H. Jeffery, J. Bissett, J. Mendham, R. C. Denney, *Quantitative Chemical Analysis*, 5th ed., 1989.

- [23] A. de S. Pinheiro, G. O. Da Rocha, J. B. de Andrade, A SDME/GC–MS methodology for determination of organophosphate and pyrethroid pesticides in water, *Microchemical. J.* 99 (2011) 303–308.
- [24] G. D. Chistian, J. E. O' Reilly, *Instrumental Analysis*, 2nd ed., 1988.
- [25] [Splitless Injection with Solvent Trapping - Liquid Chromatography \(beyonddiscovery.org\)](#). Accessed 18 May 2022.
- [26] V. R. Bella, R. Prasad, *Catalytic Oxidation: Of Diesel Soot Emissions Control*, LAP LAMBERT Academic Publishing, 2012.
- [27] D. R. Lid, *Handbook of Chemistry and Physics*, 84th. ed., CRC press, 2003–2004.

Chapter 3. Dehydroisomerisation of α -pinene and limonene to p-cymene over silica-supported ZnO in the gas phase

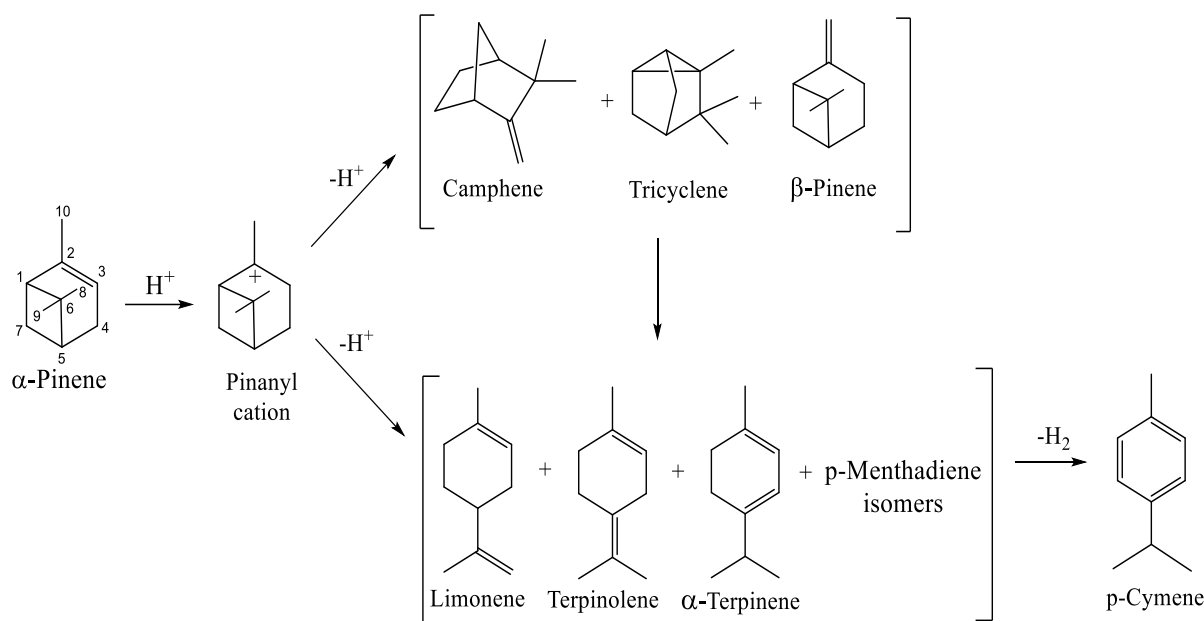
3. Introduction

p-Cymene is a versatile monoterpene with a variety of applications ranging from medicinal and cosmetic uses to industrial organic synthesis [1]. Its major application is as an intermediate for the synthesis of p-cresol, which is further processed to antioxidants [2]. p-Cymene could also be used for the production of terephthalic acid [3]. p-Cymene is commonly synthesized from the oil-based feedstock by environmentally harmful Friedel-Crafts alkylation of toluene with propene followed by isomer separation [1]. An alternative environmentally benign route to p-cymene is through dehydroisomerisation of renewable terpene raw materials, α -pinene and limonene, using acid-redox bifunctional heterogeneous catalysis [1]. α -Pinene is an inexpensive major constituent (ca. 85%) of turpentine oils obtained from coniferous trees [4]. Crude sulfate turpentine, a by-product from the pulp and paper industry, is another cheap source of terpenes including α -pinene [1]. Limonene is obtained commercially from citrus fruits [4].

Dehydroisomerisation of α -pinene to p-cymene is suggested to proceed through a bifunctional mechanism including α -pinene isomerisation on catalyst acid sites to monocyclic p-menthadienes and bi- and tricyclic terpenes followed by dehydrogenation of p-menthadienes on metal or oxo-metal redox sites [1] (Scheme 3.1). α -Pinene isomerisation has been extensively studied with a wide range of solid acid catalysts in the liquid and gas phases [1]. Among the acid catalysts are zeolites [5–7], acid-activated clays [8,9], sulfated zirconia [10],

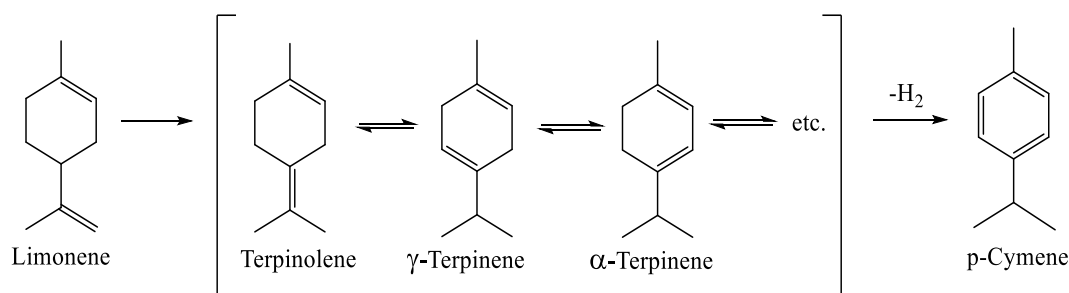
ion exchange resins [11] and heteropoly acids [12–15]. Typically, it yields 30–50% of camphene together with a complex mixture of other monoterpene by-products. The reaction is suggested to proceed through protonation of the α -pinene double bond to form pinanyl cation, followed by two parallel transformations: the rearrangement to bi- and tricyclic products (camphene, tricyclene, β -pinene, etc.) and 1–6 ring opening to form monocyclic p-menthadienes (limonene, terpinolene, terpinene, etc.) (Scheme 3.1) [1]. The first pathway is favourable at lower temperatures, whereas p-menthadienes form at higher temperatures [1]. In the α -pinene-to-p-cymene dehydroisomerisation, p-menthadiene dehydrogenation is suggested to be the rate-limiting step, whereas the isomerisation step is probably at quasi-equilibrium [1].

Usually, the synthesis of p-cymene from α -pinene is carried out in the gas phase at ambient pressure. A range of heterogenous catalysts have been reported for this reaction giving 100% α -pinene conversion at 300–460 °C [1,16–19]. These include $\text{Cr}_2\text{O}_3/\text{Al}_2\text{O}_3$ (390–460 °C, 53% p-cymene yield) [16], zeolite Y (300 °C, 54% yield) [17], Pd/SiO₂ (300 °C, 67% yield) [1], Pd-Zn/Al-SBA-15 (300 °C, 77% yield) [18] and bulk Zn(II)–Cr(III) mixed oxide (350 °C, 78% yield) [19]. The supported Pd catalysts exhibit high activity at 300 °C, but require continuous hydrogen supply to reduce catalyst coking causing catalyst deactivation [1]. The noble-metal-free bulk Zn–Cr oxide gives practically the same p-cymene yield as Pd-Zn/Al-SBA-15 without H₂ supply, although at a higher temperature of 350 °C [19].



Scheme 3.1. Dehydroisomerisation of α -pinene to p-cymene.

p-Cymene can also be produced by dehydroisomerisation of limonene occurring through double bond migration on acid sites followed by dehydrogenation on metal or oxo-metal sites (Scheme 3.2), the latter probably being the rate-limiting step [20–25]. This reaction occurs easier than the α -pinene-to-p-cymene conversion because does not include C–C bond breaking. A number of heterogeneous catalysts have been reported for this reaction in the liquid and gas phases [20–25], including Ti/SBA-15 (liquid phase, 160 °C, 56% p-cymene yield) [21], Pd/HZSM-5 (liquid phase, 260 °C, 8 bar pressure, 82% yield) [22], Pd/Al₂O₃ (supercritical EtOH, 300 °C, 65 bar pressure, 80% yield) [23], TiO₂ (gas phase, 300 °C, 90% yield) [24], Pd/SiO₂ (gas phase, 300 °C, in H₂ flow, 99% yield) [25] and others [20]. Pd/SiO₂ gives the highest yield of p-cymene in the gas phase, however, requires continuous H₂ supply to prevent catalyst deactivation [25] as in the case of α -pinene dehydroisomerisation [1].



Scheme 3.2. Dehydroisomerisation of limonene to p-cymene.

Here, the dehydroisomerisation of α -pinene and R-(+)-limonene (referred to as limonene) to p-cymene is investigated in the presence of noble-metal-free silica-supported ZnO catalyst in the gas phase in a continuous fixed-bed reactor. ZnO is an amphoteric oxide [26] it is known as a hydrogenation and dehydrogenation catalyst [2], for example, for dehydrogenation of primary alcohols to aldehydes [27]. Silica support possesses mild Brønsted acidity due to its surface silanol groups; it can readily isomerise α -pinene and limonene at 300 °C [1,25]. Therefore, the silica-supported ZnO possessing both acidic and dehydrogenating functionalities has a potential for the dehydroisomerisation of these terpenes to p-cymene. Here, it is demonstrated that this catalyst has a very high efficiency in the environmentally-friendly synthesis of p-cymene from α -pinene and limonene, exhibiting stable performance without hydrogen supply.

3.1. Results and discussion

3.1.1. Catalyst characterisation

The texture of ZnO/SiO₂ catalysts was characterised by N₂ physisorption (Table 3.1), with particular attention to the ZnO/SiO₂(300) catalysts supported on Aerosil 300, which exhibited higher activities. These catalysts showed typical adsorption/desorption isotherms for

mesoporous materials of type IV [28,29] with a H1 hysteresis loop representative of amorphous silica [30,31] (Figure 3.1). It can be seen from the pore size distribution obtained by the BJH method (Figure 3.2) that a sharp peak appeared at about 350 Å pore diameter. These results are in agreement with the previous studies [32–34].

Bulk ZnO prepared by calcining Zn(NO₃)₂ hexahydrate at 400 °C had a very low surface area of 0.01 m² g⁻¹. As expected, supported ZnO/SiO₂ catalysts had much larger surface areas; their surface area and pore volume decreased with increasing ZnO loading. At a constant ZnO loading of 10 wt%, the catalyst surface area increased with increasing the surface area of silica support with an exception of ZnO/SiO₂(750), the surface area of which is smaller than that of ZnO/SiO₂(600). This may be explained by a larger contribution of microporosity in SiO₂(750) texture, which may be blocked by ZnO.

Table 3.1. Information about catalysts.

Catalyst ^a	S _{BET} ^b (m ² g ⁻¹)	Pore volume ^c (cm ³ g ⁻¹)	Pore size ^d (Å)	Water content ^e (wt%)
ZnO	0.01	-	-	-
SiO ₂ (300)	296	1.32	179	-
5% ZnO/SiO ₂ (300)	294	0.96	155	-
10% ZnO/SiO ₂ (300)	218	1.14	209	1.2 (1.3)
15% ZnO/SiO ₂ (300)	188	0.90	191	-
20% ZnO/SiO ₂ (300)	162	0.90	222	-
30% ZnO/SiO ₂ (300)	130	0.77	237	-
10% ZnO/SiO ₂ (200)	166	0.68	163	1.5 (1.4)
10% ZnO/SiO ₂ (600)	491	0.90	74	2.0 (2.0)
10% ZnO/SiO ₂ (750)	375	1.16	124	4.5 (3.5)

^a Calcined at 400 °C for 2 h in air; in round brackets is the surface area of SiO₂ support (m² g⁻¹). ^b BET surface area. ^c Single point total pore volume. ^d Average pore diameter by BET method. ^e From TGA as weight loss in the temperature range of 40–100 °C and in round brackets in the range of 100–600 °C.

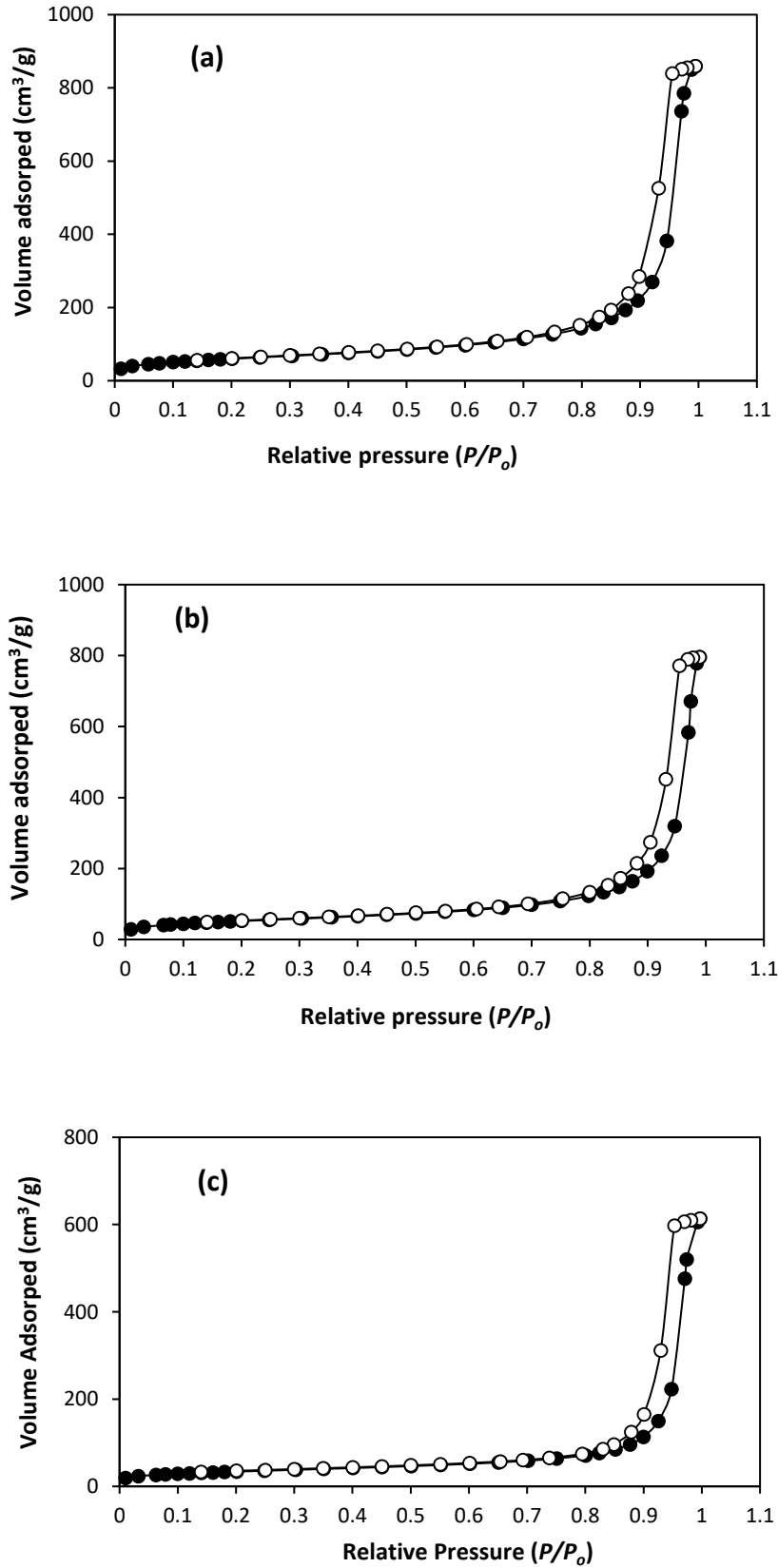


Figure 3.1. Nitrogen adsorption (solid circles) and desorption (open circles) isotherms for 10% ZnO/SiO₂(300) (a), 20% ZnO/SiO₂(300) (b) and 30% ZnO/SiO₂(300) (c).

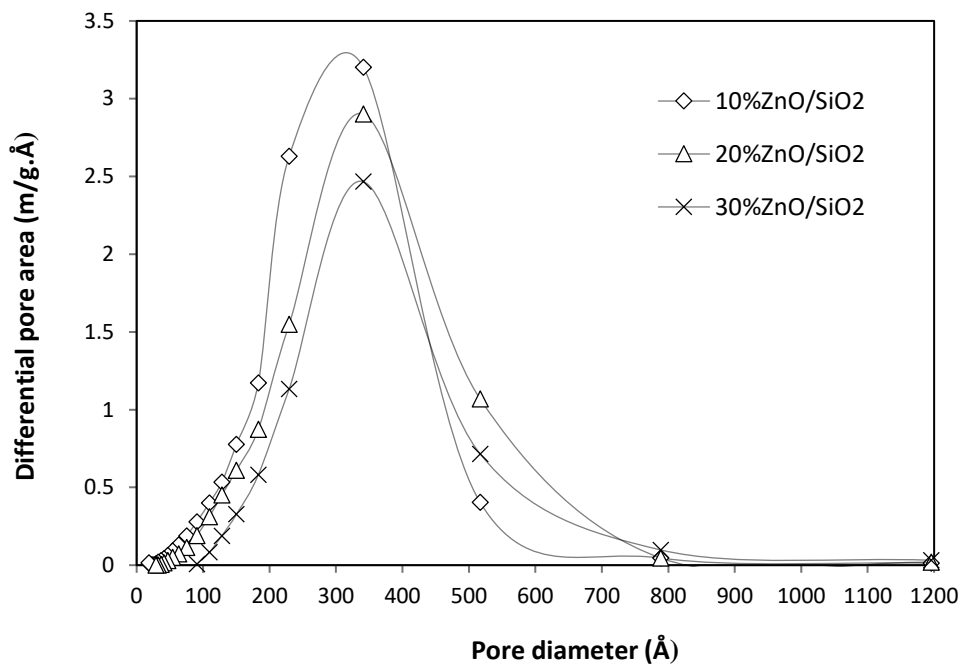


Figure 3.2. Pore size distribution for ZnO/SiO₂ catalysts.

The TGA for Zn(NO₃)₂·6H₂O, which was used as a precursor for ZnO/SiO₂ catalysts, is shown in Figure 3.3. About 35% weight loss was observed between 100 and 200 °C, corresponding to the removal of physisorbed and chemically bound water. This followed by decomposition of Zn(NO₃)₂ to ZnO which was complete at about 300 °C [35]. The total weight loss of 64% is close to the expected weight loss of 72% for the decomposition of Zn(NO₃)₂ hexahydrate to ZnO.

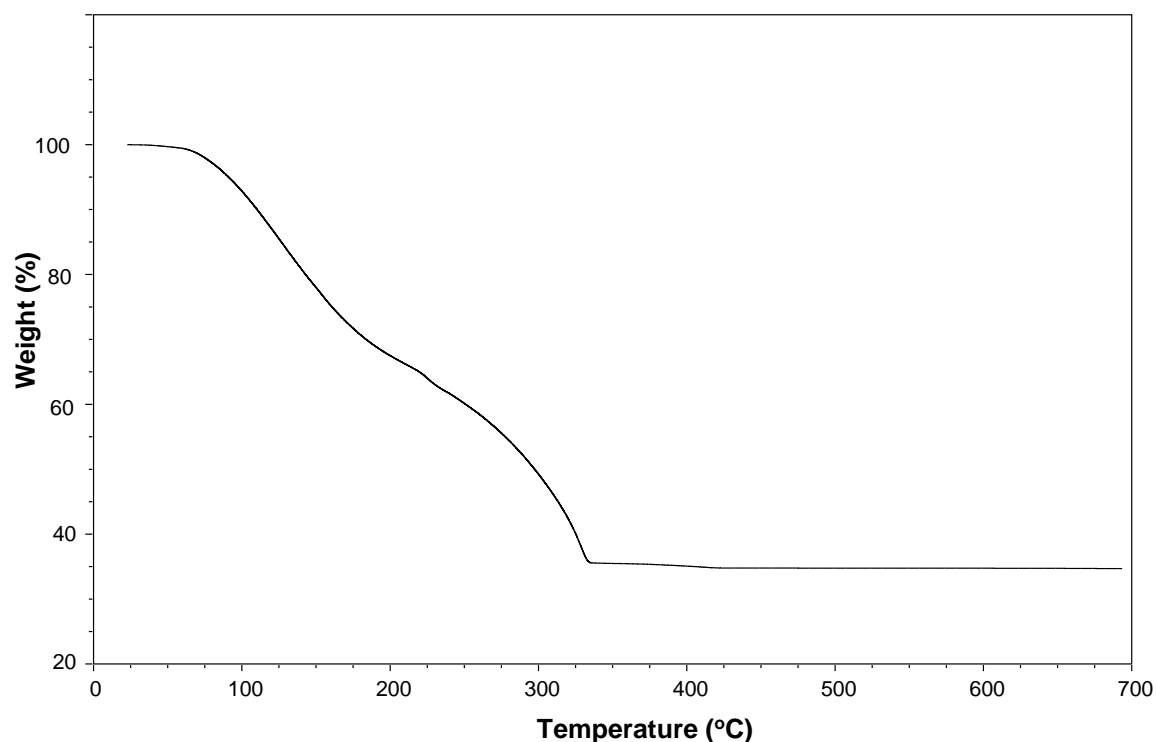


Figure 3.3. TGA for Zn(NO₃)₂·6H₂O.

From TGA, the catalysts exhibited a water loss of 1.2–4.5% upon heating up to 100 °C, which can be attributed to physisorbed water, and a further loss of chemically bound water of 1.3–3.5% in the temperature range 100–600 °C (Table 3.1) (Figure 3.4). The water loss increased with increasing the surface area of silica support. The loss of water at higher temperatures indicates the presence of silanol groups in the catalysts, which is also confirmed by DRIFT spectroscopy (see below). The silanol groups can act as active Brønsted acid sites in the dehydroisomerisation reaction [1,25].

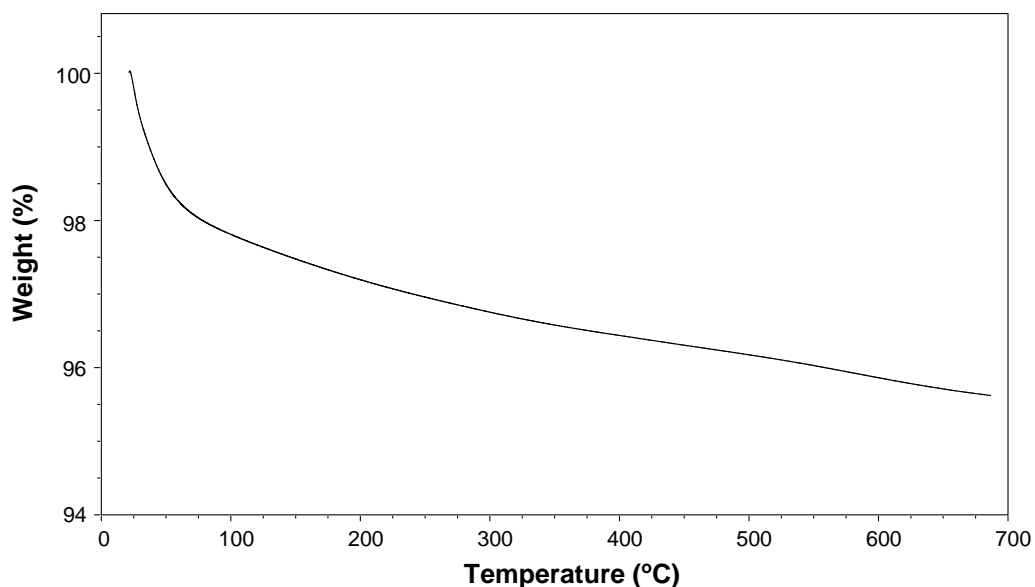


Figure 3.4. TGA for fresh 10%ZnO/SiO₂(300).

Figure 3.5 shows XRD patterns of 10%ZnO/SiO₂ catalysts supported on silica with different surface areas (200–750 m²g⁻¹) together with the pattern of bulk ZnO [19,36]. Bulk ZnO is a crystalline material (wurtzite structure), with XRD reflections at 31.8° (100), 34.4° (002), 36.3° (101), 47.6° (102), 56.7° (110), 62.9° (103), 66.3° (200), 68.0° (112), 69.2° (201) and 77.2° (202) (JCPDS No. 00-036-1451). In contrast, 10%ZnO/SiO₂ catalysts were amorphous in agreement with previous reports [37,38]. This indicates a fine dispersion of ZnO on the silica surface. Only 10%ZnO/SiO₂(200) showed a trace of ZnO crystal phase due to a relatively low surface area of the silica support.

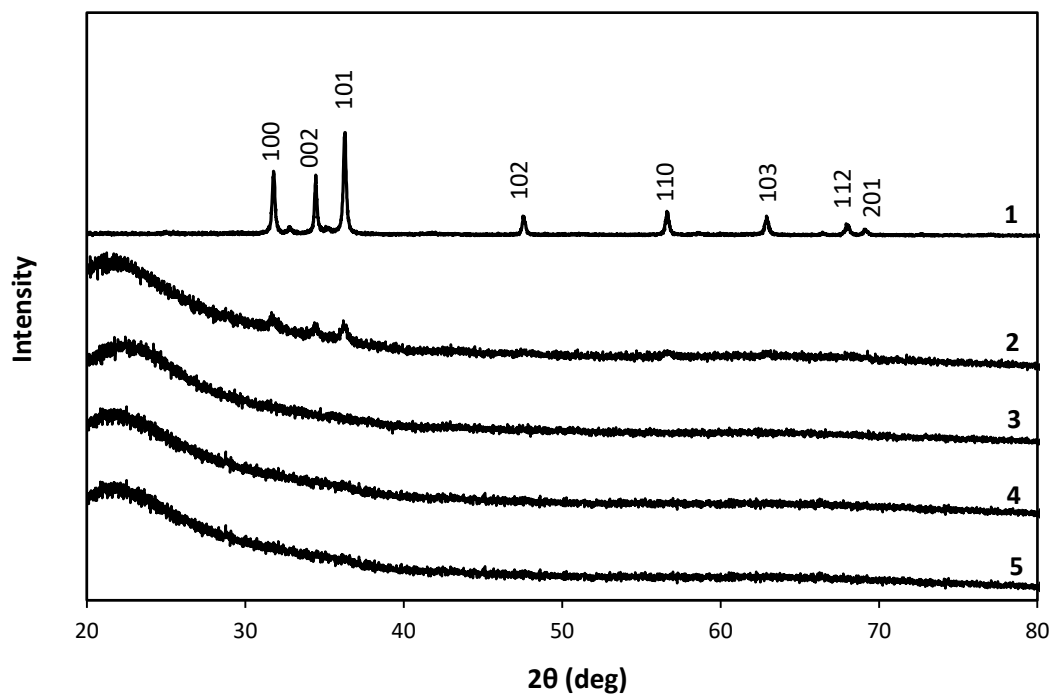


Figure 3.5. XRD patterns (CuK α) for (1) bulk ZnO, (2) 10%ZnO/SiO₂(200), (3) 10%ZnO/SiO₂(300), (4) 10%ZnO/SiO₂(600), (5) 10%ZnO/SiO₂(750).

Figure 3.6 shows XRD for ZnO/SiO₂(300) catalysts with different ZnO loadings from 10–30%. Only the catalyst with the highest ZnO loading of 30% exhibits the pattern of crystalline ZnO.

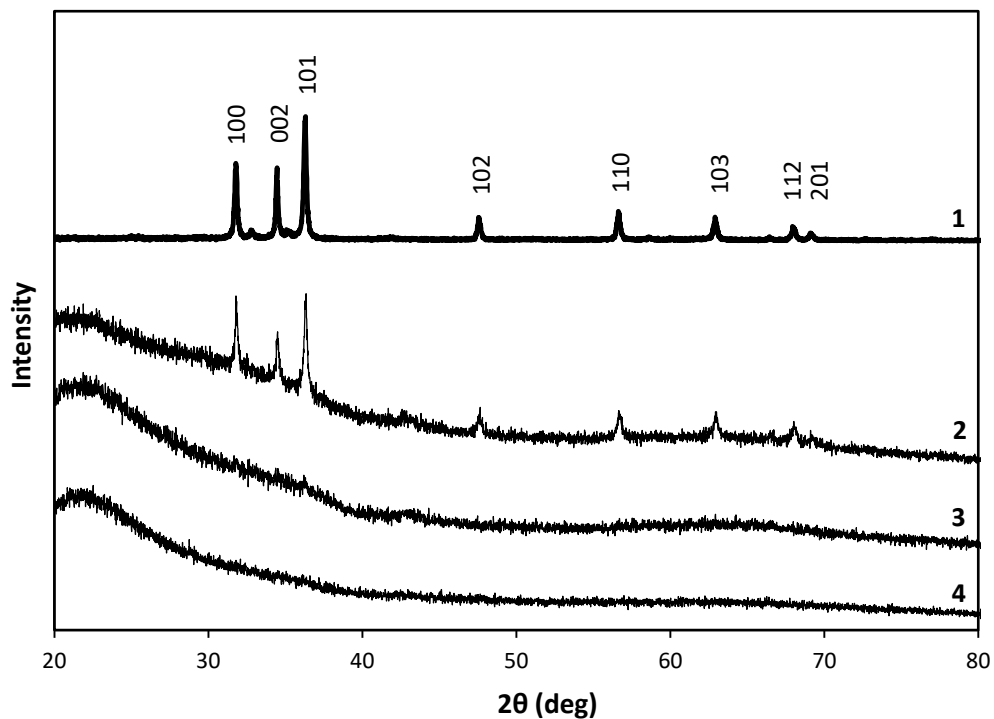


Figure 3.6. XRD patterns for ZnO catalysts (CuK α radiation): (1) bulk ZnO, (2) 30%ZnO/SiO₂, (3) 20%ZnO/SiO₂ and (4) 10%ZnO/SiO₂. Aerosil 300 was used as a support.

The acidity of the catalysts was characterised by DRIFT spectroscopy of adsorbed pyridine. Both bulk ZnO and all ZnO/SiO₂ catalysts gave a strong band at 1450 cm⁻¹ (Figure 3.7), which indicates the presence of Lewis acid sites. The absence of the characteristic band at 1540 cm⁻¹ points to the absence of Brønsted acid sites capable of protonating pyridine [39]. This is in agreement with previous DRIFTS studies of ZnO catalysts [19,36–38].

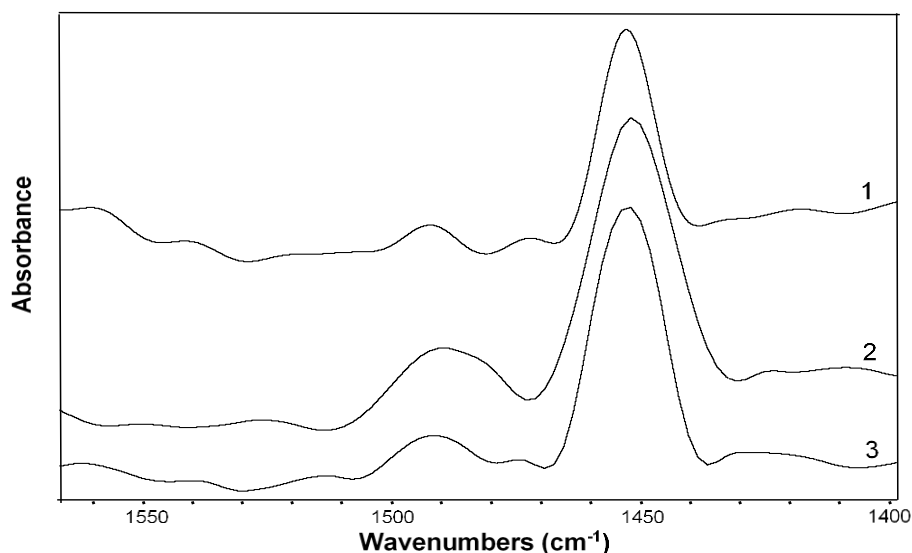


Figure 3.7. DRIFT spectra of adsorbed pyridine (powdered KBr mixtures vs. KBr): (1) bulk ZnO, (2) 10% ZnO/SiO₂(300), (3) 10% ZnO/SiO₂(750).

TGA data (Table 3.1) indicates the presence of silanol groups SiOH in the catalysts, which are weak Brønsted acid sites incapable of protonating pyridine. Figure 3.8 shows the DRIFT spectra of silica supports and 10% ZnO/SiO₂ catalysts in the region of OH stretching modes of silanol groups. In the DRIFT spectra of SiO₂ supports (Figure 3.8 A), the sharp peak at 3742 cm⁻¹ is attributed to the free terminal silanol groups and the bands around 3636–3682 cm⁻¹ to the hydrogen-bonded vicinal silanols. The broad band in the 3100–3600 cm⁻¹ region is generally ascribed to silanol nests that consist of a number of silanol groups interacting through extended hydrogen bonding [40–42]. In ZnO/SiO₂ catalysts (Figure 3.8 B), the free terminal silanol groups and silanol nests are clearly present, whereas the hydrogen-bonded vicinal silanols are less pronounced. While being weak Brønsted acid sites, the silanol groups can isomerise α -pinene and limonene at 300 °C, as demonstrated previously [1,25].

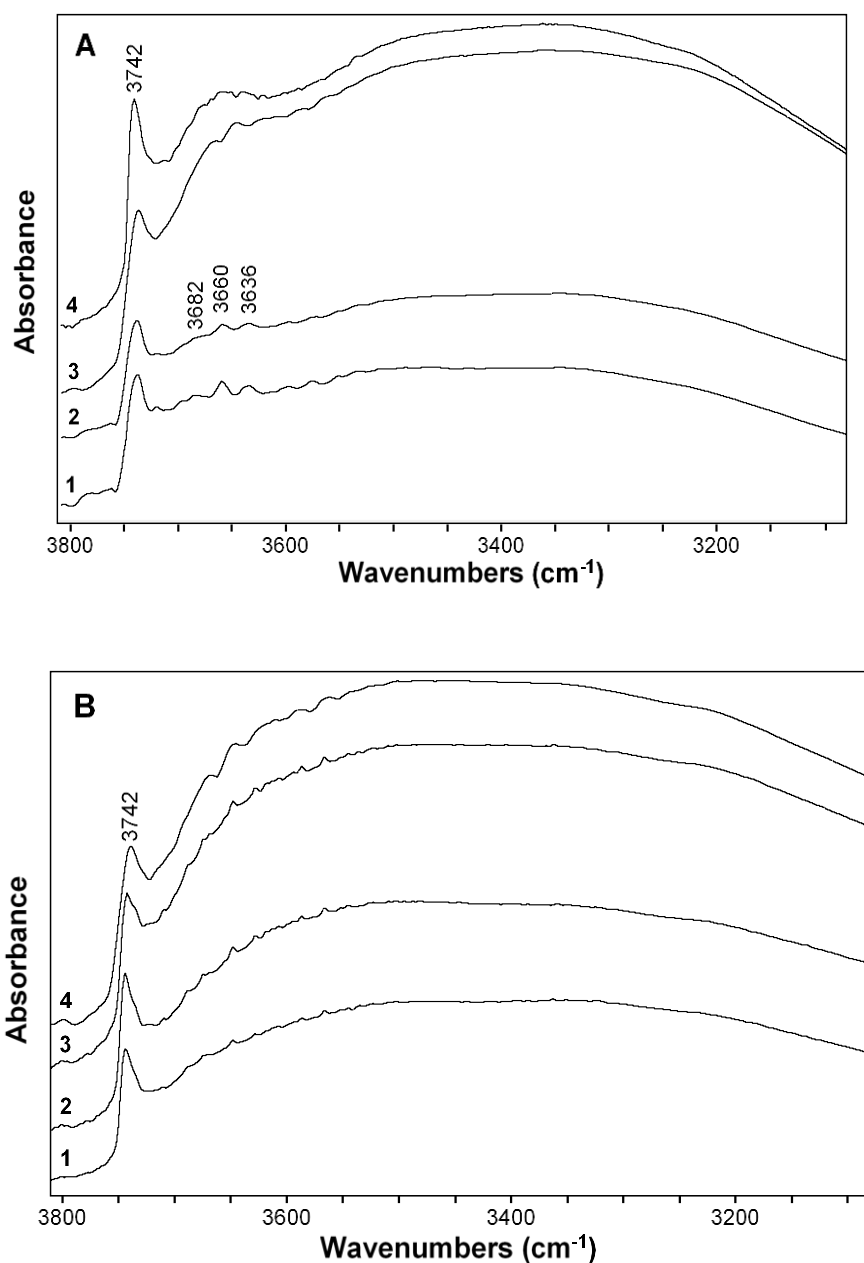


Figure 3.8. DRIFT spectra of SiO₂ supports (A) and 10%ZnO/SiO₂ catalysts (B) calcined at 400 °C in air for 2 h (powdered KBr mixtures vs. KBr). Support surface area (m² g⁻¹): (1) 200, (2) 300, (3) 600 and (4) 750.

3.1.2. Dehydroisomerisation of α -pinene

Table 3.2 shows the results of initial testing of ZnO/SiO₂(300) catalysts (Aerosil 300 support) in α -pinene dehydroisomerisation. Among silica supports used, Aerosil 300 gave the

best catalyst performance (see Table 3.3 below). The reaction was carried out for 5 h time on stream (TOS) at 370 °C and a weight hourly space velocity $WHSV = 0.020 \text{ h}^{-1}$. ZnO loading in the catalysts was varied from 5 to 30 wt%. As seen, ZnO/SiO₂(300) catalysts exhibit high activity and high p-cymene selectivity, with α -pinene conversion varying between 98–100% and p-cymene selectivity between 82–88%. The loading of ZnO had a relatively small effect on catalyst performance. Yet 10%ZnO/SiO₂(300) showed a better performance among the catalysts tested, giving 88% p-cymene at 100% conversion (entry 4). The catalyst exhibited stable p-cymene selectivity for over 5 h TOS (Figure 3.9). Without ZnO, the silica support showed a high isomerisation activity, mainly producing limonene, camphene and other p-menthadiene isomers (the other) together with some cracking products (the lights) (entry 1). Notably, no p-cymene was formed on pure SiO₂ due to the lack of dehydrogenation ability of SiO₂. On the other hand, bulk ZnO did produce p-cymene, although with a relatively low selectivity of 52% (entry 2), which can be explained by the low surface area of bulk ZnO (Table 3.1). Physical mixture ZnO + SiO₂(300) (1:9 w/w) of the same composition as the silica-supported 10%ZnO/SiO₂(300) catalyst produced mainly p-menthadienes, with a small amount of p-cymene formed (21%, entry 5).

Table 3.2. Dehydroisomerisation of α -pinene to p-cymene over ZnO/SiO₂(300).^a

Entry	Catalyst	Conversion ^b (%)	Selectivity (%mol) ^b				
			Lights	Camphene	Limonene	p-Cymene	Other
1	SiO ₂ (300)	98	9	13	20	0	59
2	ZnO	98	8	5	0	52	35
3	5%ZnO/SiO ₂ (300)	100	10	0	0	86	4
4	10%ZnO/SiO ₂ (300)	100	12	0	0	88	0
5	ZnO+SiO ₂ (300) ^c	100	9	6	0	21	64
6	10%ZnO/SiO ₂ (300) ^d	100	16	1	0	83	1
7	15%ZnO/SiO ₂ (300)	99	14	0	0	83	3
8	20%ZnO/SiO ₂ (300)	99	10	1	0	83	6
9	30%ZnO/SiO ₂ (300)	98	13	1	0	82	4

^a 370 °C, 0.40 g catalyst, 0.48 kPa α -pinene partial pressure, 5 ml min⁻¹ flow rate, 4–6 h TOS, WHSV = 0.020 h⁻¹. ^b Average conversion and product selectivity over 5 h TOS. ^c Physical mixture of bulk ZnO and SiO₂ (1:9 w/w). ^d At 0.88 kPa α -pinene partial pressure, WHSV = 0.037 h⁻¹.

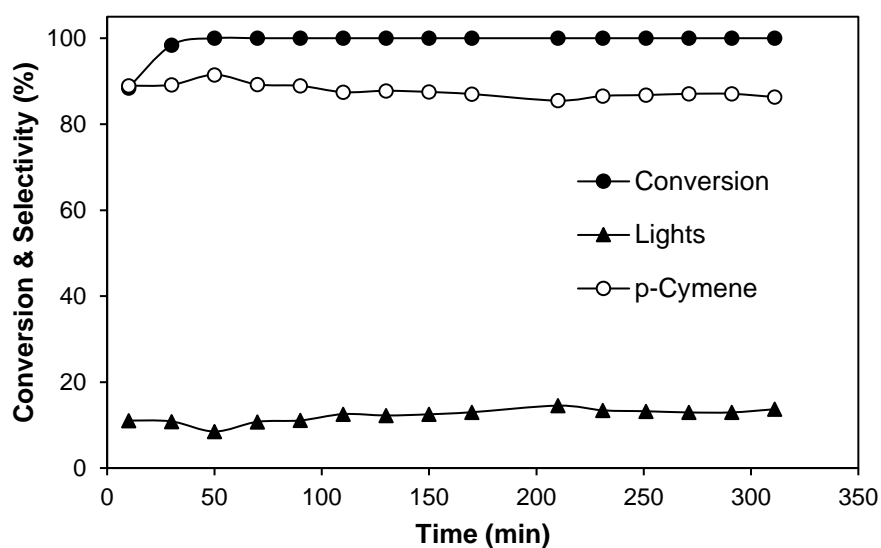


Figure 3.9. Time course for α -pinene dehydroisomerisation over 10%ZnO/SiO₂(300): 0.40 g catalyst, 370 °C, 0.48 kPa α -pinene partial pressure, 5 ml min⁻¹ flow rate, WHSV = 0.020 h⁻¹.

Figure 3.10 shows the effect of contact time, $(\text{WHSV})^{-1}$, on p-cymene selectivity in the presence of 10%ZnO/SiO₂(300) at 370 °C. The contact time was varied by changing the flow rate (5–50 ml min⁻¹) and catalyst amount (0.4–0.8 g). The conversion of p-cymene was 100% at such conditions. The results show that the selectivity increases monotonically with the contact time, as expected for a consecutive reaction (Scheme 3.1), reaching a plateau at 90% at a contact time 50–100 h ($\text{WHSV} = 0.01\text{--}0.02 \text{ h}^{-1}$).

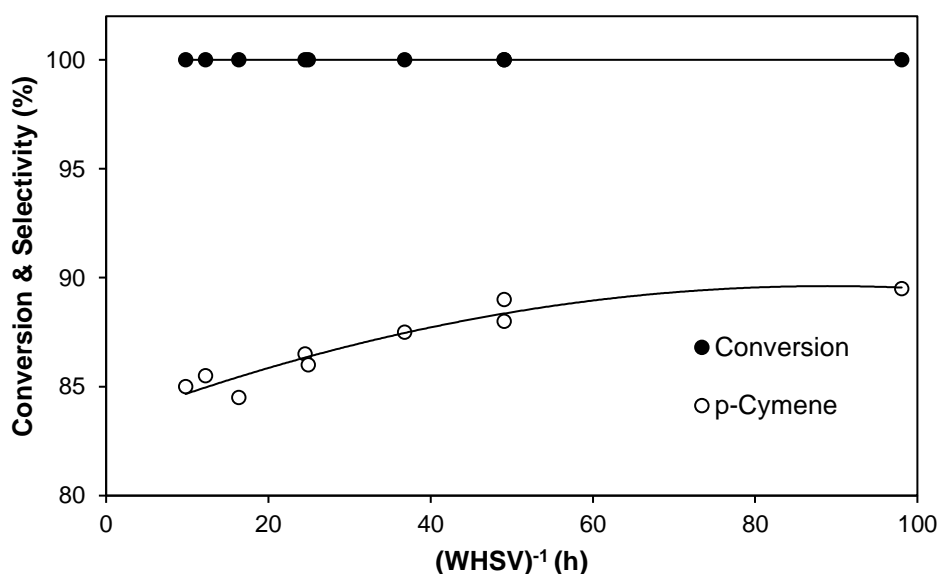


Figure 3.10. α -Pinene conversion and p-cymene selectivity over 10%ZnO/SiO₂(300) versus contact time at 370 °C and 0.48 kPa α -pinene partial pressure; the contact time varied by changing flow rate (5–50 ml min⁻¹) and catalyst amount (0.4–0.8 g).

Figure 3.11 demonstrates the effect of reaction temperature, varied between 200–400 °C, on p-cymene selectivity in the presence of 10%ZnO/SiO₂(300) at an optimum contact time of 98 h. At this contact time, the conversion of α -pinene was 100% within the temperature range studied. It can be seen that the selectivity to p-cymene increases with the temperature reaching 90% at 370 °C (90% p-cymene yield). At the same time, the selectivity to p-menthadienes (the other) decreases. These results are in agreement with the mechanism shown

in Scheme 3.1, where p-menthadienes are the intermediates to p-cymene, with the rate-limiting step of p-menthadiene dehydrogenation to form p-cymene [1]. Notably, the amount of the lights (cracking by-products) reduces as the temperature increases. This is not unexpected because the aromatic p-cymene should be more stable towards cracking than α -pinene and its isomers.

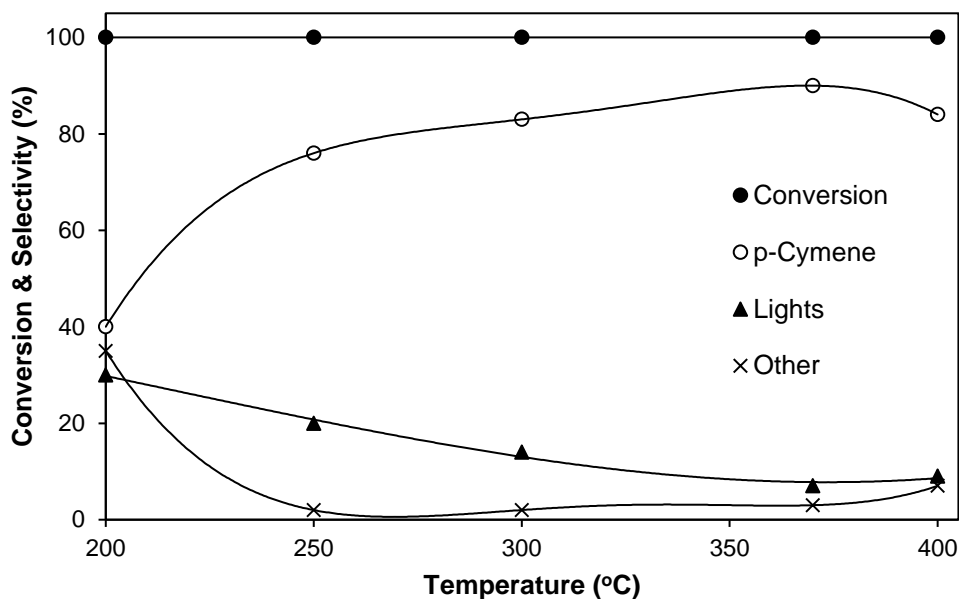


Figure 3.11. Effect of temperature on α -pinene dehydroisomerisation over 10%ZnO/SiO₂(300): 0.80 g catalyst, 0.48 kPa α -pinene partial pressure, 5 ml min⁻¹ flow rate, WHSV = 0.010 h⁻¹.

The performance of 10%ZnO/SiO₂ catalysts containing different SiO₂ supports with the surface area of 200–750 m²g⁻¹ is presented in Table 3.3 at the optimum temperature 370 °C and WHSV = 0.020 h⁻¹. 10%ZnO/SiO₂(300) showed the best performance (89% selectivity at 100% conversion) closely followed by 10%ZnO/SiO₂(200) (87% selectivity at 100% conversion). The catalysts 10%ZnO/SiO₂(600) and 10%ZnO/SiO₂(750) comprising large-area silicas (600–750 m² g⁻¹) were less efficient, giving 83% selectivity at 99% conversion. This could be the result of many factors such as catalyst pore structure, ZnO dispersion, density of

silanol groups, etc. Thus, the larger density of silanol groups (Brønsted acid sites) in 10%ZnO/SiO₂(600) and 10%ZnO/SiO₂(750) may be responsible for the larger amounts of cracking by-products (the lights) formed on these catalysts.

Table 3.3. Dehydroisomerisation of α -pinene to p-cymene over ZnO/SiO₂: effect of support.^a

Catalyst	Conversion ^b (%)	Selectivity (%mol) ^b				
		Lights	Camphene	Limonene	p-Cymene	Other
10%ZnO/SiO ₂ (200)	100	13	0	0	87	0
10%ZnO/SiO ₂ (300)	100	10	0	0	89	1
10%ZnO/SiO ₂ (600)	99	16	0	0	83	1
10%ZnO/SiO ₂ (750)	99	17	0	0	83	0

^a 370 °C, 0.80 g catalyst, 0.48 kPa α -pinene partial pressure, 10 ml min⁻¹ flow rate, 6 h TOS, WHSV = 0.020 h⁻¹. ^b Average conversion and product selectivity over 6 h TOS.

Figure 3.12 shows a longer-term test (72 h TOS) for α -pinene dehydroisomerisation over 10%ZnO/SiO₂(300) at 370 °C and WHSV = 0.020 h⁻¹. After 24 h on stream, the selectivity reduced from 89 to 83%, which was probably due to catalyst coking; 2.30% carbon deposition was found in the post reaction catalyst by combustion analysis (Table 3.4). The catalyst was regenerated in situ after 24 h TOS by air flow (10 ml min⁻¹) at 370 °C for 3 h, which allowed to restore catalyst activity. After 72 h TOS, with catalyst regeneration after each period of 24 h on stream, the average p-cymene selectivity was 85% at 100% α -pinene conversion.

Table 3.4. C and H combustion analysis for 10%ZnO/SiO₂ used in α -pinene dehydroisomerisation for a specified time on stream (TOS).

Catalyst	C (%)	H (%)
Fresh 10% ZnO/SiO ₂ (300)	-	0.30
Regenerated 10% ZnO/SiO ₂ (300)	0.01	0.20
Spent 10% ZnO/SiO ₂ (300) (4 h TOS)	0.90	0.40
Spent 10% ZnO/SiO ₂ (300) (24 h TOS)	2.30	0.30

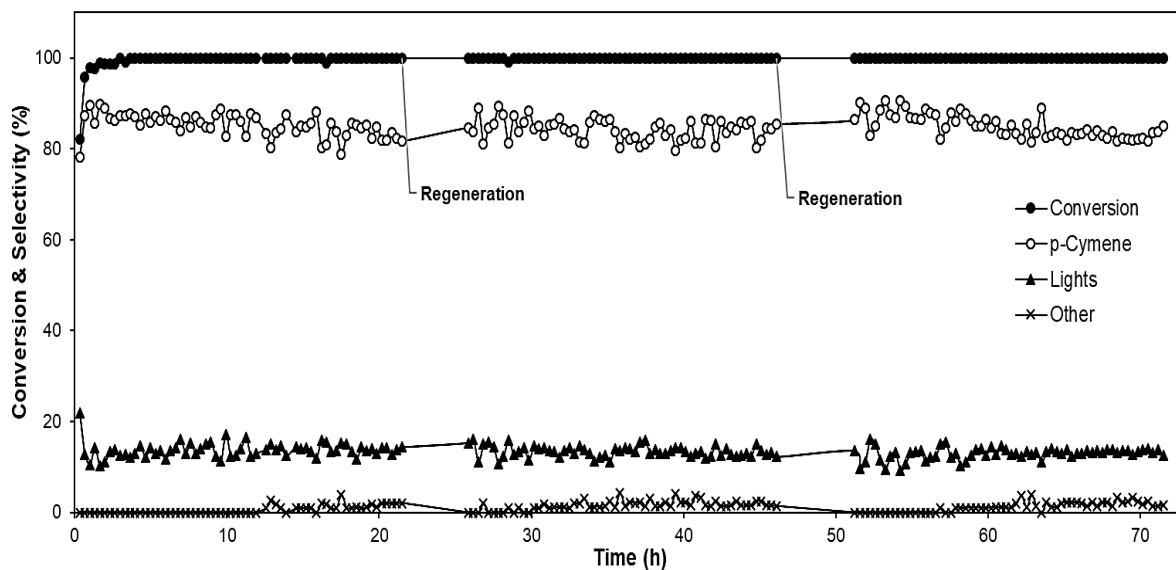


Figure 3.12. Long-term time course for α -pinene dehydroisomerisation over 10%ZnO/SiO₂(300) with catalyst regeneration: 0.80 g catalyst, 370 °C, 0.48 kPa α -pinene partial pressure, 10 ml min⁻¹ flow rate, WHSV = 0.020 h⁻¹; the catalyst regenerated in situ by air flow (10 ml min⁻¹) at 370 °C for 3 h. Average p-cymene selectivity 85% at 100% p-cymene conversion over 70 h TOS.

In summary, the developed ZnO/SiO₂ catalyst has a high activity and selectivity in one-step α -pinene-to-p-cymene dehydroisomerisation, providing 90% p-cymene yield at 100% α -pinene conversion at 370 °C and WHSV = 0.01–0.02 h⁻¹ (Figure 3.11). In terms of p-cymene yield, it outperforms the catalysts reported previously such as Pd/SiO₂ [1], Pd-Zn/Al-SBA-15 [18] and bulk Zn(II)–Cr(III) mixed oxide [19]. Although the reported catalysts operate at lower temperatures 300–350 °C, they provide considerably lower p-cymene yields. Thus, the supported Pd catalysts operate at 300 °C to yield 67–77% p-cymene; moreover, they require continuous hydrogen supply to prevent catalyst deactivation [1,18]. In contrast, the noble-metal-free Zn/SiO₂ gives stable performance without hydrogen supply and can be regenerated in situ by air at the reaction temperature.

3.1.3. Dehydroisomerisation of limonene

Limonene-to-p-cymene dehydroisomerisation occurs easier and generally with higher p-cymene yields than the reaction of α -pinene because it does not involve C–C bond breaking (Scheme 3.2). In the limonene dehydroisomerisation, ZnO/SiO₂ was found to be a highly effective catalyst, as in the case of α -pinene.

Table 3.5 shows the effect of ZnO loading (5–30 wt%) on limonene conversion and p-cymene selectivity in the presence of ZnO/SiO₂(300) at 300 °C and WHSV = 0.080 h⁻¹. As seen, the reaction occurs practically with 100% limonene conversion regardless of ZnO loading. The catalysts exhibited stable p-cymene selectivity for over 4 h TOS (Figure 3.13). The selectivity to p-cymene increased with ZnO loading reaching 98% with 30%ZnO/SiO₂(300). This is different from the reaction of α -pinene, where the optimal ZnO loading was at 10 wt% (Table 3.2). This difference could be due to the lower reaction temperature – 300 °C for limonene and 370 °C for α -pinene – hence the higher loading of dehydrogenation component ZnO is required for limonene-to-p-cymene conversion. Clearly, the reaction of limonene goes much easier than that of α -pinene, which can be seen not only from the lower reaction temperature but also from a 4-fold shorter contact time.

Table 3.5. Dehydroisomerisation of limonene to p-cymene over ZnO/SiO₂(300).^a

Catalyst	Conversion ^b (%)	Selectivity (%mol) ^b				
		Camphene	β -Pinene	α -Terpinene	p-Cymene	Terpinolene
5%ZnO/SiO ₂ (300)	>99	6	6	3	84	1
10%ZnO/SiO ₂ (300)	>99	1	2	0	97	0
20%ZnO/SiO ₂ (300)	100	0	3	0	97	0
30%ZnO/SiO ₂ (300)	100	0	2	0	98	0

^a 0.20 g catalyst, 300 °C, 10 ml min⁻¹ flow rate, 0.47 kPa limonene partial pressure, WHSV = 0.080 h⁻¹, 4 h TOS. ^b Average conversion and product selectivity over 4 h TOS.

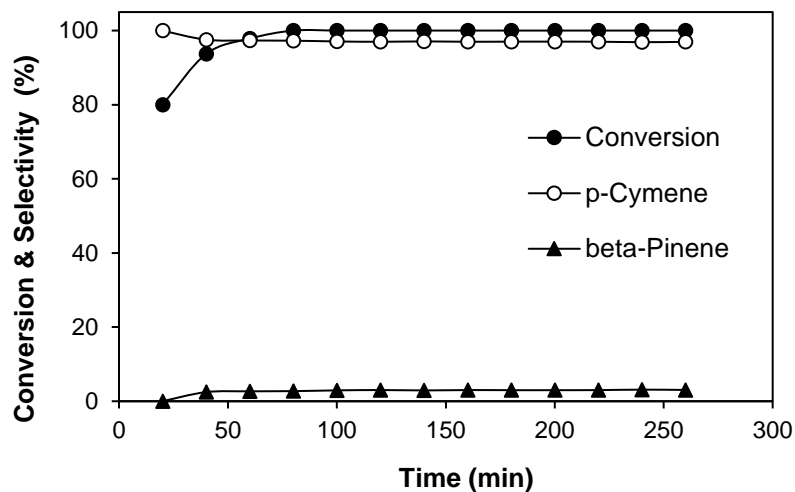


Figure 3.13. Time course for limonene dehydroisomerisation over 20%ZnO/SiO₂(300): 0.20 g catalyst, 300 °C, 0.47 kPa limonene partial pressure, 10 ml min⁻¹ flow rate, WHSV = 0.080 h⁻¹.

Figure 3.14 shows the effect of contact time, (WHSV)⁻¹, on limonene conversion and the selectivity to p-cymene and α -terpinene in the presence of 30%ZnO/SiO₂(300) at 275 °C. The contact time was varied by changing the flow rate from 10 to 50 ml min⁻¹. The results show that limonene conversion and p-cymene selectivity increase with the contact time reaching 98% p-cymene selectivity at 100% limonene conversion at a contact time of 12 h. As seen, the selectivity to p-cymene increases at the expense of α -terpinene, which indicates that α -terpinene is the main reaction intermediate in agreement with the mechanism shown in Scheme 3.2.

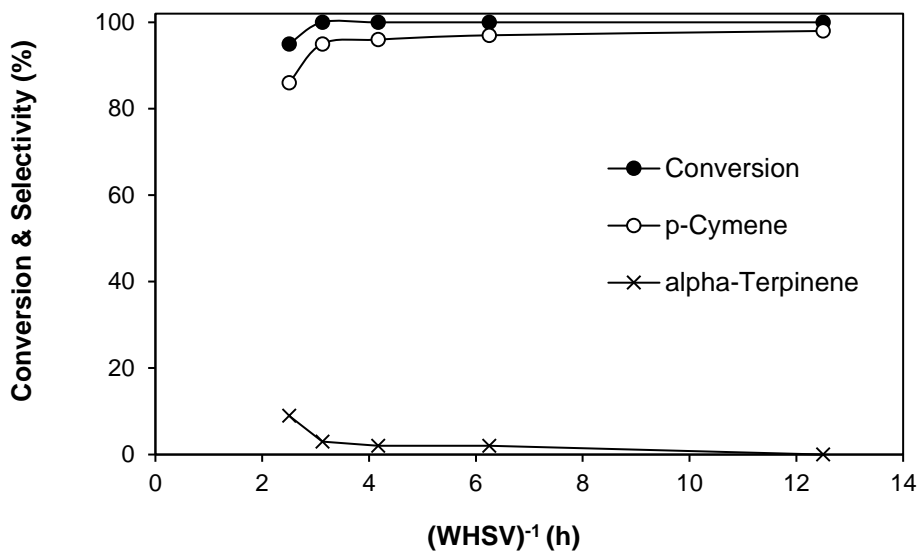


Figure 3.14. Limonene conversion and product selectivity over 30%ZnO/SiO₂(300) (0.20 g) versus contact time at 275 °C and 0.47 kPa limonene partial pressure; the contact time varied by changing the flow rate (10–50 ml min⁻¹).

Figure 3.15 shows the effect of temperature on p-cymene selectivity in the presence of 20%ZnO/SiO₂(300) and 30%ZnO/SiO₂(300) in the range of 275–350 °C at WHSV = 0.080 h⁻¹. For both catalysts, the conversion of limonene was 100% within this temperature range. It can be seen that the selectivity increases monotonically with the temperature, reaching 100% at 325 °C for 30%ZnO/SiO₂(300) (100% p-cymene yield). These results are in agreement with the mechanism shown in Scheme 3.2, with the rate-limiting step of p-menthadiene dehydrogenation.

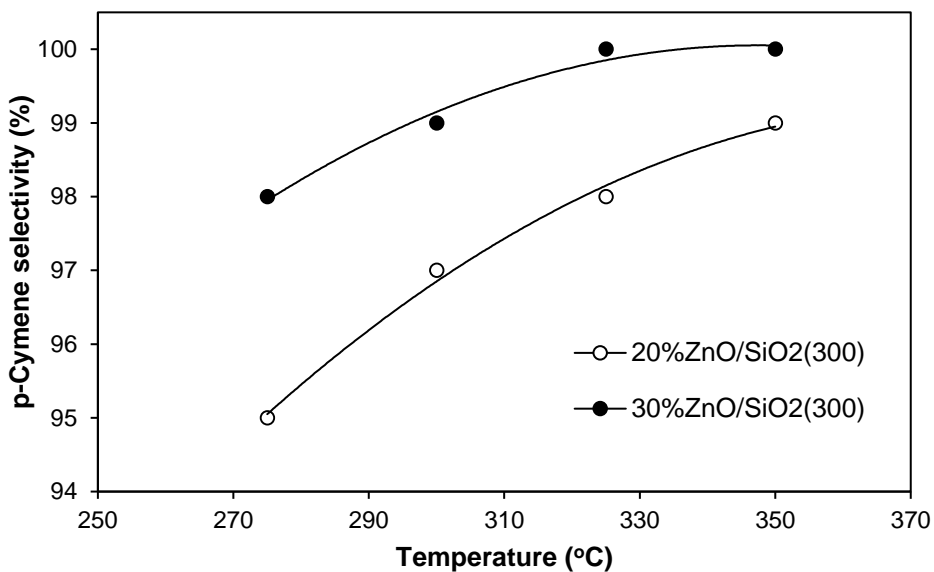


Figure 3.15. Effect of temperature on limonene dehydroisomerisation over 20%ZnO/SiO₂(300) and 30%ZnO/SiO₂(300): 0.20 g catalyst, 0.47 kPa limonene partial pressure, 10 ml min⁻¹ flow rate, 4 h TOS, WHSV = 0.080 h⁻¹; 100% limonene conversion in all cases.

The best reported catalyst for the gas-phase dehydroisomerisation of limonene so far, Pd/SiO₂, provides 99% yield of p-cymene at 300 °C, however, requires continuous hydrogen supply to prevent catalyst deactivation [25]. Our noble-metal-free ZnO/SiO₂ catalyst gives 100% p-cymene yield at 325 °C and exhibits stable performance without hydrogen supply.

3.2. Conclusions

ZnO supported on silica is a highly efficient, noble-metal-free bifunctional catalyst for the environment-friendly synthesis of p-cymene by the gas-phase dehydroisomerisation of α -pinene and limonene. Dehydroisomerisation of α -pinene over ZnO/SiO₂ produces p-cymene with 90% yield at 100% conversion at 370 °C and a contact time WHSV = 0.01–0.020 h⁻¹. The

reaction with limonene gives a 100% p-cymene yield at 325 °C and WHSV = 0.080 h⁻¹.

ZnO/SiO₂ catalyst shows stable performance for over 70 h without co-feeding hydrogen.

References

- [1] D. M. Roberge, D. Buhl, J. P. M. Niederer, W. F. Hölderich, Catalytic aspects in the transformation of pinenes to p-Cymene, *Appl.Catal. A Gen.* 215 (2001) 111–124.
- [2] K. Weissermel, H. J. Arpe, *Industrial Organic Chemistry*, 4th ed., Wiley-VCH: Weinheim, Germany, 2003.
- [3] F. Neatu, G. Culica, M. Florea, V. I. Parvulescu, F. Cavani, Synthesis of terephthalic acid by p-Cymene oxidation using oxygen: Toward a more sustainable production of bio-polyethylene terephthalate, *ChemSusChem* 9 (2016) 3102–3112.
- [4] W. F. Erman, *Chemistry of the Monoterpenes: An Encyclopedic Handbook*; M. Dekker, New York, NY, USA, 1985.
- [5] A. Severino, A. Esculcas, J. Rocha, J. Vital, L. S. Lobo, Effect of extra-lattice aluminium species on the activity, selectivity and stability of acid zeolites in the liquid phase isomerisation of α -pinene, *Appl. Catal. A Gen.* 124 (1996) 255–278.
- [6] G. Gunduz, R. Dimitrova, S. Yilmaz, L. Dimotrov, Liquid phase transformation of α -pinene over Beta zeolites containing aluminium or boron, titanium and vanadium as lattice ions, *Appl. Catal. A Gen.* 282 (2005) 61–65.
- [7] R. Rachwalik, Z. Olejniczak, J. Jiao, J. Huang, M. Hunger, B. Sulikowski, Isomerization of α -pinene over dealuminated ferrierite-type zeolites, *J. Catal.* 252 (2007) 161–170.
- [8] M. K. Yadav, C. D. Chudasama, R. V. Jasra, Isomerisation of α -pinene using modified montmorillonite clays, *J. Mol. Catal. A Gen.* 216 (2004) 51–59.
- [9] C. Volzone, O. Masini, N. A. Comelli, L. M. Grzona, E. N. Ponzi, M. I. Ponzi, α -Pinene conversion by modified-kaolinitic clay, *Mater. Chem. Phys.* 93 (2005) 296–300.
- [10] N. A. Comelli, E. N. Ponzi, M. I. Ponzi, α -Pinene isomerization to camphene: Effect of thermal treatment on sulfated zirconia, *Chem. Eng. J.* 117 (2006) 93–99.
- [11] O. Chimal-Valencia, A. Robau-Sanchez, V. Collins-Martinez, A. Aguilar Elguezabal, Ion exchange resins as catalyst for the isomerization of α -pinene to camphene, *Bioresour. Technol.* 93 (2004) 119–123.
- [12] N. A. Comelli, L. M. Grzona, O. Masini, E. N. Ponzi, M. I. Ponzi, Obtention of camphene with $H_3PW_{12}O_{40}$ catalysts supported on TiO_2 , SiO_2 and $ZrO_2 \cdot nH_2O$, *J. Chil. Chem. Soc.* 49 (2004) 245–250.

- [13] A. D. Newman, A. F. Lee, K. Wilson, N. A. Young, On the active site in $\text{H}_3\text{PW}_{12}\text{O}_{40}/\text{SiO}_2$ catalysts for fine chemical synthesis, *Catal. Lett.* 102 (2005) 45–50.
- [14] K. A. Da Silva Rocha, P. A. Robles-Dutenhefner, I. V. Kozhevnikov, E. V. Gusevskaya, Phosphotungstic heteropoly acid as efficient heterogeneous catalyst for solvent-free isomerization of α -pinene and longifolene, *Appl. Catal. A Gen.* 35 (2009) 188–192.
- [15] A. Alsalmé, E. F. Kozhevnikova, I. V. Kozhevnikov, α -Pinene isomerisation over heteropoly acid catalysts in the gas-phase, *Appl. Catal. A Gen.* 390 (2010) 219–224.
- [16] A. Stanislaus, L. M. Yeddanapalli, Vapor phase catalytic transformations of terpene hydrocarbons in the $\text{C}_{10}\text{H}_{16}$ series II. Aromatization of α -pinene over chromia-alumina, *Can. J. Chem.* 50 (1972) 113–118.
- [17] J. A. Linnekoski, M. Asikainen, H. Heikkinen, R. K. Kaila, J. Rasanen, A. Laitinen, A. Harlin, Production of p-Cymene from crude sulphate turpentine with commercial zeolite catalyst using a continuous fixed bed reactor, *Org. Process. Res. Dev.* 18 (2014) 1468–1475.
- [18] M. Golets, S. Ajaikumar, M. Mohln, J. Wärna, S. Rakesh, J. -P. Mikkola, Continuous production of the renewable p-cymene from α -pinene, *J. Catal.* 307 (2013) 305–315.
- [19] F. Al-Wadaani, E. F. Kozhevnikova, I. V. Kozhevnikov, Zn(II)–Cr(III) mixed oxide as efficient bifunctional catalyst for dehydroisomerisation of α -pinene to p-cymene, *Appl. Catal. A Gen.* 363 (2009) 153–156.
- [20] A. Satira, C. Espro, E. Paone, P. Calabrò, M. Pagliaro, R. Ciriminna, F. Mauriello, The limonene biorefinery: From extractive technologies to its catalytic upgrading into p-Cymene, *Catalysts* 11 (2021) 387.
- [21] M. Retajczyk, A. Wróblewska, Isomerization and dehydroaromatization of R-(+)-limonene over the Ti-MCM-41 catalyst: Effect of temperature, reaction time and catalyst content on product yield, *Catalysts* 508 (2019) 508.
- [22] H. Cui, J. Zhang, Z. Luo, C. Zhao, Mechanisms into dehydroaromatization of bioderived limonene to p-Cymene over Pd/HZSM-5 in the presence and absence of H_2 , *RSC Adv.* 6 (2016) 66695–66704.
- [23] E. Yilmazoglu, M. Akgün, p-Cymene production from orange peel oil using some metal catalyst in supercritical alcohols, *J. Supercrit. Fluids* 131 (2018) 37–46.

- [24] M. Kamitsou, G. D. Panagiotou, K. S. Triantafyllidis, K. Bourikas, A. Lycourghiotis, C. Kordulis, Transformation of α -limonene into p-cymene over oxide catalysts: A green chemistry approach, *Appl. Catal. A Gen.* 474 (2014) 224–229.
- [25] D. Buhl, D. M. Roberge, W. F. Hölderich, Production of p-Cymene from limonene over silica supported Pd catalysts, *Appl. Catal. A Gen.* 188 (1999) 287–299.
- [26] F. A. Cotton, G. Wilkinson, *Advanced Inorganic Chemistry*, 5th ed.; Wiley-Interscience: New York, NY, USA, 1988.
- [27] F. Monda, R. Madsen, Zinc oxide-catalyzed dehydrogenation of primary alcohols into carboxylic acids, *Chem. Eur. J.* 24 (2018) 17832–17837.
- [28] H. M. Tasdemir, S. Yasyerli, N. Yasyerli, Selective catalytic oxidation of H₂S to elemental sulfur over titanium based Ti-Fe, Ti-Cr and Ti-Zr catalysts, *Int. J. Hydrogen Energy* 40 (2015) 9989–10001.
- [29] K. Kaneko, Determination of pore size and pore size distribution 1. Adsorbents and catalysts, *J. Memb. Sci.* 96 (1994) 59–89.
- [30] G. Leofanti, M. Padovan, G. Tozzola, B. Venturelli, Surface area and pore texture of catalysts, *Catal. Today* 41 (1998) 207–219.
- [31] K. S. W. Sing, Characterization of porous materials: past, present and future, *Colloids Surfaces A Physicochem. Eng. Asp.* 241 (2004) 3–7.
- [32] R. M. Gabr, M. M. Girgis, A. M. El-Awad, B. M. Abou-Zeid, Effect of spinel (ZnCr₂O₄) formation on the texture, electrical conduction and catalytic behaviour of the ZnO-Cr₂O₃ system, *Mater. Chem. Phys.* 39 (1994) 53–62.
- [33] M. S. M. Al-Ghamdi, H. Bayahia, Zinc-Chromium oxide catalyst for gas-phase ketonisation of pentanoic acid, *Mediterr. J. Chem.* 6 (2017) 1–6.
- [34] B. S. Anandakumar, M. B. M. Reddy, K. V. Thipperudraiah, M. A. Pasha, G. T. Chandrappa, Combustion-derived CdO nanopowder as a heterogeneous basic catalyst for efficient synthesis of sulfonamides from aromatic amines using p- toluenesulfonyl chloride, *Chem. Pap.* 67 (2013) 135–144.

- [35] M. D. Arco, V. Rives, R. Trujillano, P. Malet, Thermal behaviour of Zn-Cr layered double hydroxides with hydrotalcite-like structures containing carbonate or decavanadate, *J. Mater. Chem.* 6 (1996) 1419–1428.
- [36] F. Al-Wadaani, E. F. Kozhevnikova, I. V. Kozhevnikov, Pd supported on Zn(II)–Cr(III) mixed oxide as a catalyst for one-step synthesis of methyl isobutyl ketone, *J. Catal.* 257 (2008) 199–205.
- [37] V. V. Costa, H. Bayahia, E. F. Kozhevnikova, E. V. Gusevskaya, I. V. Kozhevnikov, Highly active and recyclable metal oxide catalysts for the Prins condensation of biorenewable feedstocks, *ChemCatChem* 6 (2014) 2134–2139.
- [38] H. Bayahia, E. F. Kozhevnikova, I. V. Kozhevnikov, Ketonisation of carboxylic acids over Zn-Cr oxide in the gas phase, *Appl. Catal. B Environ.* 165 (2015) 253–259.
- [39] H. Knözinger, Infrared Spectroscopy for The Characterization of Surface Acidity and Basicity. In *Handbook of Heterogeneous Catalysis*, 2nd ed.; G. Ertl, H. Knözinger, F. Schüth, J. Weitkamp, Eds., Wiley-VCH: Weinheim, Germany, 2008; Volume 2, p. 1138.
- [40] G. P. Heitmann, G. Dahlhoff, W. F. Hoelderich, Catalytically active sites for the Beckmann rearrangement of cyclohexanone oxime to ϵ -caprolactam, *J. Catal.* 186 (1999) 12–19.
- [41] K. Barbera, F. Bonino, S. Bordiga, T. V. W. Janssens, P. Beato, Structure–deactivation relationship for ZSM-5 catalysts governed by framework defects, *J. Catal.* 280 (2011) 196–205.
- [42] H. Bayahia, E. Kozhevnikova, I. V. Kozhevnikov, High catalytic activity of silicalite in gas-phase ketonisation of propionic acid, *Chem. Commun.* 49 (2013) 3842–3844.

Chapter 4. Dehydroisomerisation of β -pinene, α -terpinene, γ -terpinene and terpinolene over silica-supported ZnO in the gas phase

4. Introduction

This chapter describes the results of investigation of the dehydroisomerisation of β -pinene, as well as other common p-menthadienes (α -terpinene, γ -terpinene and terpinolene) over ZnO/SiO₂ catalysts. These monoterpenes are often missing from the literature relevant to p-cymene synthesis but are important components of industrial turpentine feedstocks. The dehydroisomerisation of β -pinene is likely to occur via a mechanism similar to that for the reaction of α -pinene (Scheme 5.1) since α - and β -pinene isomers have similar structures differing only in the position of the C=C double bond (Table 1.3). α -Terpinene, γ -terpinene and terpinolene can be expected to undergo dehydroisomerisation similar to limonene (Scheme 3.2), p-menthadienes isomers have the same structures differing only in the position of the C=C double bond (Table 1.3).

4.1. Results and discussion

4.1.1. Dehydroisomerisation of β -pinene

The dehydroisomerisation of β -pinene was studied in the presence of 10%ZnO/SiO₂ catalyst supported on Aerosil 300 ($S_{\text{BET}} \approx 300 \text{ m}^2 \text{ g}^{-1}$) and calcined at 400 °C, which showed the best performance in the reaction of α -pinene (Chapter 3). Table 4.1 shows representative results at different reaction temperatures from 200 to 400 °C. As seen, in the whole temperature range, β -pinene conversion was 100%. The reaction had stable product selectivity for over 4 h

TOS (Figure 4.1). The selectivity to p-cymene increases with increasing reaction temperature reaching a maximum of 100% at 400 °C. Figure 4.2 displays the effect of temperature on p-cymene selectivity in more detail, with the maximum selectivity at 400 °C. The main by-products were camphene and the lights; the amount of camphene and lights decreased with increasing the temperature (Table 4.1).

Table 4.1. Effect of temperature on β -pinene dehydroisomerisation over 10%ZnO/SiO₂.^a

Temp. (°C)	Conv. ^b (%)	Selectivity (%mol) ^b						
		Lights	α -Pinene	Camphene	α -Terpinene	ρ -Cymene	γ -Terpinene	Terpinolene
200	100	8	1	22	40	3	11	15
225	100	11	1	16	35	10	10	13
250	100	10	2	10	23	38	8	9
275	100	8	0	9	19	51	6	7
300	100	7	0	7	12	66	3	5
325	100	7	0	0	3	91	0	0
350	100	4	0	0	0	96	0	0
375	100	2	0	0	0	98	0	0
400	100	0	0	0	0	100	0	0

^a 0.20 g 10%ZnO/SiO₂ catalyst, 0.47 kPa β -pinene partial pressure, 10 ml min⁻¹ flow rate, WHSV = 0.08 h⁻¹. ^b Average conversion and product selectivity within 4 h TOS.

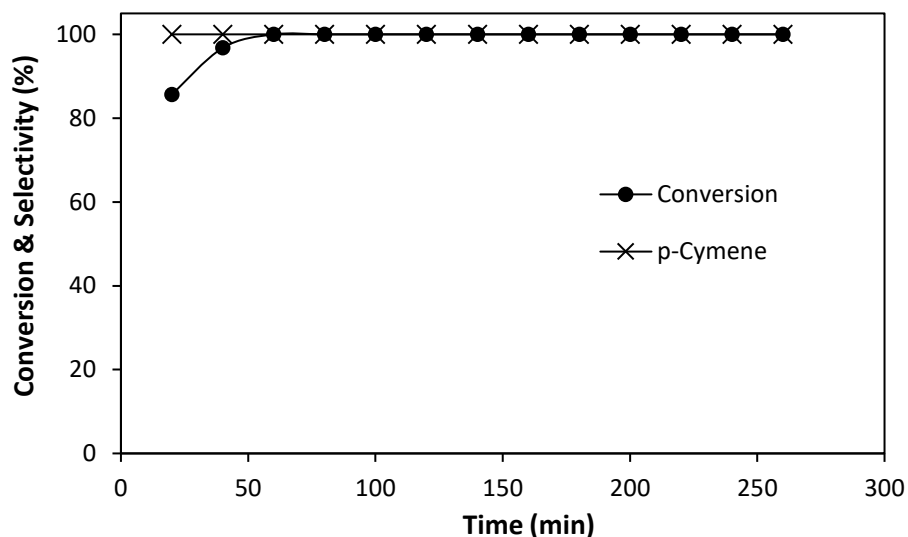


Figure 4.1. Time course for β -pinene dehydroisomerisation over 10%ZnO/SiO₂: 0.20 g catalyst, 400 °C, 0.47 kPa β -pinene partial pressure, 10 ml min⁻¹ flow rate, WHSV = 0.08 h⁻¹.

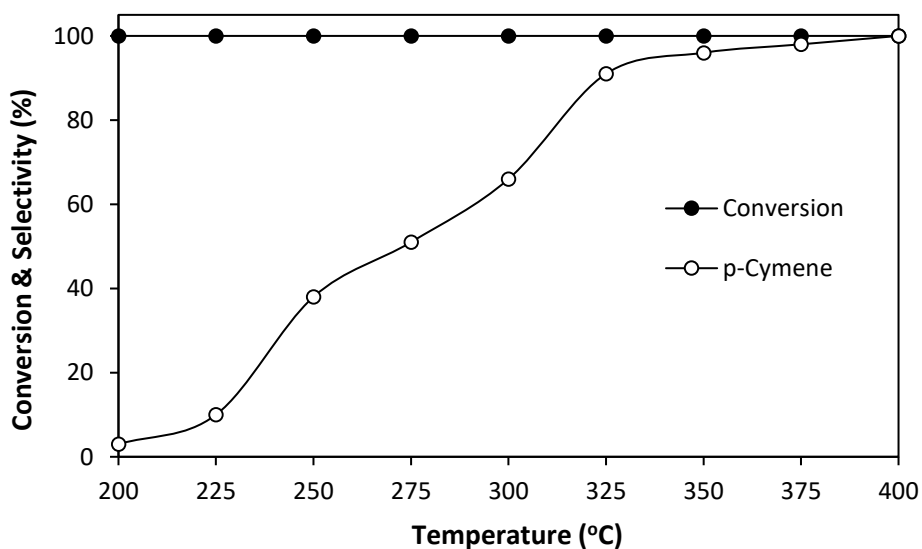


Figure 4.2. Effect of temperature on β -pinene dehydroisomerisation over 10%ZnO/SiO₂: 0.20 g catalyst, 0.47 kPa α -pinene partial pressure, 10 ml min⁻¹ flow rate, WHSV = 0.08 h⁻¹.

The selectivity to p-cymene was found to increase with increasing the contact time, (WHSV)⁻¹ (Figure 4.3), similar to the reaction of α -pinene. The contact time was varied at the

optimum temperature of 400 °C by changing the flow rate (5–20 ml min⁻¹) and catalyst amount (0.2–0.8 g) at a β -pinene partial pressure of 0.47 kPa. As can be seen, p-cymene selectivity levels off at contact time of 12 h, reaching 100% at 100% β -pinene conversion. Therefore, the dehydroisomerisation of β -pinene over ZnO/SiO₂ gives 100% p-cymene yield at 400 °C and WHSV = 0.08 h⁻¹. This is higher than the p-cymene yield obtained from α -pinene (90% at 370 °C), although achieved at a higher temperature.

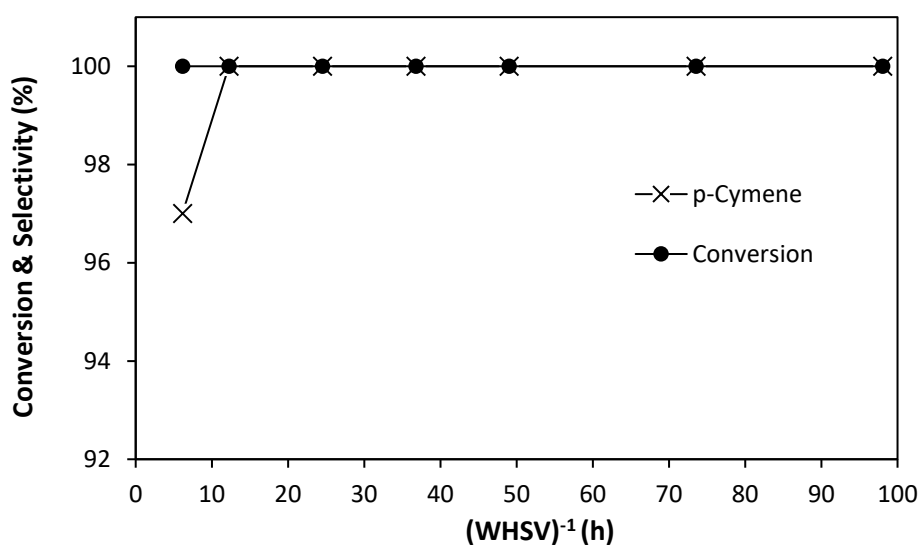


Figure 4.3. Plot of β -pinene conversion and p-cymene selectivity over 10% ZnO/SiO₂ versus contact time at 400 °C and 0.47 kPa β -pinene partial pressure; the contact time varied by changing flow rate (5–20 ml min⁻¹) and catalyst amount (0.2–0.8 g).

4.1.2. Dehydroisomerisation of α -terpinene, γ -terpinene, and terpinolene

The dehydroisomerisation of α -terpinene, γ -terpinene and terpinolene was studied using 30% ZnO/SiO₂ catalyst calcined at 400 °C, which gave the best performance in the reaction of limonene (Chapter 3). Table 4.2 shows the results for these substrates at 325 °C and WHSV = 0.08 h⁻¹. The results for limonene are also included for comparison. As expected, all these monoterpenes exhibit similar dehydrogenation activities at such conditions with a 100%

p-cymene yield. The time courses for α -terpinene, γ -terpinene and terpinolene are shown in Figures 4.4, 4.5 and 4.6, respectively. In all cases, an average monoterpene conversion is 100% within 4 h TOS, with a stable p-cymene selectivity at 100% for at least 4 h TOS.

Table 4.2. Dehydroisomerisation of monoterpenes to p-cymene over 30%ZnO/SiO₂.^a

Monoterpene	Conversion (%) ^b	Selectivity (%mol) ^b
Limonene	100	100
α -Terpinene	100	100
γ -Terpinene	100	100
Terpinolene	100	100

^a 0.20 g 30%ZnO/SiO₂ catalyst, 325 °C reaction temperature, 10 ml min⁻¹ flow rate, 0.47 kPa monoterpene partial pressure, WHSV = 0.08 h⁻¹, 4 h TOS. ^b Average conversion and product selectivity over 4 h TOS.

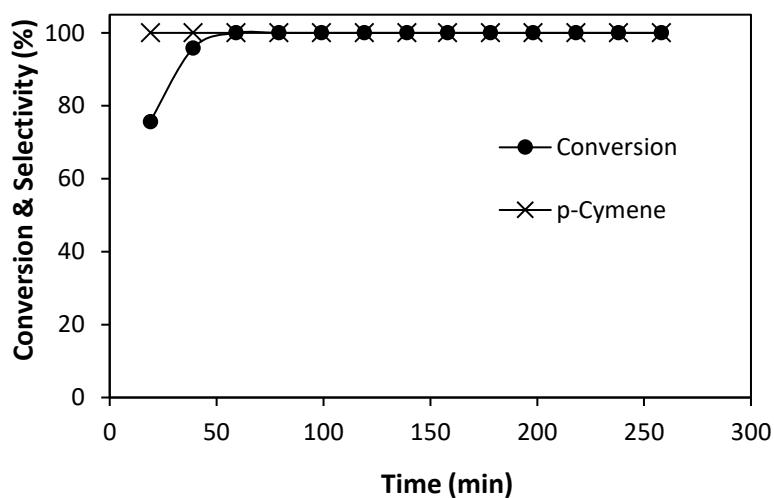


Figure 4.4. Time course for α -terpinene dehydroisomerisation over 30%ZnO/SiO₂: 0.20 g catalyst, 325 °C, 0.47 kPa α -terpinene partial pressure, 10 ml min⁻¹ flow rate, WHSV = 0.08 h⁻¹.

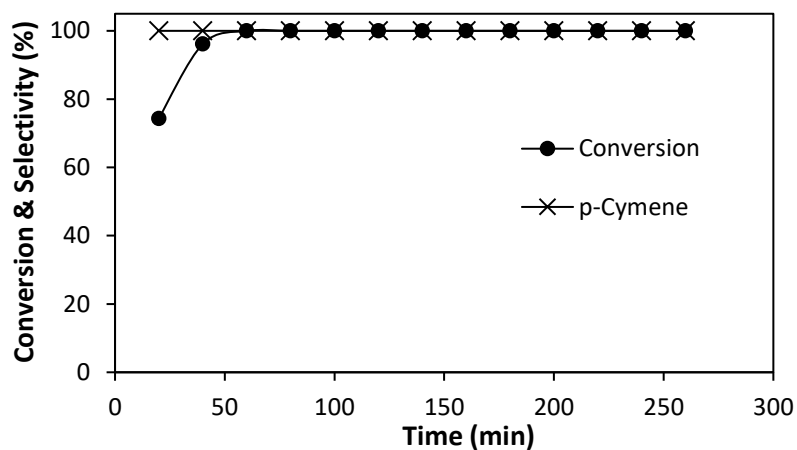


Figure 4.5. Time course for γ -terpinene dehydroisomerisation over 30%ZnO/SiO₂: 0.20 g catalyst, 325 °C, 0.47 kPa γ -terpinene partial pressure, 10 ml min⁻¹ flow rate, WHSV = 0.08 h⁻¹.

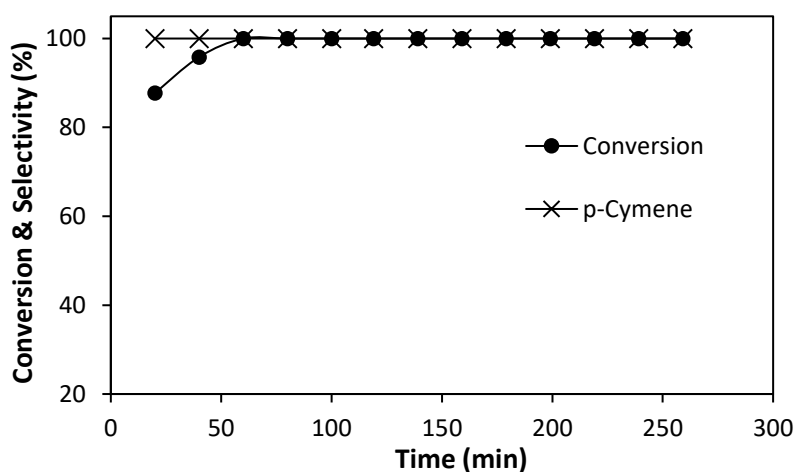


Figure 4.6. Time course for terpinolene dehydroisomerisation over 30%ZnO/SiO₂: 0.20 g catalyst, 325 °C, 0.47 kPa terpinolene partial pressure, 10 ml min⁻¹ flow rate, WHSV = 0.08 h⁻¹.

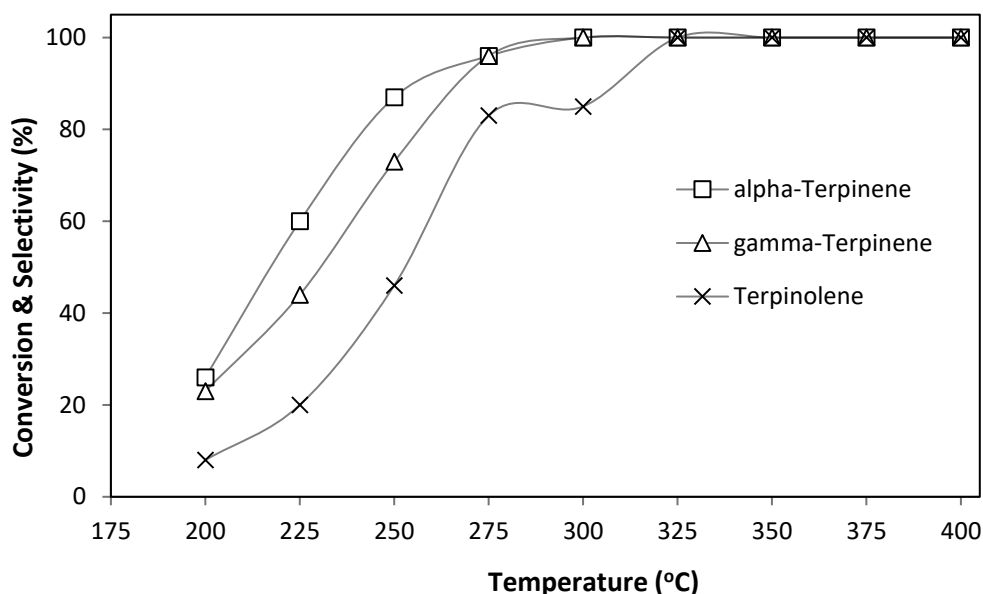


Figure 4.7. Effect of temperature on p-cymene yield in monoterpene dehydroisomerisation over 30%ZnO/SiO₂: 0.20 g catalyst, 0.47 kPa monoterpene partial pressure, 10 ml min⁻¹ flow rate, 4 h TOS, WHSV = 0.08 h⁻¹.

Figure 4.7 shows the effect of reaction temperature on p-cymene yield in dehydroisomerisation of α -terpinene, γ -terpinene and terpinolene in the temperature range of 200–400 °C at a space velocity WHSV = 0.08 h⁻¹. It can be seen that α -terpinene and γ -terpinene reach 100% yield already at 300 °C, whereas for terpinolene this yield is reached at 325 °C and remains at this level at least up to 400 °C. Figure 4.8 shows the effect of contact time on terpinolene conversion and p-cymene selectivity at 325 °C. As seen, the reaction occurs with a 100% p-cymene yield at 6–100 h contact time.

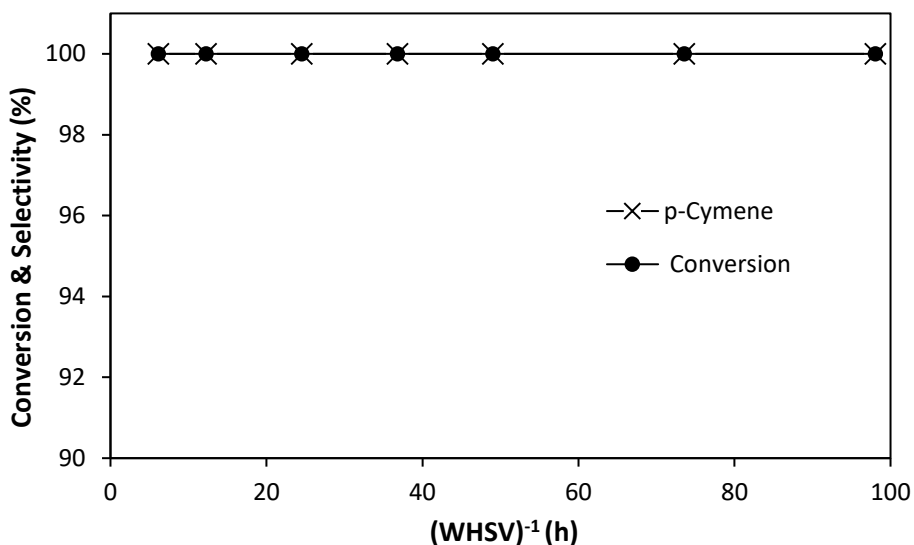


Figure 4.8. Plot of terpinolene conversion and p-cymene selectivity over 30%ZnO/SiO₂ versus contact time at 325 °C and 0.47 kPa terpinolene partial pressure; the contact time varied by changing the flow rate (5–20 ml min⁻¹) and catalyst weight (0.2–0.8 g).

4.2. Conclusions

As shown in Chapter 3, the dehydroisomerisation of α -pinene over ZnO/SiO₂ produces p-cymene with 90% yield at 100% conversion at 370 °C and a space velocity WHSV = 0.02 h⁻¹ [1]. The dehydroisomerisation of β -pinene over ZnO/SiO₂ gives 100% p-cymene yield at 400 °C and WHSV = 0.08 h⁻¹. Therefore, compared to α -pinene, the reaction of β -pinene allows for producing a higher p-cymene yield at a higher space velocity, although it was achieved at a higher temperature.

As expected, the dehydroisomerisation of α -terpinene, γ -terpinene and terpinolene over ZnO/SiO₂ occurred similarly to the reaction of limonene. The reaction with limonene gives a 100% p-cymene yield at 325 °C and WHSV = 0.08 h⁻¹ (Chapter 3) [1]. The reaction with α -terpinene, γ -terpinene and terpinolene gives 100% p-cymene yield at 300–325 °C and WHSV = 0.08–0.16 h⁻¹.

References

- [1] A. Alsharif, N. Smith, E. F. Kozhevnikova, I. V. Kozhevnikov, Dehydroisomerisation of α -pinene and limonene to p-cymene over silica-supported ZnO in the gas phase, *catalysts* 11 (2021) 1245.

Chapter 5. Dehydroisomerisation of cyclic monoterpenes to p-cymene over silica-supported CdO in the gas phase

5. Introduction

Catalytic conversion of renewable terpene feedstocks into value-added chemicals has long been an area of considerable interest [1–5]. In the past two decades, it has become one of the priority directions for sustainable development [6–17]. In this context, our work is concerned with the development of new, more efficient catalysts for sustainable synthesis of p-cymene, which has many uses, from medical and cosmetic products to manufacturing commodity chemicals [17]. The major application of p-cymene is for the synthesis of p-cresol, an intermediate in the manufacturing of antioxidants [18]. Selective oxidation of the bio-derived p-cymene is contemplated as a sustainable route to terephthalic acid ([14–16] and references therein). Traditionally, p-cymene is produced from petroleum-based feedstocks by the Friedel-Crafts alkylation of toluene by propene [17], with an adverse effect on the environment. An alternative environment-friendly route to p-cymene utilises dehydroisomerisation of renewable monoterpene feedstocks, such as α -pinene and limonene, using bifunctional heterogeneous catalysis [17]. These monoterpenes are obtained from abundantly available low-cost resources such as turpentine oils, crude sulfate turpentine, and citrus fruits [17,19,20].

The dehydroisomerisation of α -pinene to p-cymene occurs over acid-redox bifunctional catalysts at the gas-solid interface at 300–460 °C and atmospheric pressure. First, α -pinene is isomerised on acid sites to form monocyclic p-menthadienes together with bicyclic and

tricyclic terpenes; this follows by p-menthadiene dehydrogenation on metal or oxo-metal sites [17] (Scheme 3.1). It is suggested that the isomerisation proceeds through protonation of the C=C bond of α -pinene to generate pinanyl cation. The latter rearranges to bicyclic and tricyclic terpenes, such as camphene, β -pinene, and tricyclene, and to monocyclic terpenes (p-menthadienes), such as limonene, terpinolene, terpinene, etc. (Scheme 3.1) [17]. The formation of bicyclic and tricyclic terpenes is favored at lower temperatures, while p-menthadienes appear at higher temperatures [17]. In the dehydroisomerisation of α -pinene to p-cymene, p-menthadiene dehydrogenation is likely to be the rate-limiting step, with the isomerisation step probably being at quasi-equilibrium [17]. Many heterogeneous catalysts have been disclosed for α -pinene dehydroisomerisation [17,21–25]. Among them are Cr₂O₃/Al₂O₃ (390–460 °C, 53% p-cymene yield) [22], zeolite Y (300 °C, 54% yield) [23], Pd/SiO₂ (300 °C, 67% yield) [17], Pd-Zn/Al-SBA-15 (300 °C, 77% yield) [24], and bulk Zn(II)–Cr(III) mixed oxide (350 °C, 78% yield) [25]. Pd catalysts require hydrogen supply to prevent their deactivation [17].

The dehydroisomerisation of limonene to p-cymene is easier than the reaction of α -pinene. This is because the reaction of limonene does not involve C–C bond breaking. The dehydroisomerisation of limonene to p-cymene probably proceeds via a bifunctional mechanism, which involves fast limonene isomerisation on acid sites followed by slow dehydrogenation on metal or oxo-metal sites of bifunctional catalyst [26–39] (Scheme 3.2). The dehydroisomerisation of limonene can be carried out in the gas or liquid phase in the presence of various heterogeneous catalysts [27–39]. These include Ti/SBA-15 (liquid phase, 160 °C, 56% p-cymene yield) [28], Pd/HZSM-5 (liquid phase, 260 °C, 8 bar, 82% yield) [29], Pd/Al₂O₃ (supercritical ethanol, 300 °C, 65 bar, 80% yield) [30], TiO₂ (gas phase, 300 °C, 90% yield) [31], Pd/SiO₂ (gas phase, 300 °C, in H₂ flow, 99% yield) [32], and others [27]. Pd/SiO₂ gives the highest yield of p-cymene, however, it requires a hydrogen supply to prevent catalyst deactivation [32].

Recently, we have reported that silica-supported zinc oxide is an efficient noble-metal-free catalyst for the synthesis of p-cymene by the gas phase dehydroisomerisation of α -pinene and limonene (Chapter 3) [40]. The reaction of α -pinene over ZnO/SiO₂ produces p-cymene with 90% yield at 100% conversion at 370 °C. The reaction with limonene gives a 100% p-cymene yield at 325 °C. The ZnO/SiO₂ catalyst shows stable performance for over 70 h without co-feeding hydrogen.

Here, we report silica-supported cadmium oxide, CdO/SiO₂, as a new highly efficient noble-metal-free catalyst for the dehydroisomerisation of monoterpenes to p-cymene in the gas phase. Cadmium is a close Group 12 analogue of zinc. CdO is known as a multifunctional material for its application in optoelectronic devices ([41] and references therein). It has also been reported as a Lewis acid-base and dehydrogenation catalyst, for example, for condensation of aldehydes [41], dehydration of ethanol [42], and dehydrogenation of ethylbenzene and cycloalkanes [43]. Here, it is demonstrated that CdO/SiO₂ has the highest efficiency in monoterpene-to-p-cymene dehydroisomerisation among the catalysts reported so far, to the best of our knowledge. A wide range of cyclic monoterpenes is studied in this work; these include not only α -pinene and limonene, which are well documented as the feedstocks for p-cymene synthesis, but also β -pinene, α -terpinene, γ -terpinene, and terpinolene. The latter are often missing from the literature but are important components of industrial turpentine feedstocks. It is demonstrated that all these monoterpenes can be converted to p-cymene with excellent yields of 91–100% using CdO/SiO₂ as the catalyst.

5.1. Results and discussion

5.1.1. Catalyst characterisation

The CdO/SiO₂ catalysts were prepared by wet impregnation of Cd(NO₃)₂ onto Aerosil 300 silica from an aqueous solution followed by air calcination at 400 or 500 °C. Upon calcination, cadmium nitrate decomposed to form CdO on the silica surface. Bulk CdO was prepared by thermal decomposition of Cd(NO₃)₂·4H₂O at 400 °C [44]. As can be seen from the TGA trace (Figure 5.1), the thermal decomposition of Cd(NO₃)₂·4H₂O occurs in several steps including the loss of two H₂O molecules at ~100 °C and the other two at 200 °C followed by the decomposition of Cd(NO₃)₂ to CdO starting at ~400 °C and finishing at 500 °C, with no weight loss upon further heating at least up to 700 °C. These results are in good agreement with the previous report [44].

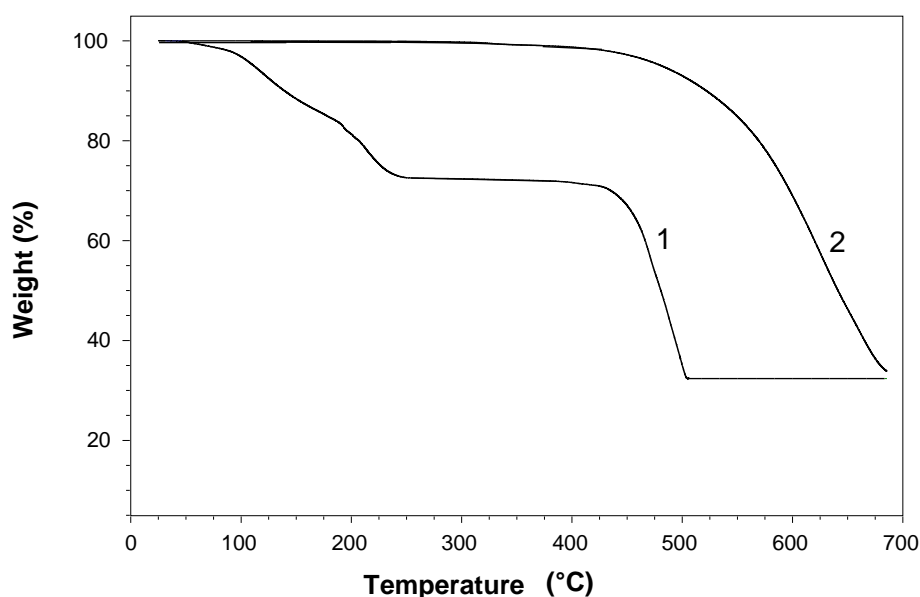


Figure 5.1. TGA of Cd(NO₃)₂·4H₂O in air flow, 10 °C min⁻¹ (1); and TGA of CdO calcined at 500 °C, in H₂-N₂ (5:95) flow, 20 °C min⁻¹ (2).

The formation of bulk CdO upon Cd(NO₃)₂·4H₂O decomposition at 400 °C (air calcination at 400 °C, 5 °C min⁻¹, 2 h) was confirmed by XRD (Figure 5.2). The bulk CdO thus

obtained was a crystalline material with a face-centered (fcc) structure and an average particle size of 156 nm. The XRD pattern of CdO is in perfect agreement with the literature data (JCPDS card no. 65-2908), with reflections at 33.0° (111), 38.3° (200), 55.3° (220), 65.9° (311), and 69.3° (222) [45]. No characteristic peaks for any impurities were detected, confirming that the CdO obtained was phase pure. CdO sample obtained by air calcination at $500^\circ\text{C}/2\text{ h}$ had the same XRD pattern. In contrast to the crystalline bulk CdO, the CdO/SiO₂ catalysts were all amorphous (Figure 5.2). Therefore, the XRD data indicates that cadmium oxide had a fine dispersion on the surface of silica.

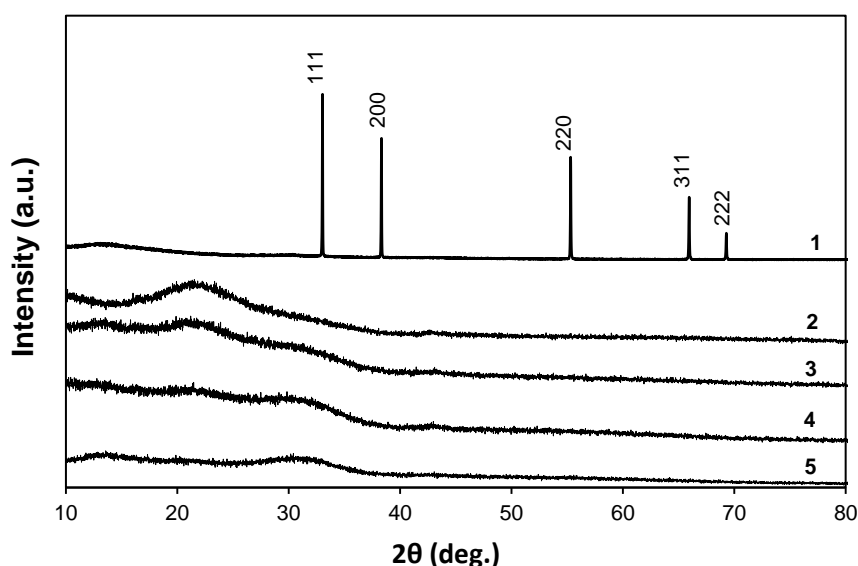


Figure 5.2. Powder XRD (CuK α) for bulk CdO (1), 5%CdO/SiO₂ (2), 10%CdO/SiO₂ (3), 20%CdO/SiO₂ (4) and 30%CdO/SiO₂ (5); all calcined at 400°C for 2 h, 5°C min^{-1} temperature ramp rate.

From the BET analysis, CdO/SiO₂ catalysts exhibited adsorption/desorption isotherms characteristic of mesoporous materials of type IV with an H1 hysteresis loop typical of amorphous silica (Figure 5.3). The pore size distribution obtained by the BJH method is presented in Figure 5.4. These results are in agreement with the previous studies [46–52].

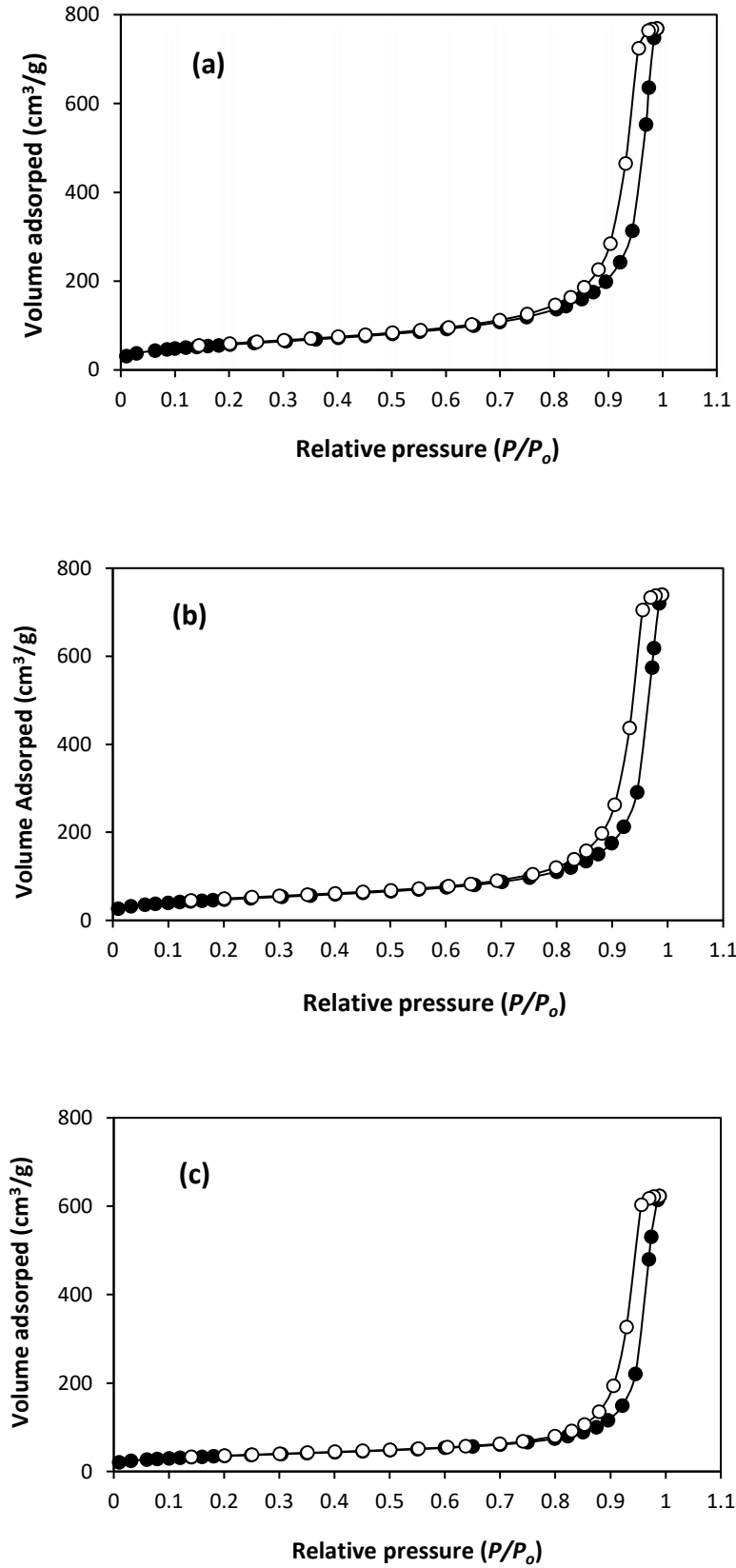


Figure 5.3. Nitrogen adsorption and desorption isotherms for 10%CdO/SiO₂ (a), 20%CdO/SiO₂ (b) and 30%CdO/SiO₂ (c) calcined at 400 °C.

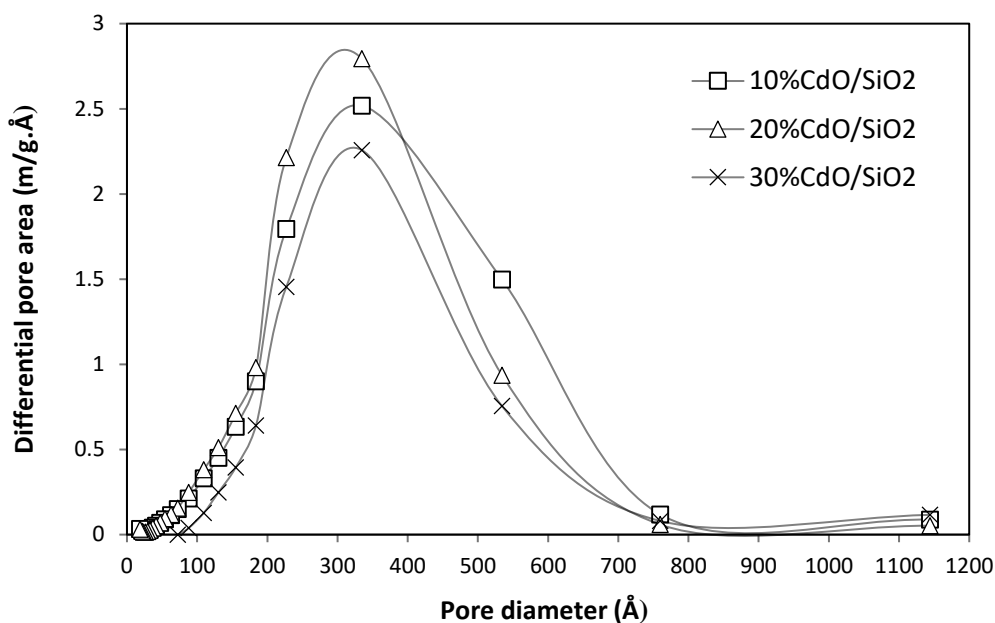


Figure 5.4. Pore size distribution for CdO/SiO₂ catalysts.

Bulk CdO prepared by calcining Cd(NO₃)₂·4H₂O at 400 °C had a low surface area of 0.35 m² g⁻¹ and a tiny pore volume. Both the surface area and pore volume of CdO increased after calcination at 500 °C to 15 m² g⁻¹ and 0.069 cm³ g⁻¹, respectively. As expected, supported CdO/SiO₂ catalysts had a much larger total surface area; the surface area and pore volume decreased with increasing CdO loading. Similar to the bulk CdO, the surface area and porosity of CdO/SiO₂ increased with increasing the calcination temperature from 400 to 500 °C (see the data for 10%CdO/SiO₂ in Table 5.1).

Table 5.1. Information about catalysts.

Catalyst ^a	$S_{\text{BET}}^{\text{b}}$ ($\text{m}^2 \text{g}^{-1}$)	Pore volume ^c ($\text{cm}^3 \text{g}^{-1}$)	Pore size ^d (\AA)	Weight loss ^e (wt%)
CdO	0.35	0.00013	15	1.0
CdO ^f	15	0.069	185	0.2
5% CdO/SiO ₂	250	1.05	167	3.0
10% CdO/SiO ₂	208	0.86	156	6.5
10% CdO/SiO ₂ ^f	230	1.04	180	4.0
20% CdO/SiO ₂	172	0.89	207	6.6
30% CdO/SiO ₂	126	0.74	235	4.2

^a Catalysts calcined in air at 400 °C for 2 h unless stated otherwise. ^b BET surface area. ^c Single point total pore volume. ^d Average pore diameter by BET method. ^e From TGA in the temperature range of 25–700 °C. ^f Catalysts calcined in air at 500 °C for 2 h.

H₂-TPR was performed on fresh 10% CdO/SiO₂ calcined at 500 °C to assess the possibility of CdO reduction during terpene dehydroisomerisation, which, along with p-cymene, produced hydrogen (less than 0.5% in the gas flow at 200–400 °C under our reaction conditions). As seen from the H₂-TPR trace (Figure 5.5), CdO in this catalyst was reduced to Cd metal at 477 °C. Additionally, TGA of bulk CdO calcined at 500 °C was performed under a mixed H₂–N₂ (5:95) flow (Figure 5.1). The TGA shows that CdO was reduced to metal above 450 °C; the Cd metal formed (m.p. 321 °C) evaporated, with a 66% weight loss to 700 °C (only a 12% weight loss expected if CdO reduced without Cd metal evaporation). These results rule out CdO reduction during the dehydroisomerisation reaction as in most cases it was carried out at 200–325 °C, with less than 0.5% H₂ produced in the gas stream.

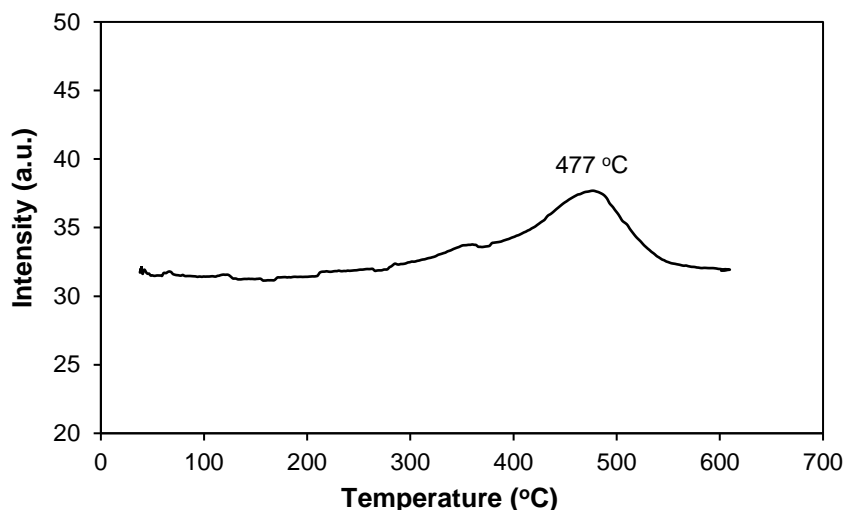


Figure 5.5. H₂-TPR of 10%CdO/SiO₂ (40 mg) calcined at 500 °C in H₂-N₂ (5:95) flow (40 ml min⁻¹), 20 °C min⁻¹.

From the DRIFT spectroscopy of adsorbed pyridine, CdO/SiO₂ catalysts exhibited a strong band at 1450 cm⁻¹ (Figure 5.6) indicating Lewis acid sites presence [53]. The band at 1540 cm⁻¹ characteristic of Brønsted acid sites [53] was hardly seen at all. We were unable to obtain good DRIFT spectra for pyridine adsorbed on bulk CdO due to its very low surface area (Table 5.1). DRIFT spectrum for anhydrous Cd(NO₃)₂, prepared by calcining Cd(NO₃)₂·4H₂O at 300 °C displays only Lewis acid sites (Figure 5.6). These results show that the CdO catalysts possess Lewis acidity and lack Brønsted acid sites capable of protonating pyridine.

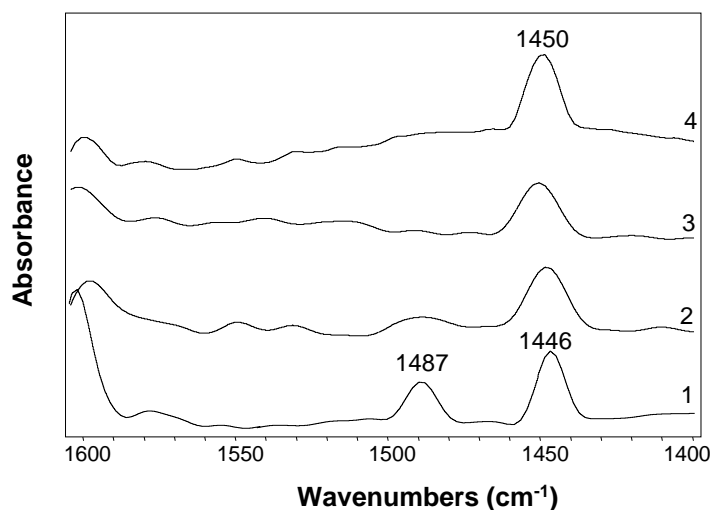


Figure 5.6. DRIFT spectra of adsorbed pyridine (powdered KBr mixtures versus KBr): anhydrous $\text{Cd}(\text{NO}_3)_2$ calcined at 300 °C (1), Aerosil 300 silica (2), 5% CdO/SiO_2 (3), and 10% CdO/SiO_2 (4).

From TGA, the CdO/SiO_2 catalysts exhibited a weight loss of 3.0–6.6% upon heating from 25 to 700 °C (Table 5.1, Figure 5.7), which can be attributed to the loss of physisorbed and chemically bound water. About half of this water was lost above 100 °C, which points to the existence of silanol groups in the catalysts. This is also supported by DRIFT spectroscopy. Figure 5.8 presents the DRIFT spectra of Aerosil 300 silica and CdO/SiO_2 catalysts in the region of the OH stretch of silanol groups. These spectra are similar to those for ZnO/SiO_2 catalysts reported previously [40]. In the DRIFT spectrum of the neat silica, the strong band at 3744 cm^{-1} is assigned to the free terminal silanol groups. The bands at 3600–3700 cm^{-1} are attributed to the hydrogen-bonded vicinal silanols. The broad band at 3100–3600 cm^{-1} is assigned to silanol nests; the latter include different silanol groups linked by extended hydrogen bonding [54–56]. In CdO/SiO_2 catalysts, the free terminal silanol groups and silanol nests are present, whereas the hydrogen-bonded vicinal silanols are less visible, similar to ZnO/SiO_2 catalysts reported previously [40]. Despite being weak Brønsted acid sites, the silanol groups can readily isomerize α -pinene and limonene at 300 °C [17, 32].

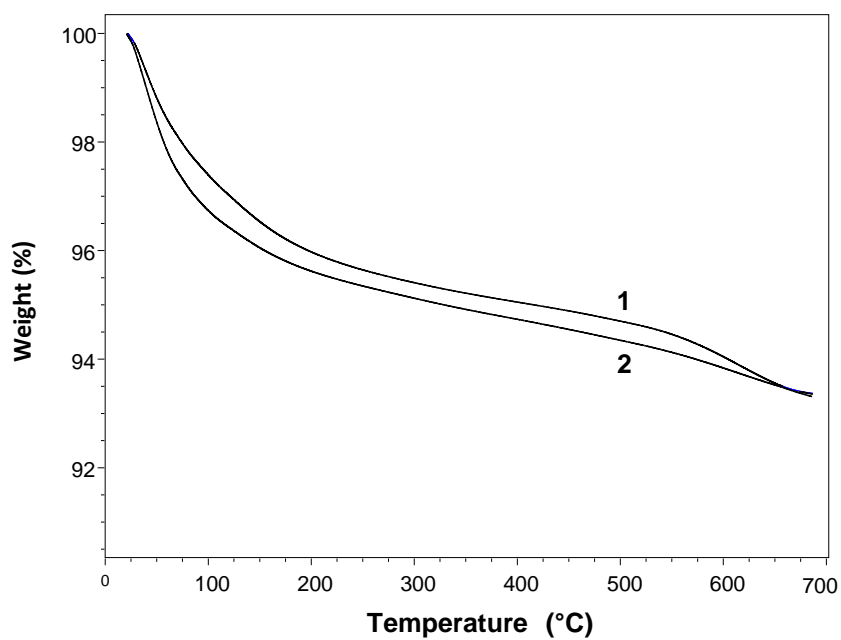


Figure 5.7. TGA of 10%CdO/SiO₂ (1) and 20%CdO/SiO₂ (2) under nitrogen, 20 °C min⁻¹ temperature ramp rate.

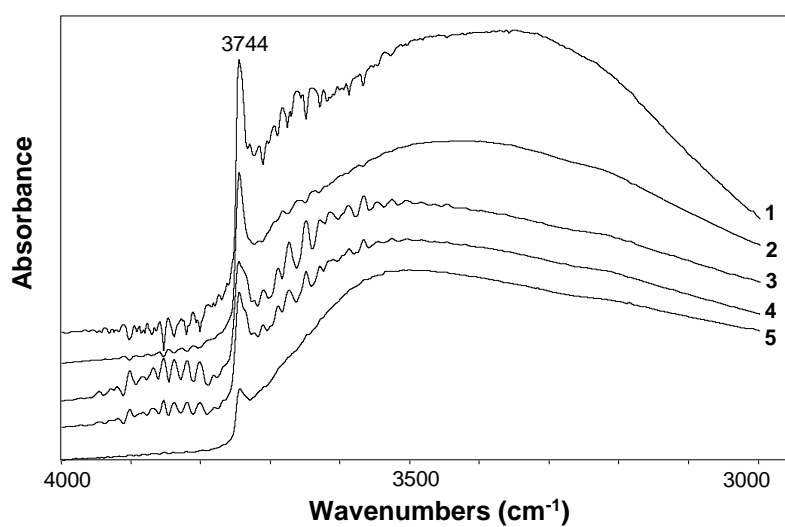


Figure 5.8. DRIFT spectra of SiO₂ (1), 5%CdO/SiO₂ (2), 10%CdO/SiO₂ (3), 20%CdO/SiO₂ (4), and 30%CdO/SiO₂ (5) calcined at 400 °C in air for 2 h (powdered KBr mixtures versus KBr).

5.1.2. Dehydroisomerisation of α -pinene

Table 5.2 shows the results of the initial testing of CdO/SiO₂ catalysts calcined at 400 °C in α -pinene dehydroisomerisation (250 °C, weight hourly space velocity WHSV = 0.08 h⁻¹, 4 h time on stream (TOS)). At such conditions, CdO/SiO₂ catalysts exhibited high activity, with p-cymene selectivity of 70–75%. α -Pinene conversion reached > 98% within 1 h TOS and further increased to 100% (Figure 5.9). The formation of hydrogen in the reaction was confirmed by GC-TCD (see GC trace in Figure 5.10). CdO loading in the range of 5–30 wt% had a small effect on catalyst performance. Nevertheless, 10%CdO/SiO₂ exhibited a better performance among these catalysts, giving 75% p-cymene selectivity at 100% conversion. As can be seen from Figure 5.9, this catalyst gave stable p-cymene selectivity for over 4 h TOS. There was an initial increase in α -pinene conversion before reaching a steady state (Figure 5.9); this may be due to catalyst coking which could provide extra adsorption sites for α -pinene and hence enhance its conversion. 10%CdO/SiO₂ calcined at 500 °C gave a higher p-cymene selectivity, 77%, compared to the catalyst calcined at 400 °C (Table 5.2).

Table 5.2. Dehydroisomerisation of α -pinene to p-cymene over CdO/SiO₂.^a

Catalyst	Conversion ^b (%)	Selectivity (%mol) ^b				
		Lights	Camphene	Limonene	p-Cymene	Other
SiO ₂	97	25	21	16	0	38
CdO ^c	1	0	0	0	0	1
5%CdO/SiO ₂ ^c	100	8	15	0	75	2
10%CdO/SiO ₂ ^c	100	8	15	0	75	2
10%CdO/SiO ₂ ^d	100	9	13	0	77	1
20%CdO/SiO ₂ ^c	100	9	17	0	73	1
30%CdO/SiO ₂ ^c	100	9	19	0	70	2

^a 0.20 g catalyst, 250 °C, 0.48 kPa α -pinene partial pressure, 10 ml min⁻¹ flow rate, 4 h TOS, WHSV = 0.08 h⁻¹. ^b Average conversion and product selectivity within 1–4 h TOS. ^c The catalysts calcined at 400 °C. ^d 10%CdO/SiO₂ calcined at 500 °C.

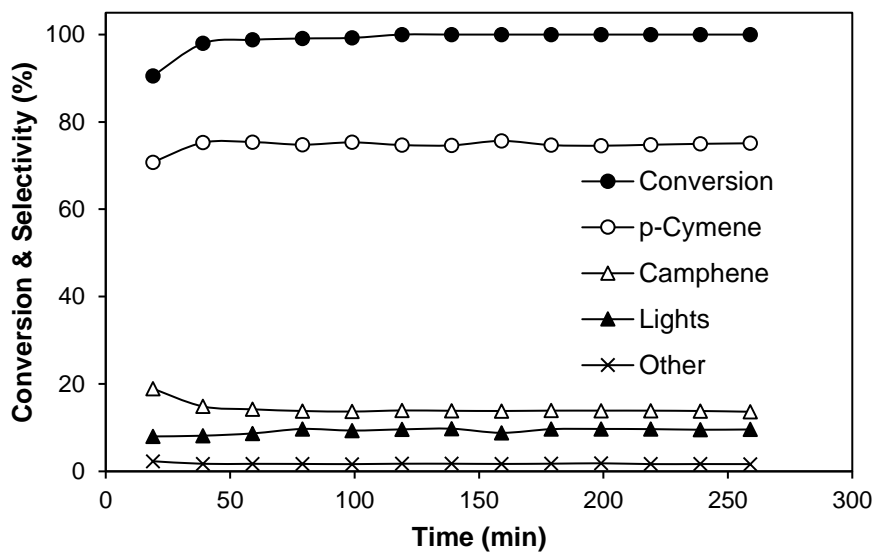


Figure 5.9. Time course for α -pinene dehydroisomerisation over 10%CdO/SiO₂ calcined at 400 °C: 0.20 g catalyst, 250 °C, 0.48 kPa α -pinene partial pressure, 10 ml min⁻¹ flow rate, WHSV = 0.08 h⁻¹.

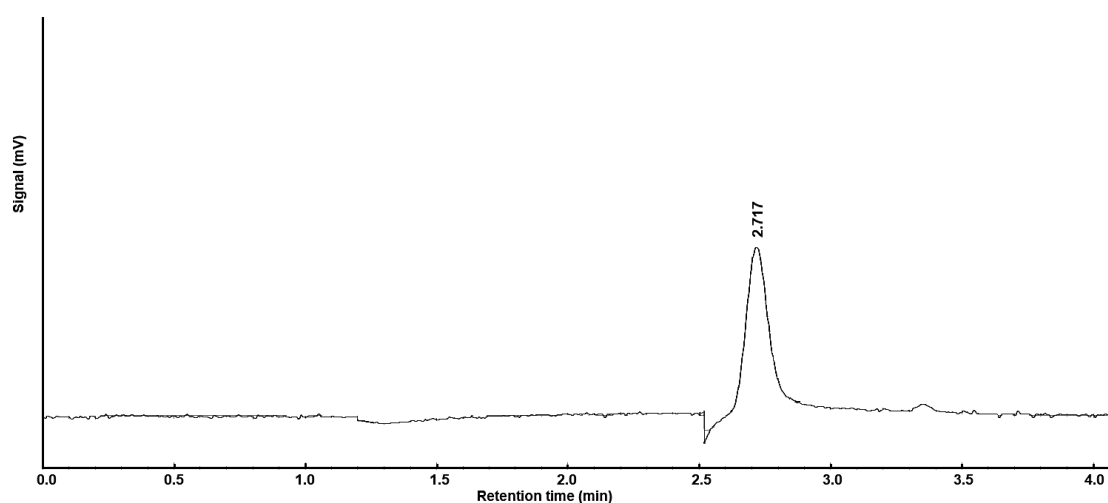


Figure 5.10. GC-TCD trace showing H₂ product evolved in α -pinene dehydroisomerisation at 250 °C and WHSV = 0.08 h⁻¹ over 10%CdO/SiO₂ (0.20.g) calcined at 400 °C (Agilent 8860 GC instrument fitted with TCD and 1.5 m packed Molsieve 5A column).

Although the difference in selectivity is within experimental error ($\leq 5\%$), this trend was observed at different contact times, with a 2–3% difference in p-cymene selectivity (Figure

5.11), hence appearing statistically significant. The better performance of 10%CdO/SiO₂ calcined at 500 °C can be attributed to a structural change of CdO on the silica surface. As seen from the data in Table 5.1, the texture of bulk CdO changed greatly upon increasing the calcination temperature from 400 to 500 °C, thus indicating a significant structural change.

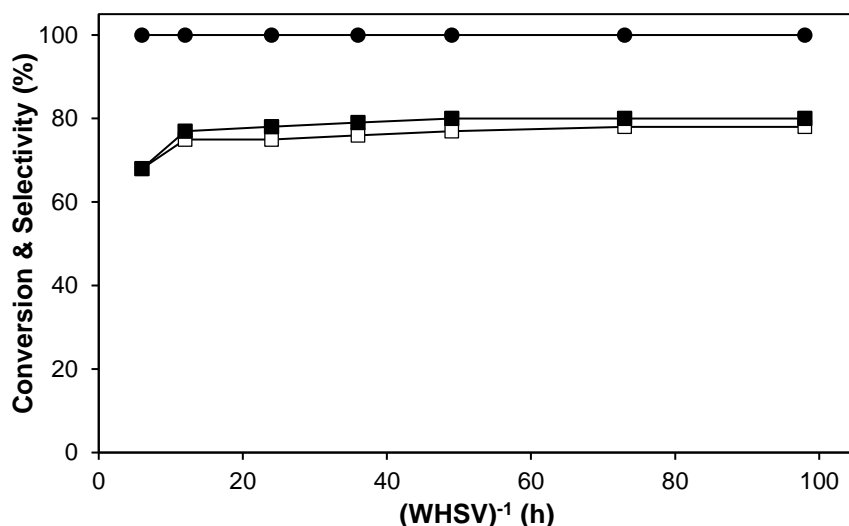


Figure 5.11. α -Pinene conversion (solid circles) and p-cymene selectivity for 10%CdO/SiO₂ calcined at 400 °C (open squares) and calcined at 500 °C (solid squares) at different contact times (250 °C, 0.48 kPa α -pinene partial pressure, 4 h TOS).

Bulk CdO hardly showed any activity at all (Table 5.2), which can be attributed to its very low surface area (Table 5.1) as well as to the lack of Brønsted acidity (see above). Pure silica support in the absence of CdO showed high isomerisation activity (97% α -pinene conversion, Table 5.2), mainly producing limonene, camphene, and other p-menthadiene isomers (referred to as “other”) together with some cracking products (referred to as “lights”). Notably, no formation of p-cymene was observed on pure SiO₂, which is not unexpected because silica lacks the dehydrogenation function. p-Cymene was formed only in the presence of CdO, which is known to possess the dehydrogenation function [43]. These results are consistent with the mechanism [17,40] involving a fast step of α -pinene isomerisation to p-

menthadienes on acid sites (silanol groups of silica) followed by a slow step of dehydrogenation of p-menthadienes to p-cymene on oxo-metal sites of cadmium oxide (Scheme 3.1).

Figure 5.12 shows a long-term test (25 h TOS) for α -pinene dehydroisomerisation over 10%CdO/SiO₂ calcined at 500 °C. After 25 h on stream at 250 °C and WHSV = 0.013 h⁻¹, the selectivity to p-cymene only slightly reduced from 78 to 74%. This could be attributed to catalyst coking. After the reaction, the initially white 10%CdO/SiO₂ catalyst became grey; 0.5% of carbon deposition was found in the post-reaction catalyst by combustion elemental analysis. The catalyst could be regenerated in situ by the air flow at 400 °C for 3 h, which reduced coke deposition to 0.1% and restored catalyst activity (Figure 5.13). XRD analysis of spent 10–30% CdO/SiO₂ catalysts after α -pinene dehydroisomerisation (250 °C, WHSV = 0.08 h⁻¹, 4 h TOS) is shown in Figure 5.14. The spent catalysts are amorphous; their diffractograms are similar to those for the corresponding fresh catalysts (Figure 5.2). No reflections of Cd metal phase (JCPDS 03–065–3363) can be seen in these diffractograms.

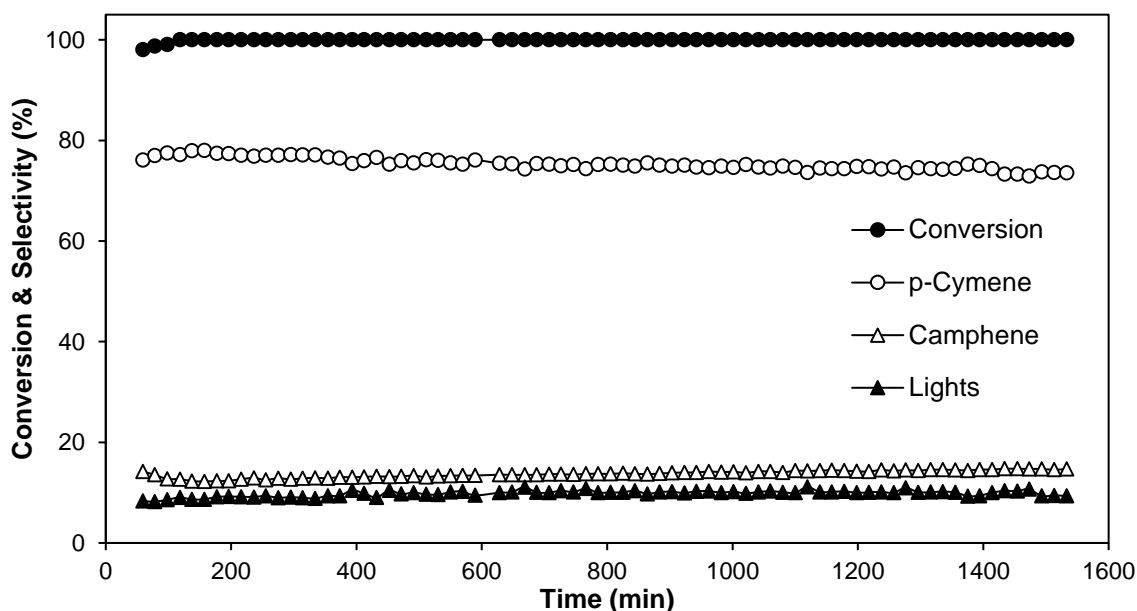


Figure 5.12. Long-term time course (25 h TOS) for α -pinene dehydroisomerisation over 10%CdO/SiO₂ calcined at 500 °C: 0.60 g catalyst, 250 °C, 0.48 kPa α -pinene partial pressure, 5 ml min⁻¹ flow rate, WHSV = 0.013 h⁻¹.

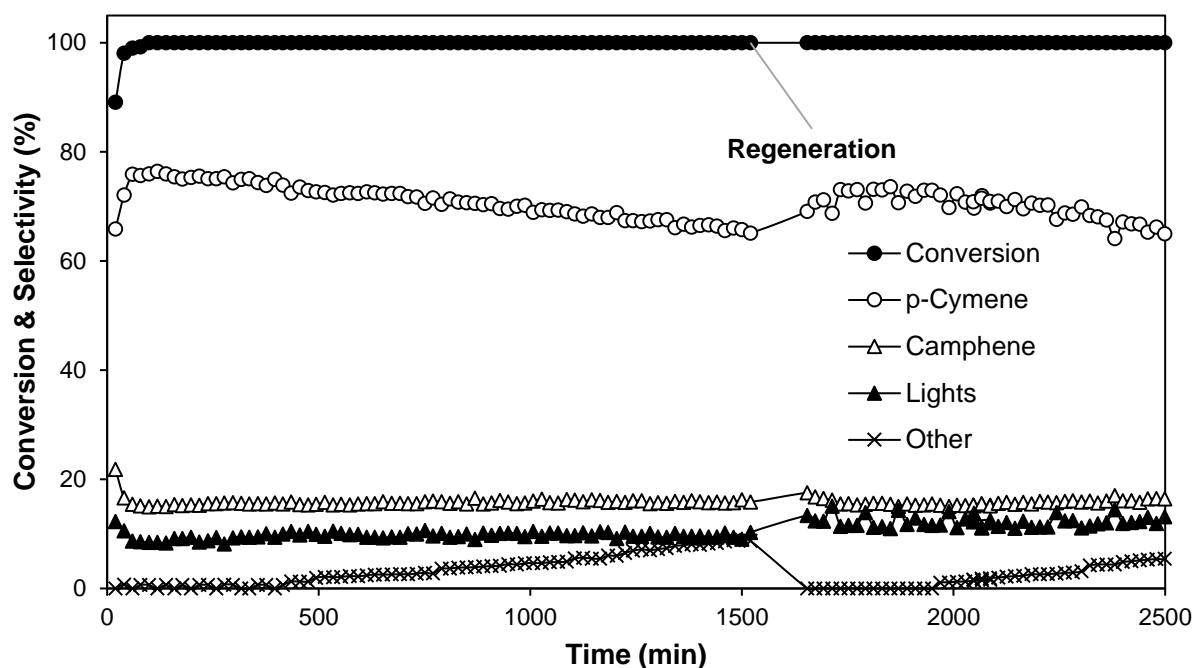


Figure 5.13. Long-term time course for α -pinene dehydroisomerisation over 20%CdO/SiO₂ calcined at 400 °C with catalyst regeneration: 0.20 g catalyst, 275 °C, 0.48 kPa α -pinene partial pressure, 10 ml min⁻¹ flow rate, WHSV = 0.08 h⁻¹; the catalyst regenerated in situ by air flow (10 ml min⁻¹) at 400 °C for 3 h.

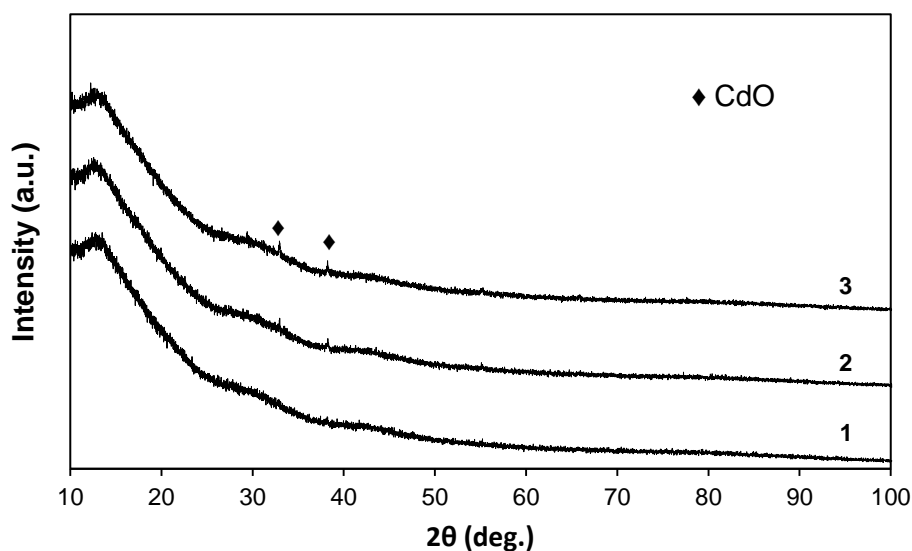


Figure 5.14. Powder XRD (CuK α) for spent 10%CdO/SiO₂ (1), 20%CdO/SiO₂ (2), and 30%CdO/SiO₂ (3) calcined at 400 °C after α -pinene dehydroisomerisation (250 °C, WHSV = 0.08 h⁻¹, 4 h TOS). Reflections at 33.0° and 38.3° in 20% and 30%CdO/SiO₂ are attributed to CdO. No Cd metal phase (JCPDS 03–065–3363) is present.

Figure 5.15 shows the effect of reaction temperature on p-cymene selectivity in the presence of 10%CdO/SiO₂ calcined at 500 °C; the temperature was varied from 200–375 °C at WHSV = 0.08 h⁻¹. The conversion of α-pinene was 100% within this temperature range. The selectivity to p-cymene increases with the temperature reaching 82% at 325 °C and then declines as the temperature is further increased. The latter can be explained by catalyst coking.

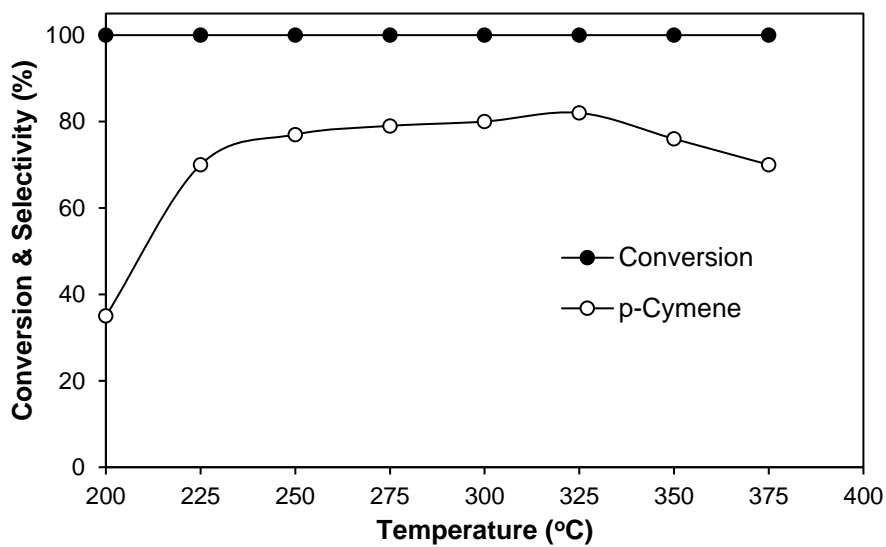


Figure 5.15. Effect of temperature on α-pinene dehydroisomerisation over 10%CdO/SiO₂ calcined at 500 °C: 0.20 g catalyst, 0.48 kPa α-pinene partial pressure, 10 ml min⁻¹ flow rate, WHSV = 0.08 h⁻¹.

Figure 5.16 shows the effect of contact time, (WHSV)⁻¹, on p-cymene selectivity at the optimum temperature of 325 °C in the presence of 10%CdO/SiO₂ calcined at 500 °C. The contact time was varied by changing the flow rate from 5–20 ml min⁻¹ and the amount of catalyst from 0.2–0.8 g. Under such conditions, α-pinene conversion was 100%. The results show that the selectivity increases steadily with the contact time, as expected for a consecutive reaction (Scheme 3.1), reaching 91% (91% p-cymene yield) at a contact time of 100 h (WHSV = 0.01 h⁻¹). From these results, the CdO/SiO₂ catalyst outperforms the ZnO/SiO₂ catalyst

reported previously [40]; the latter provides 90% p-cymene yield at the same WHSV but at a significantly higher reaction temperature of 370 °C.

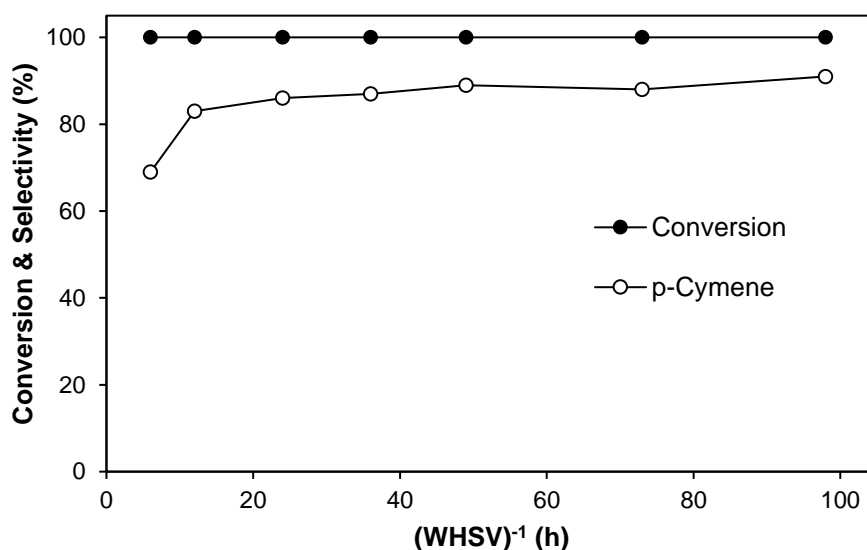
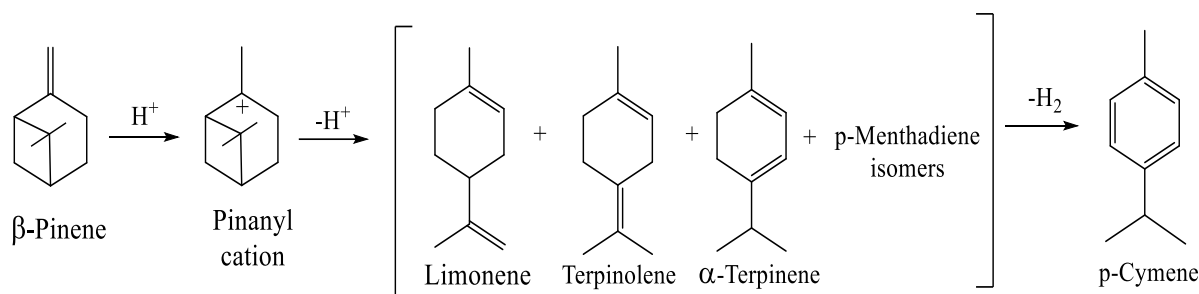


Figure 5.16. α -Pinene conversion and p-cymene selectivity for 10% CdO/SiO₂ calcined at 500 °C at different contact times (325 °C, 0.48 kPa α -pinene partial pressure, 4 h TOS); the contact time varied by changing flow rate (5–20 ml min⁻¹) and catalyst amount (0.2–0.8 g).

5.1.3. Dehydroisomerisation of β -pinene

Dehydroisomerisation of β -pinene is less well studied as compared to α -pinene. The two pinene isomers have similar structures differing only in the position of the C=C double bond (Table 1.3). The dehydroisomerisation of β -pinene is likely to occur via a mechanism similar to that for the reaction of α -pinene, involving the isomerisation of β -pinene to p-menthadienes through pinanyl cation intermediate followed by dehydrogenation to form p-cymene (Scheme 5.1).



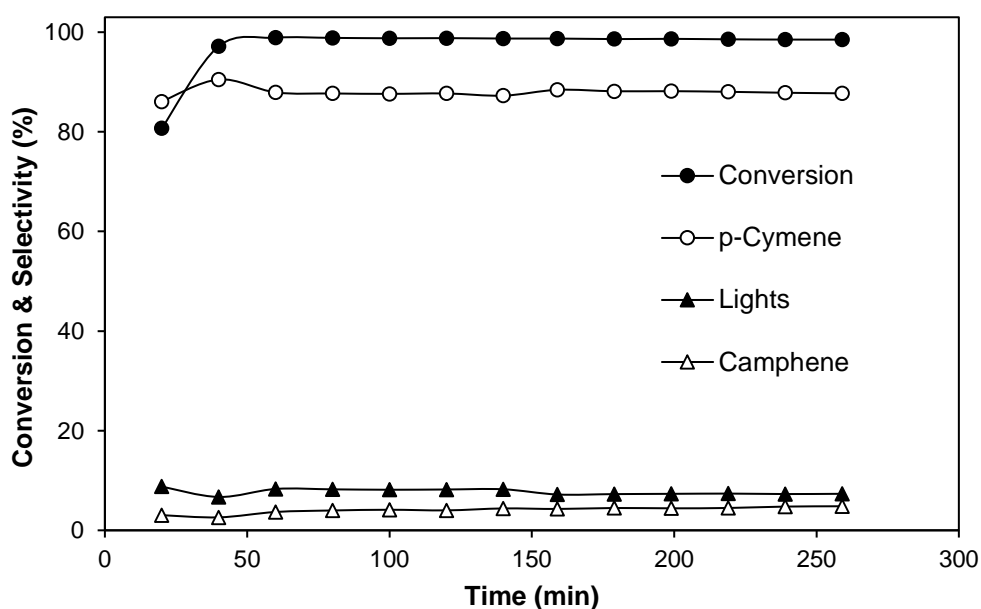
Scheme 5.1. Dehydroisomerisation of β -pinene to p-cymene.

The dehydroisomerisation of β -pinene was studied in the presence of 10% CdO/SiO₂ catalyst calcined at 500 °C, which showed the best performance in the reaction of α -pinene (see above). Table 5.3 shows representative results at different reaction temperatures 200–400 °C. The data for the reaction with 20% CdO/SiO₂ calcined at 400 °C is also included for comparison with other monoterpenes studied (see section 5.1.6 below). As seen, in the whole temperature range, β -pinene conversion on 10% CdO/SiO₂ was 99–100%. The reaction had stable product selectivity for over 4 h TOS (Figure 5.17). The selectivity to p-cymene increases with increasing reaction temperature reaching a maximum of 88% at 375 °C and then declines at higher temperatures. Figure 5.18 displays the effect of temperature on p-cymene selectivity in more detail, with the maximum selectivity at 375 °C. The main by-products were camphene and lights; the amount of camphene decreased whereas the amount of the lights increased with increasing temperature (Table 5.3).

Table 5.3. Effect of temperature on β -pinene dehydroisomerisation over 10%CdO/SiO₂.^a

Temp. (°C)	Conv. ^b (%)	Selectivity (%mol) ^b						
		Lights	α -Pinene	Camphene	α -Terpinene	p-Cymene	γ -Terpinene	Terpinolene
200	99	6	1	24	10	52	3	4
225	100	5	1	20	6	63	2	3
250	100	7	0	14	1	78	0	0
250 ^c	100	8	2	22	3	66	0	0
275	100	8	0	12	0	80	0	0
300	100	9	0	9	0	82	0	0
325	100	9	0	8	0	83	0	0
350	100	8	0	7	0	85	0	0
375	100	8	0	4	0	88	0	0
400	100	9	0	4	0	86	1	0

^a 0.20 g 10%CdO/SiO₂ catalyst calcined at 500 °C, 0.47 kPa β -pinene partial pressure, 10 ml min⁻¹ flow rate, WHSV = 0.08 h⁻¹. ^b Average conversion and product selectivity within 1–4 h TOS. ^c 20%CdO/SiO₂ catalyst calcined at 400 °C.

**Figure 5.17.** Time course for β -pinene dehydroisomerisation over 10%CdO/SiO₂ calcined at 500 °C: 0.20 g catalyst, 375 °C, 0.47 kPa β -pinene partial pressure, 10 ml min⁻¹ flow rate, WHSV = 0.08 h⁻¹.

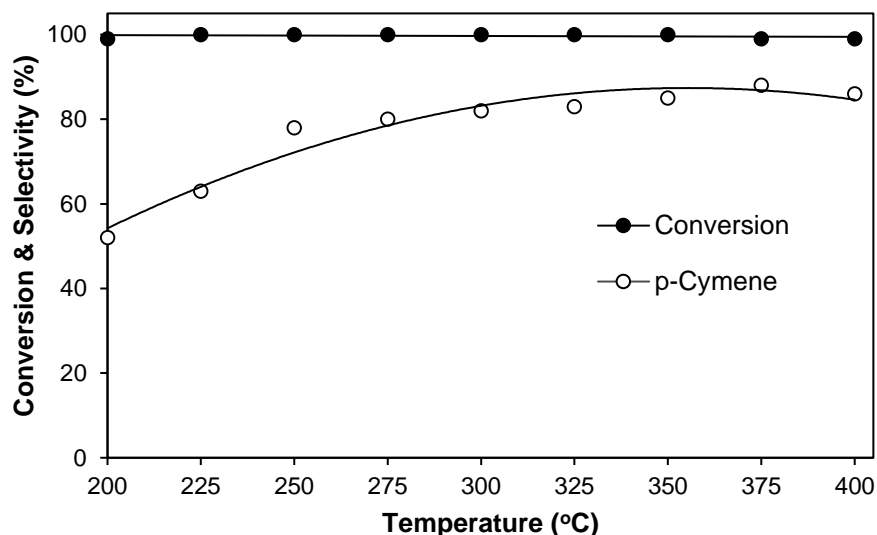


Figure 5.18. Effect of temperature on β -pinene dehydroisomerisation over 10%CdO/SiO₂ calcined at 500 °C: 0.20 g catalyst, 0.47 kPa α -pinene partial pressure, 10 ml min⁻¹ flow rate, WHSV = 0.08 h⁻¹.

The selectivity to p-cymene was found to increase with increasing the contact time, (WHSV)⁻¹ (Figure 5.19), similar to the reaction of α -pinene. The contact time was varied at the optimum temperature of 375 °C by changing the flow rate from 5–20 ml min⁻¹, the catalyst amount from 0.2–0.8 g, and the β -pinene partial pressure from 0.36–0.66 kPa. As can be seen, p-cymene selectivity levels off at contact times > 40 h, reaching 95% at 100% β -pinene conversion. Therefore, the dehydroisomerisation of β -pinene over CdO/SiO₂ gives 95% p-cymene yield at 375 °C and WHSV = 0.02 h⁻¹. This is higher than the p-cymene yield obtained from α -pinene (91% at 325 °C), although achieved at a higher temperature.

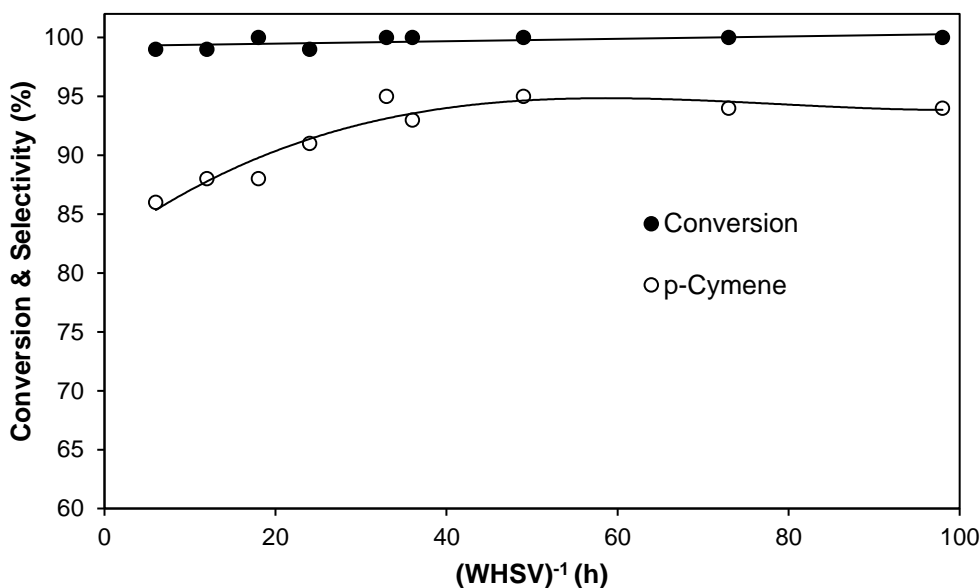


Figure 5.19. Plot of β -pinene conversion and p-cymene selectivity over 10% CdO/SiO₂ calcined at 500 °C versus contact time at 375 °C; the contact time varied by changing flow rate (5–20 ml min⁻¹), catalyst amount (0.2–0.8 g) and β -pinene partial pressure (0.36–0.66 kPa).

5.1.4. Dehydroisomerisation of limonene

Dehydroisomerisation of limonene to p-cymene occurs more easily than that of α -pinene because it does not involve C–C bond breaking during the reaction (Scheme 3.2) and generally gives a higher p-cymene yield compared to the reaction of α -pinene [17,32,40]. In the limonene dehydroisomerisation, CdO/SiO₂ calcined at 400 °C was found to be a highly efficient catalyst, providing 100% p-cymene yield at 250 °C.

Table 5.4 shows the effect of CdO loading (10–30%) on limonene conversion and p-cymene selectivity for the reaction at two temperatures of 225 and 250 °C and a space velocity $\text{WHSV} = 0.08 \text{ h}^{-1}$. It can be seen that under such conditions the reaction occurs with 97–100% limonene conversion and 97–100% p-cymene selectivity. β -Pinene was the only by product observed in this reaction. The loading of CdO had a small effect on the performance of CdO/SiO₂ catalysts. Among these catalysts, 20% CdO/SiO₂ and 30% CdO/SiO₂ exhibited a

higher efficiency, providing 100% selectivity to p-cymene at 100% limonene conversion (100% p-cymene yield) at 250 °C. This differs from the reaction of α -pinene and β -pinene, where the optimal CdO loading was 10 wt% (Table 5.2). This result can be attributed to the lower temperature for the reaction of limonene (250 °C) as compared to the reactions of α -pinene and β -pinene (325–375 °C). The lower reaction temperature necessitates a higher loading of the dehydrogenation component, cadmium oxide, for the limonene-to-p-cymene dehydroisomerisation. Similar results have been reported for a ZnO/SiO₂ catalyst [40].

Table 5.4. Dehydroisomerisation of limonene to p-cymene over CdO/SiO₂.^a

Catalyst ^b	Temperature (°C)	Conversion ^c (%)	Selectivity (%mol) ^c	
			β -Pinene	p-Cymene
10% CdO/SiO ₂	225	98	3	97
10% CdO/SiO ₂	250	100	1	99
20% CdO/SiO ₂	225	100	2	98
20% CdO/SiO ₂	250	100	0	100
30% CdO/SiO ₂	225	97	2	98
30% CdO/SiO ₂	250	100	0	100

^a 0.20 g catalyst, 10 ml min⁻¹ flow rate, 0.47 kPa limonene partial pressure, WHSV = 0.08 h⁻¹, 4 h TOS. ^b The catalysts calcined at 400 °C. ^c Average conversion and product selectivity over 1–4 h TOS.

Figure 5.20 shows the effect of temperature on the performance of 20% CdO/SiO₂ and 30% CdO/SiO₂ in the temperature range of 200–300 °C at WHSV = 0.08 h⁻¹. For both catalysts, the selectivity to p-cymene steadily grows with increasing the temperature to reach 100% at 250 °C, with limonene conversion being 100% within the entire temperature range. This confirms that the optimum temperature for the limonene-to-p-cymene conversion is 250 °C. These results are fully consistent with the view that the dehydroisomerisation of limonene occurs through the rate-limiting step of p-menthadiene dehydrogenation (Scheme 3.2).

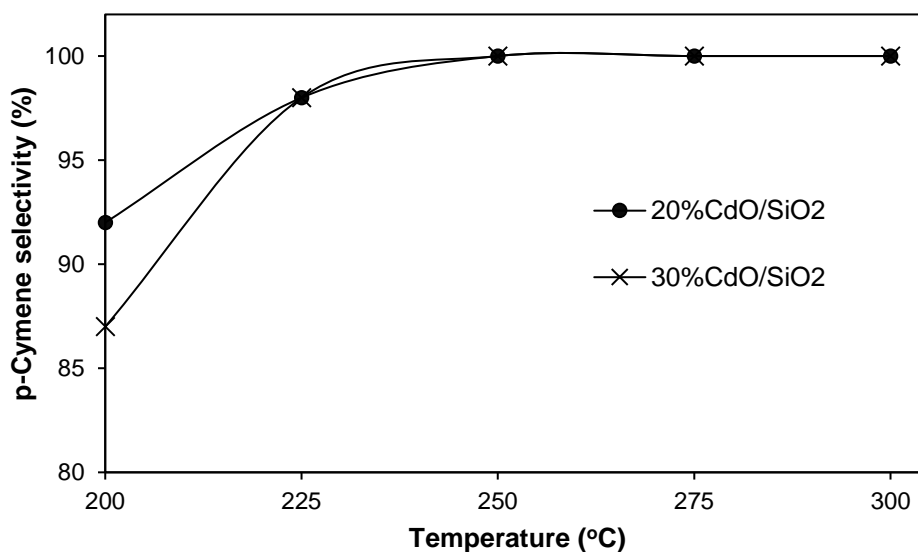


Figure 5.20. Effect of temperature on limonene dehydroisomerisation over 20%CdO/SiO₂ and 30%CdO/SiO₂: 0.20 g catalyst, 0.47 kPa limonene partial pressure, 10 ml min⁻¹ flow rate, 4 h TOS, WHSV = 0.08 h⁻¹; 100% limonene conversion in all cases.

The contact time was optimised for 20%CdO/SiO₂ catalyst; these results are presented in Figure 5.21 and Figure 5.22. The p-cymene yield increased with increasing the contact time, (WHSV)⁻¹, to reach 100% at contact times ≥ 12 h corresponding to WHSV ≤ 0.08 h⁻¹. At optimum conditions (250 °C, WHSV = 0.08 h⁻¹), the 20%CdO/SiO₂ catalyst exhibited very stable performance for 24 h TOS (Figure 5.23). Limonene conversion only slightly reduced from 100% to 97% in 24 h TOS, with an average conversion and p-cymene selectivity being 99.1% and 99.2%, respectively.

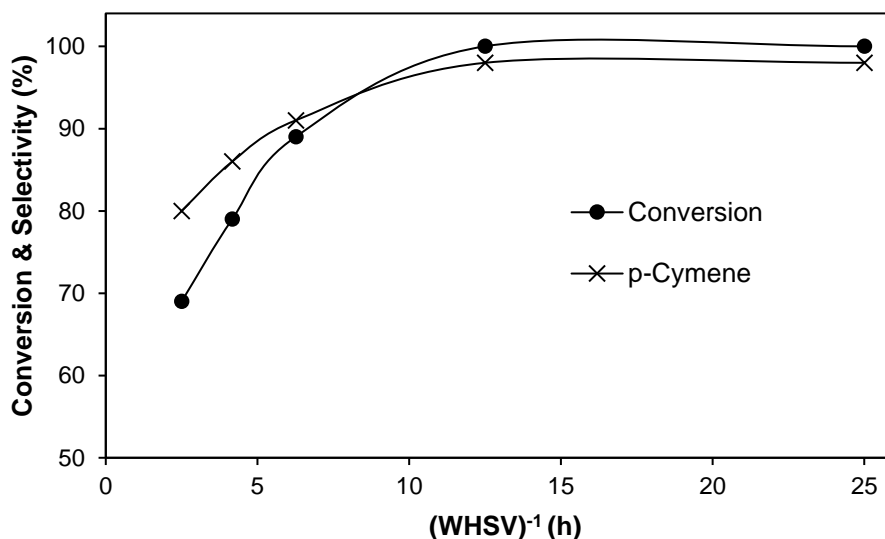


Figure 5.21. Plot of limonene conversion and p-cymene selectivity over 20%CdO/SiO₂ calcined at 400 °C (0.2–0.8 g) versus contact time at 225 °C and 0.47 kPa limonene partial pressure; the contact time varied by changing the flow rate (5–20 ml min⁻¹).

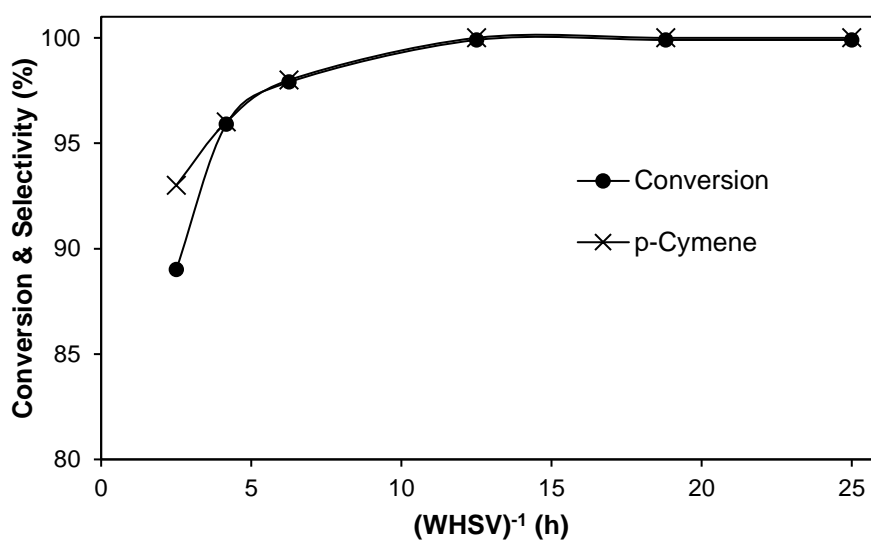


Figure 5.22. Plot of limonene conversion and p-cymene selectivity over 20%CdO/SiO₂ calcined at 400 °C (0.2–0.8 g) versus contact time at 250 °C and 0.47 kPa limonene partial pressure; the contact time varied by changing the flow rate (5–20 ml min⁻¹).

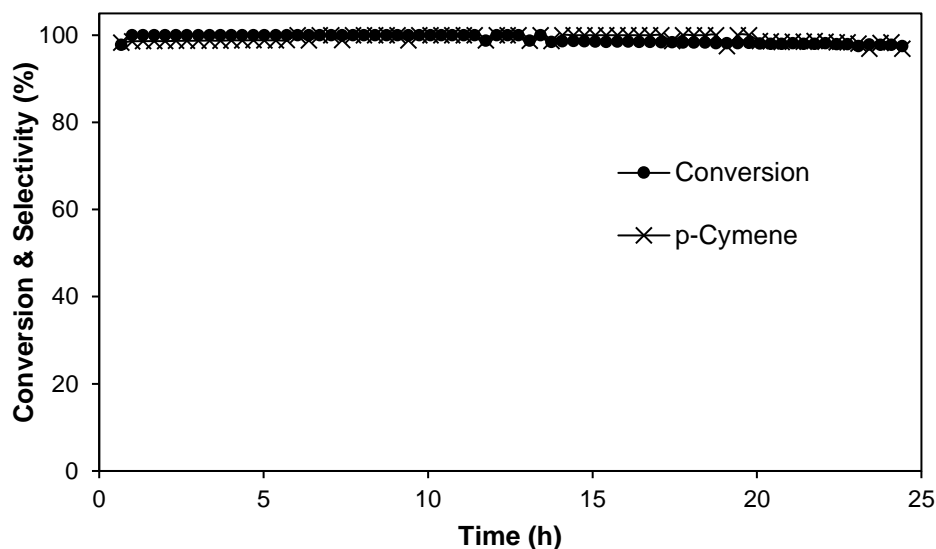


Figure 5.23. Long-term test for limonene dehydroisomerisation over 20%CdO/SiO₂: 0.20 g catalyst, 250 °C, 0.47 kPa limonene partial pressure, 10 ml min⁻¹ flow rate, WHSV = 0.08 h⁻¹.

Finally, in limonene dehydroisomerisation, 20%CdO/SiO₂ catalyst outperforms the ZnO/SiO₂ catalyst reported previously [40]. ZnO/SiO₂ provides 100% p-cymene yield at 325 °C and WHSV = 0.08 h⁻¹, whereas CdO/SiO₂ gives 100% yield at the same WHSV but at a significantly lower reaction temperature of 250 °C.

5.1.5. Dehydroisomerisation of α -terpinene, γ -terpinene, and terpinolene

There is little data on the dehydroisomerisation of the above monoterpenes in the literature. Since their framework is the same as that of limonene, differing only in the position of C=C double bonds (Table 1.3), they can be expected to undergo an easy dehydroisomerisation similar to limonene (Scheme 3.2).

The dehydroisomerisation of α -terpinene, γ -terpinene, and terpinolene was studied using 20%CdO/SiO₂ catalyst calcined at 400 °C, which gave the best performance in the reaction of limonene (see above). Table 5.5 shows the results for these substrates at 250 °C and WHSV = 0.08 h⁻¹. The results for limonene are also included for comparison. As expected, all

these monoterpenes exhibit similar dehydrogenation activities with 99–100% p-cymene yield under such conditions. The time courses for α -terpinene, γ -terpinene, and terpinolene are shown in Figure 5.24, 5.25, and 5.26, respectively. In all cases, an average monoterpene conversion is 100% within 1–4 h TOS, with a stable p-cymene selectivity at $\geq 99\%$ for at least 4 h TOS. β -Pinene was the only by-product observed ($\leq 1\%$).

Table 5.5. Dehydroisomerisation of monoterpenes to p-cymene over 20%CdO/SiO₂.^a

Monoterpene	Conversion ^b (%)	Selectivity (%mol) ^b	
		β -Pinene	p-Cymene
Limonene	100	0	100
α -Terpinene	100	0	100
γ -Terpinene	100	0	100
Terpinolene	100	1	99

^a 0.20 g 20%CdO/SiO₂ catalyst calcined at 400 °C, 250 °C reaction temperature, 10 ml min⁻¹ flow rate, 0.47 kPa monoterpene partial pressure, WHSV = 0.08 h⁻¹, 4 h TOS. ^b Average conversion and product selectivity over 1–4 h TOS.

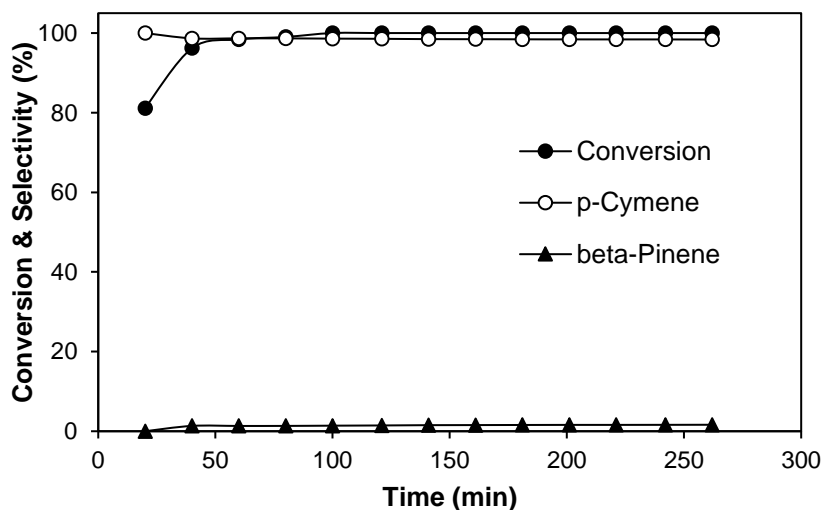


Figure 5.24. Time course for α -terpinene dehydroisomerisation over 20%CdO/SiO₂ calcined at 400 °C: 0.20 g catalyst, 250 °C, 0.47 kPa α -terpinene partial pressure, 10 ml min⁻¹ flow rate, WHSV = 0.08 h⁻¹.

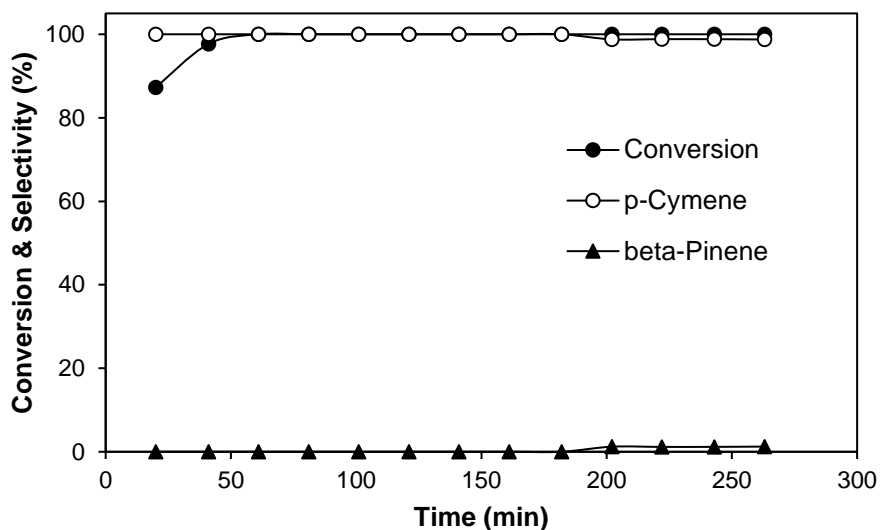


Figure 5.25. Time course for γ -terpinene dehydroisomerisation over 20%CdO/SiO₂ calcined at 400 °C: 0.20 g catalyst, 250 °C, 0.47 kPa γ -terpinene partial pressure, 10 ml min⁻¹ flow rate, WHSV = 0.08 h⁻¹.

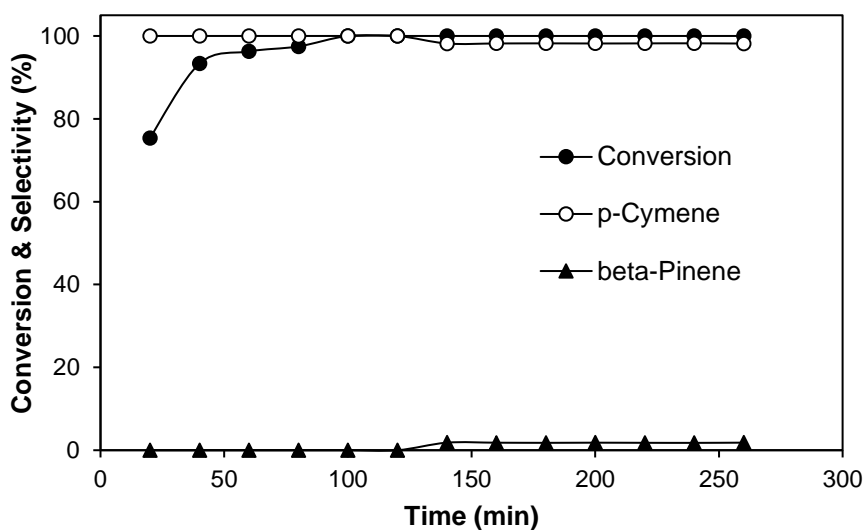


Figure 5.26. Time course for terpinolene dehydroisomerisation over 20%CdO/SiO₂ calcined at 400 °C: 0.20 g catalyst, 250 °C, 0.47 kPa terpinolene partial pressure, 10 ml min⁻¹ flow rate, WHSV = 0.08 h⁻¹.

Figure 5.27 shows the effect of reaction temperature on p-cymene yield in dehydroisomerisation of α -terpinene, γ -terpinene, and terpinolene in the temperature range of 175–400 °C at a space velocity $\text{WHSV} = 0.08 \text{ h}^{-1}$. It can be seen that α -terpinene and γ -terpinene reach 100% yield already at 200 °C, whereas for terpinolene this yield is reached at 275 °C and remains at this level at least up to 400 °C. However, at a longer contact time, $\text{WHSV} = 0.04 \text{ h}^{-1}$, terpinolene gives a 100% p-cymene yield at a lower temperature of 250 °C (Figure 5.28).

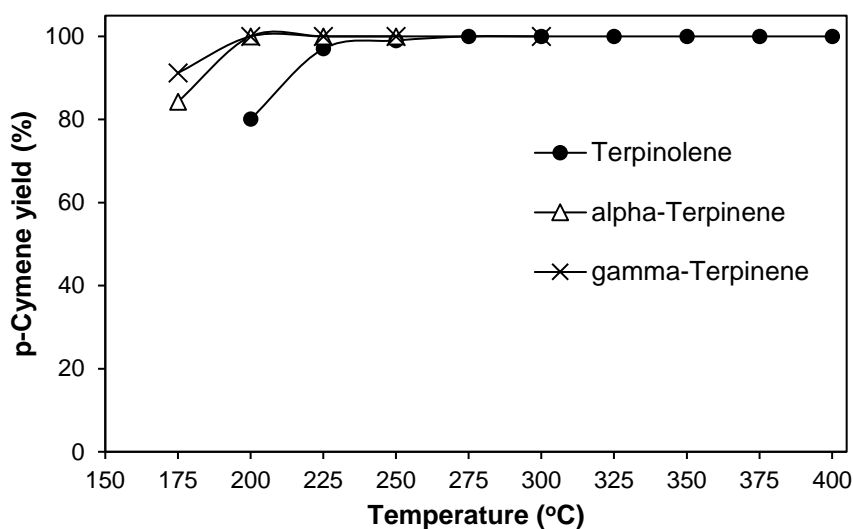


Figure 5.27. Effect of temperature on p-cymene yield in monoterpene dehydroisomerisation over 20% CdO/SiO₂ calcined at 400 °C: 0.20 g catalyst, 0.47 kPa monoterpene partial pressure, 10 ml min⁻¹ flow rate, 4 h TOS, $\text{WHSV} = 0.08 \text{ h}^{-1}$.

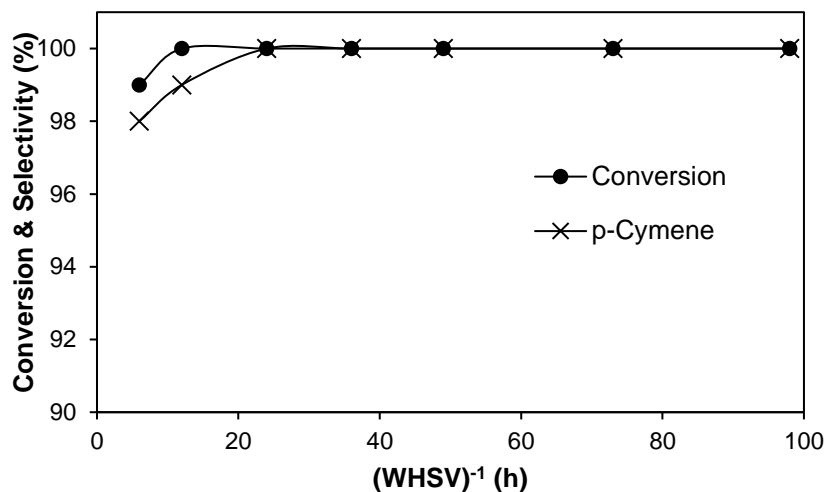


Figure 5.28. Plot of terpinolene conversion and p-cymene selectivity over 20% CdO/SiO₂ calcined at 400 °C versus contact time at 250 °C and 0.47 kPa terpinolene partial pressure; the contact time varied by changing the flow rate (5–20 ml min⁻¹) and catalyst weight (0.2–0.8 g).

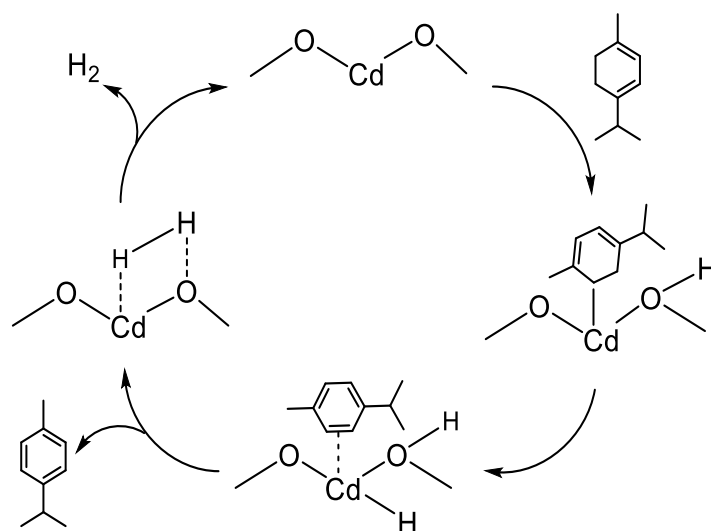
Therefore, not only α -pinene and limonene, which are well documented as the feedstocks for p-cymene synthesis, but also β -pinene, α -terpinene, γ -terpinene, and terpinolene that are important components of industrial turpentine feedstocks can be converted to p-cymene with excellent yields using CdO/SiO₂ as the catalyst.

Industrial turpentine streams are often contaminated with sulfur compounds [17]. It has been shown that sulfur can poison Pd catalysts during crude sulfate turpentine dehydroisomerisation [17]. In contrast to Pd catalysts, CdO/SiO₂ may be expected to be tolerant to sulfur impurities because silica-supported metal sulfides, such as ZnS, CuS, CoS, etc., have been found to perform significantly better in alkane dehydrogenation than their corresponding oxides [57]. However, the tolerance of CdO/SiO₂ catalysts to sulfur impurities is an open research issue.

5.1.6. Reaction mechanism

It is suggested that the mechanism of dehydroisomerisation of monoterpenes to p-cymene on bifunctional catalysts involves two steps: fast isomerisation of monoterpene reactant on Brønsted acid sites to form p-menthadiene intermediates followed by their slow dehydrogenation on metal or oxo-metal sites to p-cymene [17,25,32,40]. The mechanism of the first step is well documented in the literature. It is presented in Scheme 3.1. In the case of Pd/SiO₂ [17,32] and ZnO/SiO₂ [40] catalysts, this step has been shown to occur on the silanol groups of silica support possessing mild Brønsted acidity. This is also the case for our CdO/SiO₂ catalyst, as demonstrated by the data in Table 5.2. This data shows that α -pinene isomerisation to p-menthadienes proceeds in the presence of silica alone with almost 100% conversion at 250 °C, whereas CdO alone, lacking Brønsted acidity, exhibits no isomerisation activity. On the other hand, silica, lacking dehydrogenation ability, is incapable to dehydrogenate p-menthadienes to p-cymene, which occurs efficiently on CdO.

A proposed mechanism for the dehydrogenation step on oxo-metal sites of CdO/SiO₂ catalyst is shown in Scheme 5.2 for the dehydrogenation of α -terpinene as an example. The dehydrogenation is suggested to proceed through the abstraction of allylic hydrogen from the substrate by the oxo-Cd(II) site followed by the elimination of another hydrogen atom to form p-cymene π -bonded to Cd(II). Then, the elimination of the p-cymene molecule and H₂ closes the catalytic cycle. The same mechanism can also be suggested for the reaction on ZnO/SiO₂ catalyst. This mechanism is based on knowledge about the mechanism of hydrocarbon dehydrogenation on metal oxides [58].



Scheme 5.2. Proposed mechanism of monoterpene dehydrogenation on oxo-metal sites of CdO/SiO₂ catalyst.

The bicyclic monoterpenes, such as α -pinene and β -pinene, are less reactive than the monocyclic ones, such as limonene, α -terpinene, γ -terpinene, and terpinolene, since the latter do not require C–C bond breaking to form p-cymene. The bicyclic monoterpenes give the 91–95% p-cymene yields at 325–375 °C, whereas the monocyclic ones give a 100% yield at 200–250 °C. The monoterpenes can be ranked more accurately in their reactivity by comparing p-cymene selectivity at 100% conversion under the same reaction conditions (250 °C, 20% CdO/SiO₂, WHSV = 0.08 h⁻¹): β -pinene (66%) < α -pinene (73%) < terpinolene (99%) \leq limonene, α -terpinene, γ -terpinene (100%). The importance of these results is twofold: (i) all these monoterpenes give p-cymene with excellent yields on CdO/SiO₂; and (ii) the results support the bifunctional reaction mechanism. It should be noted that ranking the reactivity of monoterpenes by measuring differential rates or conversions is not possible because monoterpene conversion is determined by the fast isomerisation step (~100% above 200 °C), and practically no p-cymene is formed at low conversions.

5.2. Conclusions

In summary, CdO/SiO₂ is a new highly efficient noble-metal-free catalyst for the green synthesis of p-cymene by the dehydroisomerisation of cyclic monoterpenes (α -pinene, β -pinene, limonene, α -terpinene, γ -terpinene, and terpinolene). In the α -pinene-to-p-cymene reaction, this catalyst provides 91% p-cymene yield at 100% α -pinene conversion at 325 °C and WHSV = 0.01 h⁻¹. The CdO/SiO₂ catalyst surpasses Pd/SiO₂ [17], Pd-Zn/Al-SBA-15 [24], bulk Zn(II)–Cr(III) mixed oxide [25], and ZnO/SiO₂ [40], which provide either lower p-cymene yields (Pd catalysts) or operate at a higher temperature (ZnO/SiO₂ at 370 °C) or both (Zn-Cr oxide). Moreover, the Pd catalysts require continuous hydrogen supply to prevent catalyst deactivation [17,24]. The noble-metal-free CdO/SiO₂ catalyst does not require any hydrogen supply and it can be regenerated by air. The dehydroisomerisation of β -pinene over CdO/SiO₂ gives 95% p-cymene yield at 375 °C and WHSV = 0.02 h⁻¹, which is higher than the p-cymene yield obtained from α -pinene, although achieved at a higher temperature. The dehydroisomerisation of limonene is much more feasible than that of α -pinene and β -pinene. The CdO/SiO₂ catalyst outperforms the best catalysts for the gas-phase limonene-to-p-cymene dehydroisomerisation reported so far. Thus, Pd/SiO₂ provides a 99% yield of p-cymene at 300 °C and requires hydrogen supply to prevent catalyst deactivation [32]. ZnO/SiO₂ catalyst gives 100% p-cymene yield at 325 °C and WHSV = 0.08 h⁻¹. In contrast, the 20% CdO/SiO₂ catalyst gives 100% p-cymene yield at 250 °C and the same space velocity. α -Terpinene, γ -terpinene, and terpinolene readily undergo dehydroisomerisation over CdO/SiO₂ similar to limonene with 100% p-cymene yield at 200–250 °C and WHSV = 0.04–0.08 h⁻¹. The most abundant monoterpenes, such as α -pinene and limonene, and industrial waste turpentine streams, such as the crude sulfate turpentine, containing a mixture of common p-menthadienes, are the renewable feedstocks for the sustainable production of p-cymene. The new CdO/SiO₂ catalyst is promising for the sustainable synthesis of p-cymene from renewable terpene feedstocks.

References

- [1] K. A. D. Swift, Catalytic transformations of the major terpene feedstocks, *Top. Catal.* 27 (2004) 1–4.
- [2] J. L. F. Monteiro, C. O. Veloso, Catalytic conversion of terpenes into fine chemicals, *Top. Catal.* 27 (2004) 169–180.
- [3] E. Breitmaier, *Terpenes. Flavors, Fragrances, Pharmaca, Pheromones*, Wiley-VCH, Weinheim, 2006.
- [4] A. Corma, S. Iborra, A. Velty, Chemical routes for the transformation of biomass into chemicals. *Chem. Rev.* 107 (2007) 2411–2502.
- [5] M. Eggersdorfer, Terpenes, in: *Ullmann’s Encyclopedia of Industrial Chemistry*, Wiley-VCH, Weinheim, Germany, 2012, Vol. 36, pp. 29–45.
- [6] E. V. Gusevskaya, Reactions of terpenes catalyzed by heteropoly compounds: valorization of bio renewables, *ChemCatChem* 6 (2014) 1505–1515.
- [7] C. S. Sell (Ed.), *The Chemistry of fragrances: From perfumer to consumer*, second ed., RSC Publishing, Dorset, UK, 2015.
- [8] G. J. H. Buisman, J.H.M. Lange, in: P. D. de María (Ed.), *Industrial Bio renewables: A Practical Viewpoint*, Wiley, 2016, pp. 21–62.
- [9] J. D. Tibbetts, S. D. Bull, p-Menthadienes as bio renewable feedstocks for a monoterpene-based biorefinery, *Adv. Sustain. Syst.* (2021) 2000292.
- [10] A. E. Harman-Ware, Conversion of Terpenes to Chemicals and Related Products, in: M. Crocker, E. Santillana-Jimenez (Eds.), *Chemical Catalysts for Biomass Upgrading*, Wiley, New York, 2019, pp. 529–568.
- [11] W. B. Cunningham, J. D. Tibbetts, M. Hutchby, K. A. Maltby, M.G. Davidson, U. Hintermair, P. Plucinski, S. D. Bull, Sustainable catalytic protocols for the solvent free epoxidation and antidihydroxylation of the alkene bonds of bio renewable terpene feedstocks using H₂O₂ as oxidant, *Green Chem.* 22 (2020) 513–524.
- [12] W. P. Teh, D. C. Obenschain, B. M. Black, F. E. Michael, Catalytic metal-free allylic C-H amination of terpenoids, *J. Am. Chem. Soc.* 142 (2020) 16716–16722.
- [13] J. D. Tibbetts, S. D. Bull, Dimethyl sulfide facilitates acid catalysed ring opening of the bicyclic monoterpenes in crude sulfate turpentine to afford p-menthadienes in good yield, *Green Chem.* 23 (2021) 597–610.

- [14] D. I. Collias, A. M. Harris, V. Nagpal, I. W. Cottrell, M. W. Schultheis, Bio based terephthalic acid technologies: A literature review, *Ind. Bio technol.* 10 (2014) 91–105.
- [15] F. Neatu, G. Culica, M. Florea, V. I. Parvulescu, F. Cavani, Synthesis of terephthalic acid by p-cymene oxidation using oxygen: Toward a more sustainable production of biopolyethylene terephthalate, *ChemSusChem* 9 (2016) 3102–3112.
- [16] J. D. Tibbetts, D. Russo, A. A. Lapkin, S. D. Bull, Efficient syntheses of bio based terephthalic acid, p-toluic acid, and p-methyl acetophenone via one-pot catalytic aerobic oxidation of monoterpene derived bio-p-cymene, *ACS Sustain. Chem. Eng.* 9 (2021) 8642–8652.
- [17] D. M. Roberge, D. Buhl, J. P. M. Niederer, W. F. Hölderich, Catalytic aspects in the transformation of pinenes to p-cymene, *Appl. Catal. A Gen.* 215 (2001) 111–124.
- [18] K. Weissermel, H. J. Arpe, *Industrial Organic Chemistry*, forth ed., Weinheim, Wiley-VCH, 2003.
- [19] W. F. Erman, *Chemistry of The Monoterpenes: An Encyclopedic Handbook*, M. Dekker, New York, 1985.
- [20] B. Ozturk, J. Winterburn, M. Gonzalez-Miquel, Orange peel waste valorisation through limonene extraction using bio-based solvents. *Biochem. Eng. J.* 151 (2019) 107298.
- [21] P. Jorayev, D. Russo, J. D. Tibbetts, A. M. Schweidtmann, P. Deutsch, S. D. Bull, A. A. Lapkin, Multi-objective Bayesian optimization of a two-step synthesis of p-cymene from crude sulphate turpentine. *Chem. Eng. Sci.* 247 (2021) 116938.
- [22] A. Stanislaus, L. M. Yeddanapalli, Vapor phase catalytic transformations of terpene hydrocarbons in the C₁₀H₁₆ series. II. Aromatization of α -pinene over chromia-alumina, *Can. J. Chem.* 50 (1972) 113–118.
- [23] J. A. Linnekoski, M. Asikainen, H. Heikkinen, R. K. Kaila, J. Rasanen, A. Laitinen, A. Harlin, Production of p-cymene from crude sulphate turpentine with commercial zeolite catalyst using a continuous fixed bed reactor, *Org. Process. Res. Dev.* 18 (2014) 1468–1475.
- [24] M. Golets, S. Ajaikumar, M. Mohln, J. Wärna, S. Rakesh, J.P. Mikkola, Continuous production of the renewable p-cymene from α -pinene, *J. Catal.* 307 (2013) 305–315.
- [25] F. Al-Wadaani, E. F. Kozhevnikova, I. V. Kozhevnikov, Zn(II)–Cr(III) mixed oxide as efficient bifunctional catalyst for dehydroisomerization of α -pinene to p-cymene, *Appl. Catal. A Gen.* 363 (2009) 153–156.

- [26] M. A. Martin-Luengo, M. Yates, M. J. Martinez Domingo, B. Casal, M. Iglesias, M. Esteban, E. Ruiz-Hitzky, Synthesis of p-cymene from limonene, a renewable feedstock, *Appl. Catal. B Environ.* 81 (2008) 218–224.
- [27] A. Satira, C. Espro, E. Paone, P. Calabrò, M. Pagliaro, R. Ciriminna, F. Mauriello, The limonene biorefinery: From extractive technologies to its catalytic upgrading into p-cymene, *Catalysts* 11 (2021) 387.
- [28] M. Retajczyk, A. Wróblewska, Isomerization and dehydroaromatization of R-(+)-limonene over the Ti-MCM-41 catalyst: Effect of temperature, reaction time and catalyst content on product yield, *Catalysts* 9 (2019) 508.
- [29] H. Cui, J. Zhang, Z. Luo, C. Zhao, Mechanisms into dehydroaromatization of bioderived limonene to p-cymene over Pd/HZSM-5 in the presence and absence of H₂, *RSC Adv.* 6 (2016) 66695–66704.
- [30] E. Yilmazoglu, M. Akgün, p-Cymene production from orange peel oil using some metal catalyst in supercritical alcohols, *J. Supercrit. Fluids* 131 (2018) 37–46.
- [31] M. Kamitsou, G. D. Panagiotou, K. S. Triantafyllidis, K. Bourikas, A. Lycourghiotis, C. Kordulis, Transformation of α -limonene into p-cymene over oxide catalysts: A green chemistry approach, *Appl. Catal. A Gen.* 474 (2014) 224–229.
- [32] D. Buhl, D. M. Roberge, W. F. Hölderich, Production of p-cymene from limonene over silica supported Pd catalysts, *Appl. Catal. A Gen.* 188 (1999) 287–299.
- [33] M. A. Martin-Luengo, M. Yates, S. E. Rojoa, D. H. Arribas, D. Aguilar, R. E. Hitzky, Sustainable p-cymene and hydrogen from limonene. *Appl. Catal. A Gen.* 387 (2010) 141–146.
- [34] A. C. Bueno, B. B. N. S. Brandao, E. V. Gusevskaya, Aromatization of para-menthenic terpenes by aerobic oxidative dehydrogenation catalyzed by p-benzoquinone, *Appl. Catal. A Gen.* 351 (2008) 226–230.
- [35] C. P. Tavera Ruiz, P. Gauthier-Maradei, M. Capron, C. Pirez, O. Gardoll, B. Katryniok, F. Dumeignil, Transformation of DL limonene into aromatic compounds using supported heteropolyacid catalysts, *Catal. Lett.* 149 (2019) 328–337.
- [36] D. Makarouni, S. Lycourghiotis, E. Kordouli, K. Bourikas, C. Kordulis, V. Dourtoglou, Transformation of limonene into p-cymene over acid activated natural mordenite utilizing atmospheric oxygen as a green oxidant: A novel mechanism, *Appl. Catal. B Environ.* 224 (2018) 740–750.

- [37] R. Rachwalik, M. Hunger, B. Sulikowski, Transformations of monoterpene hydrocarbons on ferrierite type zeolites, *Appl. Catal. A Gen.* 427–428 (2012) 98–105.
- [38] S. Lycourghiotis, D. Makarouni, E. Kordouli, K. Bourikas, C. Kordulis, V. Dourtoglou, V. Activation of natural mordenite by various acids: Characterization and evaluation in the transformation of limonene into p-cymene, *Mol. Catal.* 450 (2018) 95–103.
- [39] J. Zhang, C. Zhao, Development of a bimetallic Pd-Ni/HZSM-5 catalyst for the tandem limonene dehydrogenation and fatty acid deoxygenation to alkanes and arenes for use as biojet fuel, *ACS Catal.* 6 (2016) 4512–4525.
- [40] A. Alsharif, N. Smith, E. F. Kozhevnikova, I. V. Kozhevnikov, Dehydroisomerization of α -pinene and limonene to p-cymene over silica-supported ZnO in the gas phase, *Catalysts* 11 (2021) 1245.
- [41] S. Dahi-Azar, S. Abdolmohammadi, J. Mokhtari, CdO Nanoparticles: A highly effective catalyst in cyclocondensation reaction of 3,4-methylenedioxyphenol, aromatic aldehydes, and active methylene compounds under ultrasonic irradiation, *J. Nanostruct.* 11 (2021) 57–65.
- [42] K. M. Abd El-Salaam, E. A. Hassan, Active surface centres in a heterogeneous CdO catalyst for ethanol decomposition, *Surf. Technol.* 16 (1982) 121–128.
- [43] V. A. Ferapontov, A. A. Balandin, A. A. Tolstopyatova, Catalytic dehydrogenation of ethylbenzene to styrene on cadmium oxide in the presence of water vapor, *Bull. Acad. Sci. USSR, Div. Chem. Sci.* 12 (1963) 373–380.
- [44] K. T. Wojciechowski, A. Maøeckci, Mechanism of thermal decomposition of cadmium nitrate $\text{Cd}(\text{NO}_3)_2 \cdot 4\text{H}_2\text{O}$, *Thermochim. Acta* 331 (1999) 73–77.
- [45] M. Tariq, A. K. Qureshi, S. Karim, M. Sirajuddin, N. Abbas, M. Imran, J. H. Shirazi, Synthesis, characterization and fuel parameters analysis of linseed oil biodiesel using cadmium oxide nanoparticles, *Energy* 222 (2021) 1–8.
- [46] H. M. Tasdemir, S. Yasyerli, N. Yasyerli, Selective catalytic oxidation of H_2S to elemental sulfur over titanium based Ti-Fe, Ti-Cr and Ti-Zr catalysts, *Int. J. Hydrogen Energy* 40 (2015) 9989–10001.
- [47] K. Kaneko, Determination of pore size and pore size distribution 1. Adsorbents and catalysts, *J. Memb. Sci.* 96 (1994) 59–89.
- [48] G. Leofanti, M. Padovan, G. Tozzola, B. Venturelli, Surface area and pore texture of catalysts, *Catal. Today* 41 (1998) 207–219.

- [49] K. S. W. Sing, Characterization of porous materials: past, present and future, *Colloids Surfaces A Physicochem. Eng. Asp.* 241 (2004) 3–7.
- [50] R. M. Gabr, M. M. Girgis, A. M. El-Awad, B. M. Abou-Zeid, Effect of spinel (ZnCr_2O_4) formation on the texture, electrical conduction and catalytic behaviour of the $\text{ZnO-Cr}_2\text{O}_3$ system, *Mater. Chem. Phys.* 39 (1994) 53–62.
- [51] M. S. M. Al-Ghamdi, H. Bayahia, Zinc-Chromium oxide catalyst for gas-phase ketonisation of pentanoic acid, *Mediterr. J. Chem.* 6 (2017) 1–6.
- [52] B. S. Anandakumar, M. B. M. Reddy, K. V. Thipperudraiah, M. A. Pasha, G. T. Chandrappa, Combustion-derived CdO nanopowder as a heterogeneous basic catalyst for efficient synthesis of sulfonamides from aromatic amines using p- toluenesulfonyl chloride, *Chem. Pap.* 67 (2013) 135–144.
- [53] H. Knözinger, Infrared Spectroscopy for The Characterization of Surface Acidity and Basicity, in: G. Ertl, H. Knözinger, F. Schüth, J. Weitkamp (Eds.), *Handbook of Heterogeneous Catalysis*, Second ed. Vol. 2, Wiley-VCH, Weinheim, Germany, 2008, p. 1138.
- [54] G. P. Heitmann, G. Dahlhoff, W. F. Hölderich, Catalytically active sites for the Beckmann rearrangement of cyclohexanone oxime to ϵ -caprolactam, *J. Catal.* 186 (1999) 12–19.
- [55] K. Barbera, F. Bonino, S. Bordiga, T. V. W. Janssens, P. Beato, Structure–deactivation relationship for ZSM-5 catalysts governed by framework defects, *J. Catal.* 280 (2011) 196–205.
- [56] H. Bayahia, E. Kozhevnikova, I. V. Kozhevnikov, High catalytic activity of silicalite in gas-phase ketonisation of propionic acid, *Chem. Commun.* 49 (2013) 3842–3844.
- [57] G. Wang, C. Li, H. Shan, Highly efficient metal sulfide catalysts for selective dehydrogenation of isobutane to isobutene, *ACS Catal.* 4 (2014) 1139–1143.
- [58] J. J. H. B. Sattler, J. Ruiz-Martinez, E. Santillan-Jimenez B. M. Weckhuysen, Catalytic dehydrogenation of light alkanes on metals and metal oxides, *Chem. Rev.* 114 (2014) 10613–10653.

Chapter 6. Conclusions and future outlook

The conversion of biomass resources into value-added chemical products is a major goal in the academy and industry [1,2]. Particularly, monoterpenes are an attractive renewable material that can be converted to p-cymene. p-Cymene is a valuable product that has many applications in medicinal and cosmetic uses and industrial organic synthesis [3]. Its major application is as an intermediate for the synthesis of p-cresol, which is further transformed into antioxidants [4]. Conventionally, p-cymene is produced by Friedel-Crafts liquid-phase alkylation of toluene with propene catalysed by Lewis acids. This method is problematic because it uses non-renewable feedstocks as well as corrosive and toxic homogeneous acid catalysts, with adverse effect on the environment. Also, there are problems associated with separation processes [5]. Therefore, the dehydroisomerisation of monoterpenes over multifunctional heterogeneous catalysts is a promising direction for the sustainable synthesis of p-cymene.

In this study, the new bifunctional metal-acid catalysts ZnO/SiO₂ and CdO/SiO₂ were investigated for the direct synthesis of p-cymene from monoterpenes such as α -pinene, β -pinene, limonene, α -terpinene, γ -terpinene and terpinolene. These catalysts possess oxo-metal and acid sites and allow for producing p-cymene in excellent yields.

The main aims of this work were:

1. To investigate the dehydroisomerisation of α -pinene and limonene to p-cymene in the gas phase over ZnO/SiO₂ and CdO/SiO₂ catalysts .
2. To investigate the dehydroisomerisation of other terpenes such as β -pinene, α -terpinene, γ -terpinene and terpinolene over ZnO/SiO₂ and CdO/SiO₂ catalysts.

These terpenes are much less studied in the literature, but are significant

components of industrial turpentine streams that can be used as a renewable feedstock for p-cymene production.

3. To gain mechanistic insights into monoterpene dehydroisomerisation over bifunctional metal-acid catalysts.

The new catalysts used in this work were prepared by an impregnation method according to the procedures documented in the literature and characterised using various techniques. ICP analysis was used to determine the loading of ZnO and CdO on the silica support. TGA was used to determine the thermal stability of the catalysts and the water content. The surface area and porosity of catalysts were determined using N₂ physisorption (BET method). The catalysts under study were all mesoporous solids with an average pore diameter of 155–237 Å and relatively high surface area of 126–294 m² g⁻¹. XRD studies were carried out to determine the catalyst composition. DRIFT spectroscopy of silanol groups and adsorbed pyridine was used to characterise the acid properties of ZnO/SiO₂ and CdO/SiO₂ catalysts.

The catalysts were tested for the gas-phase dehydroisomerisation of monoterpenes using the continuous flow fixed-bed quartz tubular reactor (9 mm internal diameter) with online GC analysis of reaction products described in Chapter 2.

ZnO/SiO₂ was found to be a highly efficient, noble-metal-free bifunctional catalyst for the environment-friendly synthesis of p-cymene by the gas-phase dehydroisomerisation of α -pinene and limonene. Dehydroisomerisation of α -pinene over ZnO/SiO₂ produces p-cymene with 90% yield at 100% conversion at 370 °C and a space velocity WHSV = 0.020 h⁻¹. The reaction with limonene gives a 100% p-cymene yield at 325 °C and WHSV = 0.080 h⁻¹. The dehydroisomerisation of β -pinene over ZnO/SiO₂ gives 100% p-cymene yield at 400 °C and WHSV = 0.080 h⁻¹, whereas dehydroisomerisation of α -terpinene, γ -terpinene, and terpinolene over ZnO/SiO₂ gives 100% p-cymene yield at 300–325 °C and WHSV = 0.160–0.080 h⁻¹. ZnO/SiO₂ catalyst shows stable performance for over 70 h without co-feeding hydrogen.

The CdO/SiO₂ catalyst is an even more efficient noble-metal-free catalyst for the green synthesis of p-cymene by the dehydroisomerisation of bicyclic monoterpenes (α -pinene and β -pinene), and monocyclic monoterpenes (limonene, α -terpinene, γ -terpinene, and terpinolene). The bicyclic monoterpenes give 91–95% p-cymene yields at 325–375 °C and WHSV = 0.010–0.020 h⁻¹, whereas the monocyclic ones give a 100% yield at 200–250 °C and WHSV = 0.040–0.080 h⁻¹. The CdO/SiO₂ catalyst does not require any hydrogen supply and can be regenerated by air. This catalyst is superior to the catalysts reported in the literature, such as Pd/SiO₂ [6], Pd-Zn/Al-SBA-15 [4], bulk Zn(II)–Cr(III) mixed oxide [7], and ZnO/SiO₂ [8], which provide either lower p-cymene yields (Pd catalysts) or operate at a higher temperature (ZnO/SiO₂ at 370 °C) or both (Zn–Cr oxide).

A mechanism for the dehydroisomerisation of monoterpenes over bifunctional metal-acid catalysts was proposed. It involves acid-catalysed cyclic monoterpene isomerisation to form p-menthadienes, followed by dehydrogenation of p-menthadienes on oxo-metal sites to produce p-cymene. The dehydrogenation is suggested to proceed through the abstraction of allylic hydrogen from the substrate by an oxo-metal site followed by the elimination of another hydrogen atom to form p-cymene π -bonded to metal ion (Zn(II) or Cd(II)). Then, the elimination of the p-cymene molecule and H₂ closes the catalytic cycle.

Future work may be focussed on the following issues:

1. Better characterisation of oxo-metal active sites in these catalysts using techniques such as XPS, EXAFS and adsorption of probe molecules (CO, etc.).
2. Further catalyst improvement by optimising catalyst composition using doping with metal and non-metal additives.
3. Testing the catalysts on the crude sulfate turpentine (CST) and other industrial turpentine feedstocks.
4. Further studies of catalyst stability and life time.

References

- [1] Y. Zhu, C. Romain, C. K. Williams, Sustainable polymers from renewable resources, *Nature* 540 (2016) 354–362.
- [2] M. S. Cui, J. Deng, X. L. Li, Y. Fu, Production of 4-hydroxymethylfurfural from derivatives of biomass-derived glycerol for chemicals and polymers, *ACS Sustain. Chem. Eng.* 4 (2016) 1707–1714.
- [3] E. Yılmazoğlu, M. Akgün, p-cymene production from orange peel oil using some metal catalyst in supercritical alcohols, *J. Supercrit. Fluids* 131 (2018) 37–46.
- [4] M. Golets, S. Ajaikumar, M. Mohln, J. Wärnå, S. Rakesh, J. P. Mikkola, Continuous production of the renewable p-cymene from α -pinene, *J. Catal.* 307 (2013) 305–315.
- [5] A. Marchese, C. R. Arciola, R. Barbieri, A. S. Silva, S. F. Nabavi, A. J. T. Sokeng, M. Izadi, N. J. Jafari, I. Suntar, M. Daglia, S. M. Nabavi, Update on monoterpenes as antimicrobial agents: A particular focus on p-cymene, *Materials* 10 (2017) 1–15.
- [6] D. M. Roberge, D. Buhl, J. P. M. Niederer, W. F. Hölderich, Catalytic aspects in the transformation of pinenes to p-cymene, *Appl. Catal. A Gen.* 215 (2001) 111–124.
- [7] F. Al-Wadaani, E. F. Kozhevnikova, I. V. Kozhevnikov, Zn(II)–Cr(III) mixed oxide as efficient bifunctional catalyst for dehydroisomerisation of α -pinene to p-cymene, *Appl. Catal. A Gen.* 363 (2009) 153–156.
- [8] A. Alsharif, N. Smith, E. F. Kozhevnikova, I. V. Kozhevnikov, Dehydroisomerisation of α -pinene and limonene to p-cymene over silica-supported ZnO in the gas phase, *Catalysts* 11 (2021) 1245.